

2010-10-07

# Transport and Metabolism of Glucose in Intervertebral Disc

Alicia R. Jackson

University of Miami, a.jackson2@umiami.edu

Follow this and additional works at: [https://scholarlyrepository.miami.edu/oa\\_dissertations](https://scholarlyrepository.miami.edu/oa_dissertations)

## Recommended Citation

Jackson, Alicia R., "Transport and Metabolism of Glucose in Intervertebral Disc" (2010). *Open Access Dissertations*. 479.  
[https://scholarlyrepository.miami.edu/oa\\_dissertations/479](https://scholarlyrepository.miami.edu/oa_dissertations/479)

This Open access is brought to you for free and open access by the Electronic Theses and Dissertations at Scholarly Repository. It has been accepted for inclusion in Open Access Dissertations by an authorized administrator of Scholarly Repository. For more information, please contact [repository.library@miami.edu](mailto:repository.library@miami.edu).



UNIVERSITY OF MIAMI

TRANSPORT AND METABOLISM OF GLUCOSE IN INTER VERTEBRAL DISC

By

Alicia R. Jackson

A DISSERTATION

Submitted to the Faculty  
of the University of Miami  
in partial fulfillment of the requirements for  
the degree of Doctor of Philosophy

Coral Gables, Florida

December 2010

©2010  
Alicia R. Jackson  
All Rights Reserved



UNIVERSITY OF MIAMI

A dissertation submitted in partial fulfillment of  
the requirements for the degree of  
Doctor of Philosophy

TRANSPORT AND METABOLISM OF GLUCOSE IN INTERVERTEBRAL DISC

Alicia R. Jackson

Approved:

\_\_\_\_\_  
Weiyong Gu, Ph.D.  
Professor of  
Biomedical Engineering

\_\_\_\_\_  
Terri A. Scandura, Ph.D.  
Dean of the Graduate School

\_\_\_\_\_  
Chun-Yuh Huang, Ph.D.  
Assistant Professor of  
Biomedical Engineering

\_\_\_\_\_  
Fotios Andreopoulos, Ph.D.  
Associate Professor of  
Biomedical Engineering

\_\_\_\_\_  
Mark D. Brown, M.D., Ph.D.  
Professor of Orthopaedics

\_\_\_\_\_  
Zhongmin Lu, Ph.D.  
Associate Professor of Biology

JACKSON, ALICIA R.

(Ph.D., Biomedical Engineering)

Transport and Metabolism of Glucose in  
Intervertebral Disc

(December 2010)

Abstract of a dissertation at the University of Miami.

Dissertation supervised by Professor Weiyong Gu

No. of pages in text. (164)

Low back pain is a major social and economic dilemma in the United States. Despite its high impact, the origins of low back remain unclear. Nonetheless, degenerative changes to the intervertebral discs (IVD) of the spine have been implicated as a possible source leading to pain. Poor nutritional supply to the IVD is believed to play a primary role in the pathophysiology of disc degeneration.

Since the disc is avascular, vital nutrients, such as glucose, must be supplied by surrounding blood vessels. However, the transport and metabolic properties of glucose in the IVD have not been fully delineated. This knowledge is necessary in order to elucidate the nutrition-related mechanisms of disc degeneration. Therefore, in this dissertation, experimental and theoretical methods are used to investigate the transport and metabolism of glucose in the intervertebral disc.

Strain-dependent and anisotropic (i.e., direction-dependent) transport of glucose in human annulus fibrosus (AF) was investigated using custom apparatuses. Results indicate that diffusivity and partitioning of glucose in human AF decreases with increasing compressive strain. Furthermore, diffusivity of glucose is anisotropic, being lower in the radial direction than the axial or circumferential directions at all strain levels. Transport of glucose in human AF was also found to diminish with increasing disc degeneration.

A new method was developed to measure the rate of glucose consumption by IVD cells; this method was then validated with porcine AF and nucleus pulposus (NP) cells at varying levels of oxygen tension. Results show a positive Pasteur effect, with the glucose consumption rate by AF and NP cells increasing at low levels of oxygen. Moreover, results indicate that the rate of consumption of glucose by NP cells is significantly higher than that by AF cells.

A new, three-dimensional finite element model of the IVD was developed in order to theoretically predict nutrient distributions in the disc. This model incorporated anatomical disc geometry, nutrient transport coupled to cellular metabolism, and mechanical loading conditions. The model was used to investigate the effects of endplate calcification and *in vivo* loading conditions on glucose distributions in the disc. Both calcification and compressive loading resulted in diminished glucose concentrations in the tissue. The model was also used to analyze the effects of degeneration and compression on cell viability in IVD by incorporating viability criteria. Our model could predict cell death in degenerated tissue, and compressive loading augmented this effect. The model prediction can be used to supplement experimental results, and may also serve as a useful tool in developing new strategies for the treatment of disc degeneration.

The findings of this dissertation greatly enhance the knowledge of glucose transport and metabolism in the intervertebral disc. Given that glucose is a critical nutrient for disc cell survival, this knowledge can provide important insight into nutritional pathways and mechanisms in the IVD, as well as related disc degeneration.

## ACKNOWLEDGEMENTS

There are many people to whom I am incredibly grateful for their support and encouragement over the past years. Without them, this achievement would not have been possible.

First and foremost, I would like to thank Dr. Weiyong Gu for serving as my advisor for the past 6+ years, as an undergraduate and graduate student. You have always provided me with great advice, thoughtful insights, and all the necessary tools to allow me to become a better engineer and scientist. Your constant encouragement and confidence in me has been invaluable. I thank you for the opportunity to work with you in the Tissue Biomechanics Lab.

I would also like to thank the other members of my committee: Dr. Charles Huang, Dr. Mark Brown, Dr. Fotios Andreopoulos, and Dr. Zhongmin Lu. I greatly appreciate the time you have spent and advice you have provided while kindly serving on my committee.

To all the members of the Tissue Biomechanics Lab, I thank you for helping to make working and doing research enjoyable. I especially want to thank Tai for always offering me his advice, time, and guidance – I will always be indebted to you for all you have done to help me. Francesco, I want to thank you for answering my questions and offering me your opinion when I needed it. And to Andre, thanks for always lightening the mood in the lab, and for machining my chambers in an (almost always) timely fashion.

I have accomplished my goals because of the support of my family: my parents, Mark and Mary Lou, and my siblings, Adam and Amanda. Thank you for helping me to become the person I am today.

And most of all, I want to thank my husband, Chris Bennett, for always supporting me, guiding me, encouraging me, and loving me. I could not have achieved this without you. I dedicate this to you.

# TABLE OF CONTENTS

<b><u>LIST OF FIGURES</u></b>	<b>viii</b>
<b><u>LIST OF TABLES</u></b>	<b>xiii</b>
<b><u>CHAPTER 1. SPECIFIC AIMS</u></b>	<b>1</b>
<b>1.1 INTRODUCTORY REMARKS</b>	<b>1</b>
<b>1.2 SPECIFIC AIMS</b>	<b>2</b>
<b>1.3 CONTENTS OF THIS DISSERTATION</b>	<b>4</b>
<b><u>CHAPTER 2. BACKGROUND AND SIGNIFICANCE</u></b>	<b>7</b>
<b>2.1 FUNCTION OF THE INTERVERTEBRAL DISC IN SPINE BIOMECHANICS</b>	<b>7</b>
<b>2.2 THE INTERVERTEBRAL DISC</b>	<b>9</b>
2.2.1 <i>COMPOSITION AND STRUCTURE OF THE INTERVERTEBRAL DISC</i>	9
2.2.2 <i>CELLS OF THE INTERVERTEBRAL DISC</i>	11
<b>2.3 INTERVERTEBRAL DISC DEGENERATION</b>	<b>13</b>
<b>2.4 NUTRITIONAL TRANSPORT IN THE INTERVERTEBRAL DISC</b>	<b>16</b>
2.4.1 <i>PATHWAYS OF TRANSPORT</i>	16
2.4.2 <i>MECHANISMS OF TRANSPORT</i>	17
2.4.3 <i>EXPERIMENTAL STUDIES OF SOLUTE TRANSPORT IN IVD TISSUES</i>	19
<b>2.5 METABOLISM OF DISC CELLS</b>	<b>20</b>
<b>2.6 EFFECT OF MECHANICAL LOADING ON THE IVD</b>	<b>22</b>
<b>2.7 SIGNIFICANCE AND CLINICAL RELEVANCE</b>	<b>25</b>
<b><u>CHAPTER 3. MEASUREMENT OF STRAIN-DEPENDENT AND ANISOTROPIC DIFFUSION OF GLUCOSE IN HUMAN ANNULUS FIBROSUS</u></b>	<b>28</b>
<b>3.1 INTRODUCTORY REMARKS</b>	<b>28</b>
<b>3.2 THEORETICAL APPROACH</b>	<b>29</b>
<b>3.3 MATERIALS AND METHODS</b>	<b>32</b>
3.3.1 <i>DESIGN OF EXPERIMENTAL APPARATUS</i>	32
3.3.2 <i>SPECIMEN PREPARATION</i>	35
3.3.3 <i>WATER CONTENT MEASUREMENT</i>	38
3.3.4 <i>MEASUREMENT OF GLUCOSE DIFFUSIVITY</i>	40
3.3.5 <i>STATISTICAL ANALYSES</i>	43
<b>3.4 RESULTS</b>	<b>44</b>
<b>3.5 DISCUSSION</b>	<b>50</b>
3.5.1 <i>EFFECT OF COMPRESSION ON THE DIFFUSION OF GLUCOSE</i>	50
3.5.2 <i>ANISOTROPIC BEHAVIOR OF GLUCOSE DIFFUSIVITY IN HUMAN IVD</i>	52
3.5.3 <i>EFFECT OF DISC DEGENERATION ON DIFFUSIVITY OF GLUCOSE</i>	55
3.5.4 <i>EXPERIMENTAL LIMITATIONS</i>	56

3.6 SUMMARY AND CONCLUSIONS	57
<b><u>CHAPTER 4. MEASUREMENT OF STRAIN-DEPENDENT GLUCOSE PARTITION COEFFICIENT IN HUMAN INTERVERTEBRAL DISC</u></b>	<b>59</b>
4.1 INTRODUCTORY REMARKS	59
4.2 THEORETICAL APPROACH	60
4.3 MATERIALS AND METHODS	62
4.3.1 DESIGN OF EXPERIMENTAL APPARATUS	62
4.3.2 SPECIMEN PREPARATION	64
4.3.3 WATER CONTENT MEASUREMENT	65
4.3.4 MEASUREMENT OF PARTITION COEFFICIENT	66
4.3.5 STATISTICAL ANALYSES	68
4.4 RESULTS	68
4.5 DISCUSSION	72
4.5.1 EFFECT OF COMPRESSION ON GLUCOSE PARTITIONING IN HUMAN IVD	72
4.5.2 EFFECT OF DEGENERATION ON GLUCOSE PARTITIONING IN HUMAN IVD	73
4.5.3 EXPERIMENTAL LIMITATIONS	74
4.6 SUMMARY AND CONCLUSIONS	75
<b><u>CHAPTER 5. EFFECTIVE DIFFUSIVITY OF GLUCOSE IN HUMAN ANNULUS FIBROSUS</u></b>	<b>77</b>
5.1 INTRODUCTORY REMARKS	77
5.2 COMBINATION OF DIFFUSIVITY AND PARTITIONING RESULTS	77
5.3 COMPARISON WITH PREVIOUS STUDIES	80
5.4 SUMMARY	81
<b><u>CHAPTER 6. DEVELOPMENT OF NOVEL METHOD FOR MEASURING OXYGEN-TENSION-DEPENDENT RATE OF GLUCOSE CONSUMPTION BY IVD CELLS</u></b>	<b>83</b>
6.1 INTRODUCTORY REMARKS	83
6.2 THEORETICAL APPROACH	84
6.3 MATERIALS AND METHODS	86
6.3.1 CELL ISOLATION	86
6.3.2 CELL – GEL CONSTRUCT PREPARATION	88
6.3.3 ASSESSMENT OF CELL VIABILITY	89
6.3.4 EXPERIMENTAL SETUP	89
6.3.5 MEASUREMENT OF GLUCOSE CONCENTRATION	91
6.3.6 MEASUREMENT OF DNA CONTENT	95
6.3.7 DETERMINATION OF EVAPORATION EFFECT	96
6.3.8 CALCULATION OF GLUCOSE CONSUMPTION RATE	96
6.3.9 STATISTICAL ANALYSES	97
6.4 RESULTS	97
6.5 DISCUSSION	101

6.5.1	<i>COMPARISON OF CONSUMPTION RATES WITH STUDIES IN THE LITERATURE</i>	101
6.5.2	<i>EFFECT OF OXYGEN TENSION LEVEL ON GLUCOSE CONSUMPTION RATE</i>	102
6.5.3	<i>DIFFERENCE IN GLUCOSE CONSUMPTION RATE FOR NP AND AF CELLS</i>	105
6.5.4	<i>EXPERIMENTAL LIMITATIONS</i>	106
6.6	<b>SUMMARY AND CONCLUSIONS</b>	<b>109</b>
<b><u>CHAPTER 7. INVESTIGATION OF GLUCOSE DISTRIBUTIONS IN THE INTERVERTEBRAL DISC USING THREE-DIMENSIONAL FINITE ELEMENT ANALYSIS</u></b>		<b>110</b>
7.1	<b>INTRODUCTORY REMARKS</b>	<b>110</b>
7.2	<b>THEORETICAL MODEL</b>	<b>111</b>
7.3	<b>FINITE ELEMENT FORMULATION</b>	<b>114</b>
7.4	<b>CASE 1: EFFECT OF ENDPLATE CALCIFICATION AND MECHANICAL LOADING ON GLUCOSE DISTRIBUTIONS IN IVD</b>	<b>120</b>
7.4.1	<i>BOUNDARY CONDITIONS</i>	120
7.4.2	<i>RESULTS</i>	122
7.4.3	<i>DISCUSSION</i>	130
7.5	<b>CASE 2: EFFECT OF DEGENERATION ON CELL VIABILITY IN IVD</b>	<b>133</b>
7.5.1	<i>TISSUE PROPERTIES AND MODEL PARAMETERS</i>	133
7.5.2	<i>RESULTS</i>	135
7.5.3	<i>DISCUSSION</i>	141
7.6	<b>LIMITATIONS</b>	<b>143</b>
7.7	<b>SUMMARY AND CONCLUSIONS</b>	<b>144</b>
<b><u>CHAPTER 8. CONCLUSIONS AND RECOMMENDATIONS FOR FUTURE WORK</u></b>		<b>146</b>
8.1	<b>SUMMARY AND CONCLUDING REMARKS</b>	<b>146</b>
8.1.1	<i>STRAIN-DEPENDENT TRANSPORT PROPERTIES IN IVD</i>	147
8.1.2	<i>GLUCOSE CONSUMPTION RATE BY IVD CELLS AT VARYING OXYGEN TENSION LEVELS</i>	147
8.1.3	<i>FINITE ELEMENT MODEL OF THE IVD</i>	148
8.2	<b>RECOMMENDATIONS FOR FUTURE WORK</b>	<b>149</b>
<b><u>REFERENCES</u></b>		<b>152</b>



## LIST OF FIGURES

<b>2-1</b>	Posterior, lateral, and anterior views of the human spine, showing the four main divisions (cervical, thoracic, lumbar and sacral).	<b>8</b>
<b>2-2</b>	(a) The basic functional spinal unit and its components; (b) schematic of the IVD showing the layered structure of the annulus fibrosus (AF).	<b>9</b>
<b>2-3</b>	Photographs showing the visible differences between (a) a non-degenerate disc and (b) a degenerated disc.	<b>15</b>
<b>2-4</b>	Sagittal view of the intervertebral disc, highlighting the two main nutritional pathways into the disc from the surrounding vasculature.	<b>16</b>
<b>2-5</b>	Intradiscal pressure in common postures and activities normalized to standing posture. For Nachemson study, lifting weight = 10 kg. For Wilke study, lifting weight =20 kg. (Nachemson 1966; Wilke et al. 1999)	<b>22</b>
<b>2-6</b>	Pressures created in the disc during compressive loading; adapted from (White and Panjabi 1990).	<b>23</b>
<b>2-7</b>	Schematic showing possible causes and pathways related to disc degeneration. Adapted from (Urban et al. 2004).	<b>27</b>
<b>3-1</b>	Schematic of diffusion chamber. Solute diffuses from upstream to downstream chamber (left to right), passing through the tissue specimen.	<b>29</b>
<b>3-2</b>	Schematic illustrating linear distribution of solute in tissue when at equilibrium.	<b>31</b>
<b>3-3</b>	Engineering drawing showing the front and top views of the diffusion chamber halves.	<b>34</b>
<b>3-4</b>	Schematic showing orientation and size of specimens obtained from human annulus fibrosus (AF).	<b>37</b>
<b>3-5</b>	Schematic showing setup for analytical balance with density determination kit used for measuring tissue water content.	<b>39</b>
<b>3-6</b>	Results for apparent glucose diffusivity at varying levels of compressive strain in the three principal directions in human annulus fibrous tissue. A: axial, C: circumferential, R: radial.	<b>46</b>

<b>3-7</b>	Variation of apparent glucose diffusivity with compressive strain in the three principal directions in human annulus fibrous tissue. A: axial, C: circumferential, R: radial.	<b>47</b>
<b>3-8</b>	Graph of apparent glucose diffusivity versus compressive strain for the three principal directions of diffusion: (a) axial, (b) circumferential, and (c) radial. For each, n=48. Linear curve fits for each were used to determine diffusivity at 0% compressive strain level.	<b>48</b>
<b>3-9</b>	Variation of apparent glucose diffusivity with Thompson degenerative grade in the three principal directions in human annulus fibrous tissue. A: axial, C: circumferential, R: radial. For Grade I, n=8 for all groups; for Grades II and III, n=4 for all groups.	<b>49</b>
<b>3-10</b>	Scanning electron microscopy (SEM) images showing no obviously visible microtubes in the radial section of human AF (a), the clear presence of microtubes in the axial (b) and circumferential sections (c), along with magnified view of microtube (d).	<b>54</b>
<b>3-11</b>	Various possible arrangements for lamellae in radial specimens which may affect diffusivity measurements in radial direction. Note that diffusion is measured across the specimen, in the direction indicated by the arrows.	<b>56</b>
<b>4-1</b>	Schematic showing the procedure for determining the partition coefficient in a tissue specimen.	<b>60</b>
<b>4-2</b>	Engineering drawing showing the top and front views of the two halves of the custom partition coefficient chamber. See Figure 4-4 for schematic of assembled apparatus.	<b>63</b>
<b>4-3</b>	Schematic showing orientation and size of specimens obtained from human annulus fibrosus (AF).	<b>65</b>
<b>4-4</b>	Schematic of (a) the compression apparatus and (b) the custom chamber for measuring the partition coefficient of a compressed IVD tissue sample.	<b>66</b>
<b>4-5</b>	Results for glucose partition coefficient in human annulus fibrosus tissue at varying levels of compressive strain.	<b>70</b>
<b>4-6</b>	Relationship between partition coefficient and compressive strain for normal and degenerated human annulus fibrosus tissue. Note that normal tissue signifies Thompson Grade I, while degenerated tissue is for Grades II and III.	<b>71</b>

<b>4-7</b>	Relationship between partition coefficient and tissue porosity for human annulus fibrosus tissue. A linear curve-fit was performed using Origin 6.1.	<b>76</b>
<b>5-1</b>	Relationship between effective diffusivity and tissue porosity for human AF in the three principal directions (axial, circumferential, and radial).	<b>79</b>
<b>6-1</b>	Schematic showing how consumption rate is measured. Cells are placed in culture media with cell density $\rho(=V_s/N$ , where $V_s$ is the volume of media in the chamber, and $N$ is the number of cells) and initial concentration $C_1$ ; as cells consume glucose, the concentration in the media decreases to $C_2$ . The rate is calculated based the change in concentration over time.	<b>84</b>
<b>6-2</b>	(a) Porcine lumbar spine harvested from 3-6 month old pig; (b) transverse view of porcine IVD showing AF, NP and transition zone.	<b>87</b>
<b>6-3</b>	Cell-gel construct having a diameter of 8 mm and containing approximately 1 million cells in 2% agarose gel.	<b>88</b>
<b>6-4</b>	Schematic showing the basic experimental setup. The chamber was housed in a controlled environment in order to maintain constant oxygen tension, humidity and temperature. There was a free exchange of gas between the culture medium and the inner controlled environment. Glucose concentrations were measured outside the incubator using an electrochemical method connected to data acquisition.	<b>90</b>
<b>6-5</b>	Schematic illustrating the chain of transport of electrons from the glucose molecule, to the enzyme (here, PQQ-GDH), to the mediator, and finally to the working electrode.	<b>92</b>
<b>6-6</b>	Photographs showing (a) the Accu-Chek Aviva test strip and relative size; (b) the electrode configuration of the test strip, with working electrode (W) and counter/reference electrode (C/R) labeled; and (c) schematic of electrical circuit, with the working electrode connected to the positive terminal and the counter/reference electrode connected to the negative terminal; a constant 100 mV was applied and the current generated was measured.	<b>93</b>
<b>6-7</b>	Example of calibration curve used for calculating glucose concentration from current measurements measured with a constant 100 mV applied voltage.	<b>95</b>
<b>6-8</b>	Results for $V_{max}$ and $K_m$ for porcine NP cells at three oxygen tension levels: 2.5%, 5%, and 21%.	<b>99</b>

<b>6-9</b>	Comparison of glucose consumption rates for porcine AF and NP cells at varying oxygen tension levels. For NP cells, consumption rates were calculated at 5 mM glucose concentrations based on values for $V_{max}$ and $K_m$ determined and Equation (6-8).	<b>100</b>
<b>6-10</b>	Comparison of glucose consumption rates for porcine NP cells at varying oxygen tension levels, calculated based on values for $V_{max}$ and $K_m$ determined and Equation (6-8).	<b>103</b>
<b>7-1</b>	<b>(a)</b> Photograph of L2-L3 IVD used for determining disc geometry; <b>(b)</b> disc geometry; <b>(c)</b> disc mesh; <b>(d)</b> test configuration.	<b>115</b>
<b>7-2</b>	Loading on the disc for <b>(a)</b> supine and <b>(b)</b> standing configurations.	<b>121</b>
<b>7-3</b>	Typical glucose concentrations in the IVD for the six cases investigated: <b>(a)</b> normal CEP, supine; <b>(b)</b> normal CEP, standing; <b>(c)</b> normal CEP, weight-bearing standing; <b>(d)</b> ‘calcified’ CEP, supine; <b>(e)</b> ‘calcified’ CEP, standing; and <b>(f)</b> ‘calcified’ CEP, weight-bearing standing. Note in (b)-(c) and (e)-(f), the deformed shape is shown, while the black outline signifies the original geometry.	<b>125</b>
<b>7-4</b>	Minimum glucose concentration in the disc for the three loading configurations (supine, standing, and weight-bearing standing) and for normal (orange) and ‘calcified’ (green) endplate cases. Note the dashed line at 0.5 mM, which denotes the glucose concentration below which cells begin to die (Horner and Urban 2001).	<b>126</b>
<b>7-5</b>	Distribution of glucose in the IVD under three loading conditions (supine, standing, and weight-bearing standing) and for normal (orange) and ‘calcified’ (green) endplate cases along the y axis at $x = z = 0$ (from posterior to anterior, see figure).	<b>127</b>
<b>7-6</b>	Distribution of glucose in the IVD under three loading conditions (supine, standing, and weight-bearing standing) and for normal (orange) and ‘calcified’ (green) endplate cases along the x axis at $y = z = 0$ (from center to lateral edge, see figure).	<b>128</b>
<b>7-7</b>	pH distribution in IVD for <b>(a)</b> normal and <b>(b)</b> ‘calcified’ endplate cases.	<b>129</b>
<b>7-8</b>	Schematic showing the criteria used for cell viability based on glucose concentrations in the tissue.	<b>135</b>

- 7-9** Typical glucose concentrations in the IVD for the four cases investigated: **(a)** normal disc, reference configuration; **(b)** normal disc, 10% static compressive strain; **(c)** degenerated disc, reference configuration; **(d)** degenerated disc, 10% static compressive strain. Note in (b) and (d), the deformed shape is shown, while the black outline signifies the original geometry. **137**
- 7-10** Distribution of glucose in the normal (orange) and degenerated (green) IVD under two loading conditions [supine or reference (solid) and 10% static compression (dashed)] along the x axis at  $y = z = 0$  (from center to lateral edge, see figure). **138**
- 7-11** Distribution of glucose in the normal (orange) and degenerated (green) IVD under two loading conditions [supine or reference (solid) and 10% static compression (dashed)] along the y axis at  $x = z = 0$  (from posterior to anterior, see figure). **139**
- 7-12** Cell density in degenerated IVD for **(a)** reference and **(b)** compressed tissue at cross section shown. Values are normalized by initial cell density (see Table 7-2). Note that cell death occurs moving away from nutritional supply. **140**

## LIST OF TABLES

<b>2-1</b>	Percentage of Major Components in the Intervertebral Disc and in the Two Major Regions, Annulus Fibrosus and Nucleus Pulposus	<b>11</b>
<b>2-2</b>	Description of Thompson Morphologic Grading	<b>14</b>
<b>3-1</b>	Photographs of Intervertebral Discs Used in Diffusivity Studies, Along with Patient Information and Degenerative Grades	<b>36</b>
<b>3-2</b>	Results for Apparent Glucose Diffusivity at Varying Levels of Compressive Strain in the Three Principal Directions in Human Annulus Fibrous Tissue	<b>44</b>
<b>3-3</b>	Summary of Experimental Results for Anisotropic Diffusion in IVD	<b>55</b>
<b>4-1</b>	Results for Glucose Partition Coefficient at Varying Levels of Compressive Strain in Human Annulus Fibrous Tissue	<b>69</b>
<b>5-1</b>	Results for Effective Diffusion Coefficient and Relative Diffusivity for Human AF in the Three Principal Directions	<b>80</b>
<b>5-2</b>	Summary of Experimental Results for Diffusion Coefficient, $D$ , in IVD from the Literature	<b>82</b>
<b>6-1</b>	Results for $V_{max}$ and $K_m$ for Porcine NP Cells at Varying Oxygen Levels	<b>98</b>
<b>7-1</b>	Diffusivity in Aqueous Solution and Hydrodynamic Radius of Solutes Used in Model	<b>114</b>
<b>7-2</b>	Solute Concentrations at the AF Edge and CEP edge of the IVD	<b>118</b>
<b>7-3</b>	Tissue Properties Incorporated Into Finite Element Model of the Intervertebral Disc	<b>119</b>
<b>7-4</b>	Tissue Properties Incorporated Into Finite Element Model for Degenerated Intervertebral Disc Tissue	<b>134</b>

## **CHAPTER 1. SPECIFIC AIMS**

### **1.1 INTRODUCTORY REMARKS**

Low back pain is a condition that has a significant impact on society and the economy in the United States. Each year, it is estimated that 15 to 45% of the population of this country experiences some type of symptom of low back pain; furthermore, upwards of 70% of all individuals suffer from low back pain at some point in their lifetime. It is the second most common complaint heard by primary care physicians, behind only upper respiratory infections (i.e., the common cold). Moreover, low back pain is the most frequent cause of disability in workers under the age of 45 years. It has been previously proposed that the total cost of low back pain ranges from \$100 to \$200 billion each year in the United States alone. Two thirds of this is attributed to indirect costs, which include lost wages and reduced productivity due to the condition. Clearly, these statistics indicate that low back pain is a condition that warrants significant scientific research efforts.

Despite the high prevalence and costs of low back pain, the exact cause of this condition remains unclear to physicians and researchers. Nonetheless, degenerative changes to the intervertebral discs (IVD) in the spine have been charged as a primary etiological factor leading to the condition. As the disc degenerates, it may lose its ability to perform its primary function in the spine, leading to pain. Poor nutritional supply to the disc and its cells is believed to be the principal mechanism leading disc degeneration.

The lumbar IVD is the largest avascular structure in the human body, making transport of water and solutes into the disc an important mechanism of nutrition.

Knowledge of transport and metabolic properties of important nutrients, such as glucose, is important in understanding etiologic factors involved in disc degeneration. Furthermore, the extracellular matrix of the disc provides a unique environment for IVD cells, being subjected to a variety of conditions including mechanical loading and low nutrient (i.e., glucose and oxygen) concentrations. Mechanical forces at the tissue level can affect the physical signals at the cellular level as well as the way tissue remodeling changes physical signals through changes in tissue material properties of the extracellular matrix. Also, mechanical factors may regulate cellular responses in IVD that could govern the initiation and progression of disc degeneration. Additionally, nutrient levels in the disc may affect cellular consumption, which in turn alters the concentration gradients and transport of nutrients through disc tissue. Therefore, better understanding how these factors affect the transport and metabolism in IVD tissues is important for better understanding the *in vivo* environment in the disc, as well as the pathology of disc degeneration. However, there remains a lack of knowledge regarding nutritional transport and metabolism in the disc. This information is of utmost importance in fully delineating the causes of disc degeneration and subsequent low back pain. Therefore, this dissertation aims to close this gap by investigating both the transport and metabolism of glucose, an important nutrient, in IVD tissues.

## 1.2 SPECIFIC AIMS

The **long-term goals** of this project are to (1) better understand the pathophysiology involved in the development of low back pain; (2) further elucidate transport and metabolic properties in normal and degenerated intervertebral discs; and (3)



develop new strategies for assessing and treating the changes occurring in tissue during disc degeneration. In order to address these goals, the following specific aims will be pursued:

**Specific Aim #1: To determine the strain-dependent transport properties of glucose in non-degenerated and degenerated human IVD tissues.** Using a one-dimensional steady-state diffusion experiment, the diffusivity of glucose in human IVD tissues will be determined. The glucose diffusivity will be measured for three different degenerative grades (I, II, and III) and under three levels of compressive strain (0%, 10%, and 20%). Additionally, the anisotropic (i.e., direction-dependent) behavior of glucose diffusivity will also be examined. Moreover, the partition coefficient of glucose in human IVD tissues will be measured under three levels of compressive strain (0%, 10%, and 20%) and for three degenerative grades (I, II, and III) of tissue.

**Specific Aim #2: To determine the oxygen tension-dependent rate of glucose consumption by porcine IVD cells.** Using methods similar to those previously developed for the measurement of oxygen consumption rate, the glucose consumption rate of porcine IVD cells will be determined. These measurements will be carried out under various oxygen tensions to determine the effect of these conditions on cellular metabolism. The inhomogeneous behavior of glucose metabolism in cells will also be examined.

**Specific Aim #3: To develop a three-dimensional finite element model for analyzing transport and metabolism of glucose in IVD tissues.** A new three-dimensional finite element model of the intervertebral disc will be developed for theoretical prediction of nutritional levels in the disc. The model incorporates anatomical disc geometry, nutrient concentrations coupled to cellular metabolism, and mechanical loading along with strain-dependent tissue properties. Various boundary conditions will be considered, including mechanical loading configurations and disc degeneration.

### 1.3 CONTENTS OF THIS DISSERTATION

The overall objective of this dissertation is to investigate the transport and metabolism of glucose in intervertebral disc, in order to better elucidate the pathophysiology of disc degeneration and related low back pain. A background of the intervertebral disc and its structure, composition, function, and transport and metabolic properties is given in Chapter 2. In order to pursue the objectives of this work, new experimental techniques for investigating nutrient transport and metabolism in intervertebral disc have been developed. Furthermore, a theoretical model of the intervertebral disc, based on mixture theory and including nutrient transport coupled to cellular metabolism, is developed for investigating the distribution of glucose in the disc.

First, the transport properties of glucose in human IVD are investigated. In Chapter 3, a new experimental method is developed for measuring the strain-dependent diffusion of glucose in intervertebral disc tissue. This method is used to measure not only the diffusivity under various compressive strains, but also the anisotropic behavior of

glucose diffusion in human annulus fibrosus tissue. The detailed methods and experimental findings are discussed; results are compared with those in the literature.

In Chapter 4, a new method is developed for determining the strain-dependent partition coefficient in intervertebral disc tissue. This method is applied to measure the partition coefficient of glucose in human annulus fibrosus tissue under three levels of compressive strain. Details regarding the custom apparatus, experimental techniques, and results are fully delineated.

In Chapter 5, results from glucose diffusivity and partitioning are combined to determine the effective diffusivity of glucose in human AF. These results are also compared with those in the literature for solute transport in IVD tissues.

A new experimental approach is developed for measuring the rate of glucose consumption by cells in Chapter 6. The method employs a diffusional uptake problem, along with a custom technique for measuring glucose concentrations in culture media and curve-fitting of the Michaelis-Menten equation. The approach was validated using porcine annulus fibrosus and nucleus pulposus cells under varying levels of oxygen tension. Results are discussed and compared with previous studies in the literature.

In Chapter 7, a new finite element model of the intervertebral disc is developed. The theoretical background and new finite element formulation is described. Several boundary conditions are considered, including *in vivo* mechanical loading configurations and disc degeneration changes (i.e., endplate calcification); glucose distributions in the disc are predicted using the finite element model. Findings are discussed in the context of experimental findings in the literature as well as clinical implications.

Finally, in Chapter 8, the major findings of these investigations are summarized. Recommendations for future research initiatives in the field are also presented.

## **CHAPTER 2. BACKGROUND AND SIGNIFICANCE**

### **2.1 FUNCTION OF THE INTERVERTEBRAL DISC IN SPINE BIOMECHANICS**

The spine functions in many capacities in the human body by transmitting loads, allowing for a wide range of motion, and protecting the vital neural components of the spinal cord. The human spine is divided into four main regions: cervical, thoracic, lumbar and sacral (Figure 2-1). The cervical, thoracic and lumbar divisions are composed of seven, twelve, and five vertebral bodies, respectively. Each bony vertebra is separated by a soft tissue structure known as the intervertebral disc (IVD). The sacral region, unlike the three other regions, is a rigid structure absent of IVD between vertebrae. Instead, this region is composed of the sacrum and the coccyx, which include five and four to five fused vertebrae, respectively.

The intervertebral discs separating the vertebrae in the three upper regions of the spine play an integral role in allowing the spine to fulfill its functions. The discs allow for spinal flexibility and a wide range of motion. Furthermore, these soft tissue structures are also responsible for distributing the loads which are imposed upon the spine throughout normal daily activities.

The lumbar discs are the largest IVD in the spine, allowing for the highest range of motion in the lumbar region. Furthermore, the lumbar spine is also responsible for bearing the largest stresses, caused not only by body weight but also by normal daily activities, such as lifting or bending. Hence, given the normal conditions on these discs, it is easy to see why the lumbar discs are the most frequent site of disc degeneration, leading to low back pain in millions of Americans.

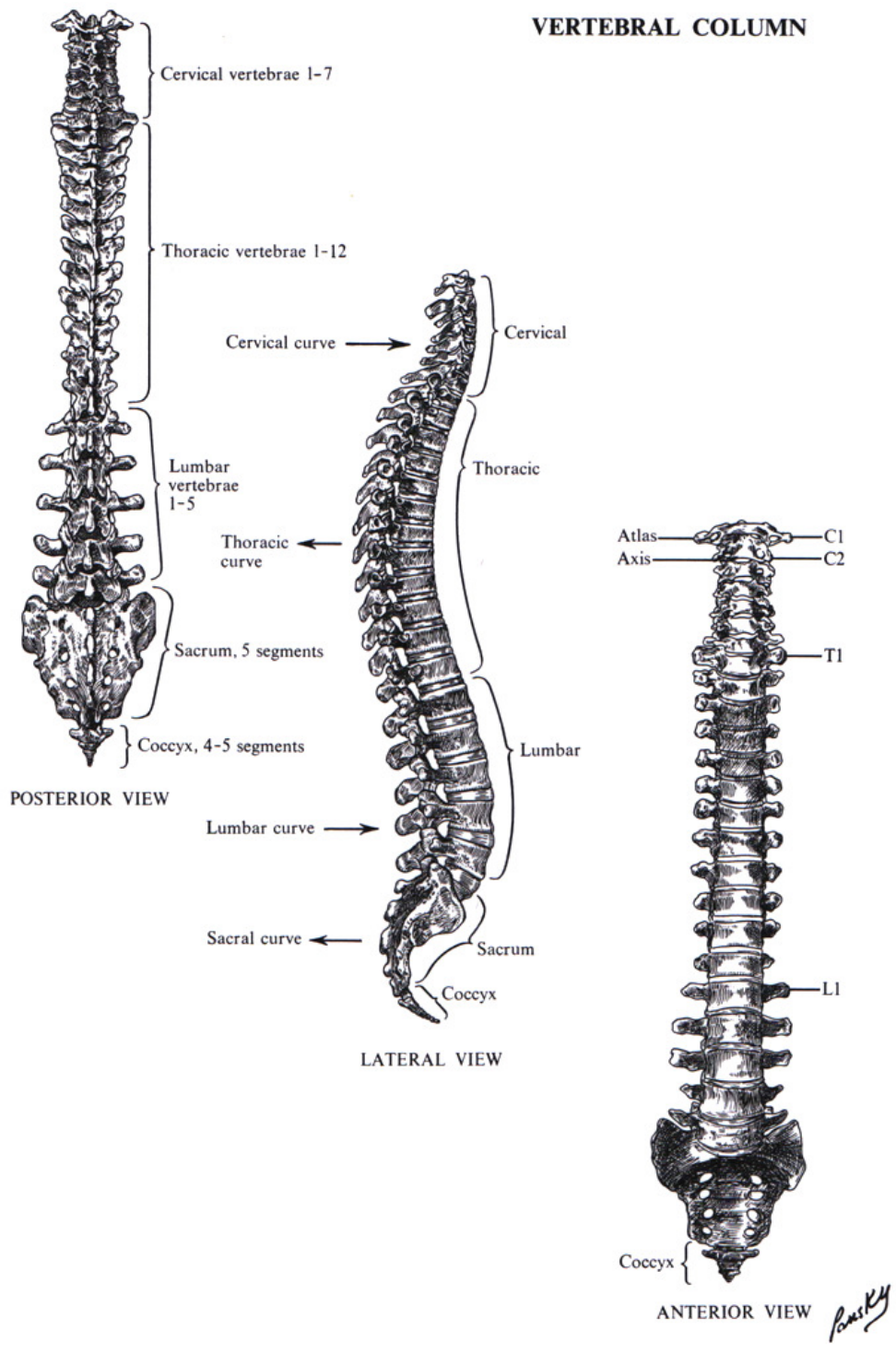


**Figure 2-1:** Posterior, lateral, and anterior views of the human spine, showing the four main divisions (cervical, thoracic, lumbar and sacral).

## 2.2 THE INTERVERTEBRAL DISC

### 2.2.1 COMPOSITION AND STRUCTURE OF THE INTERVERTEBRAL DISC

The intervertebral disc is comprised of three primary components: the annulus fibrosus (AF), the nucleus pulposus (NP) and the cartilaginous end plate (CEP) (Figure 2-2a). The composition and structure of each of these components is distinct, indicating a unique mechanical role for each (Guiot and Fessler 2000; Lundon and Bolton 2001).

The fluid-like NP is composed of randomly-oriented collagen fibrils enmeshed in a proteoglycan gel. In the lumbar intervertebral discs, the NP region fills approximately 50% of the total disc cross-sectional area (Mirza and White, III 1995). In this portion of the spine, the nucleus is located more posterior than central. The main function of the NP is to distribute loads throughout the disc.

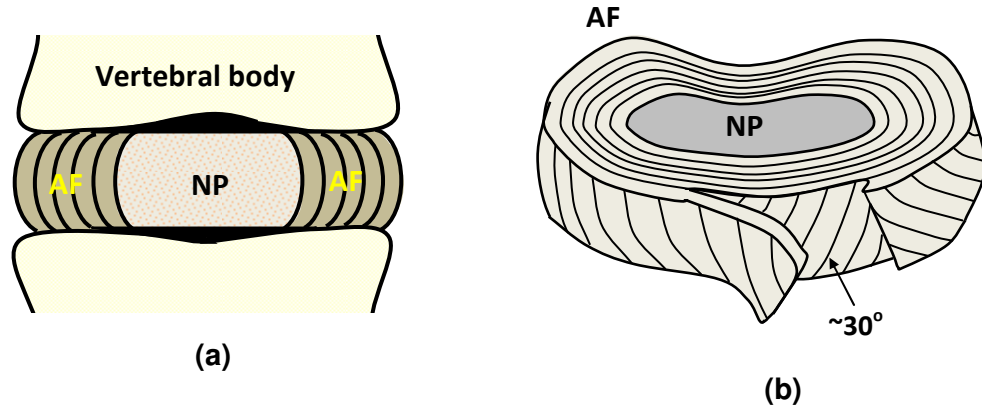


**Figure 2-2:** (a) The basic functional spinal unit and its components; (b) schematic of the IVD showing the layered structure of the annulus fibrosus (AF).

The AF surrounds the NP on its periphery and is composed of a series of concentric lamellae consisting of collagen fibers. The fibers run parallel to each other within each lamellae, but opposite those in adjacent lamellae, at approximately  $\pm 30^\circ$  to

the horizontal axis (Figure 2-2b) (Hickey and Hukins 1980; Marchand and Ahmed 1990). Depending on age and location in the spine, the AF is composed of 15 to 25 concentric lamellae, which become progressively thinner and less distinct moving inward from outer to inner AF (Marchand and Ahmed 1990). This layered structure results in anisotropic mechanical properties in the AF [e.g. (Ebara et al. 1996; Fujita et al. 1995; Galante 1967; Marchand F. and Ahmed A.M 1989)]. The AF region of the disc functions primarily in containing the gelatinous nucleus pulposus as well as withstanding forces in the radial direction.

The CEP is located on the top and bottom of the disc, connecting the soft tissue structure to the adjacent bony vertebrae. The CEP surrounds the NP as well as the inner third of the AF. It consists of a thin layer of hyaline cartilage. Along with the AF, the CEP functions to constrain the nucleus. Furthermore, the end plates also play an integral role in nutritional transport in the disc, allowing for passage of nutrients and metabolites.

The major component of the IVD is water, making up 65-90% of the wet weight. The IVD also has significant amounts of collagen (15-65% dry weight), proteoglycan (PG) (10-60% dry weight) and other matrix proteins (15-45% dry weight) (Eyre et al. 1989; Gu et al. 1999; Hendry 1958; Johnstone et al. 1992; Kraemer et al. 1985; Panagiotacopulos et al. 1987; Pearce 1993). The different components have distinct biochemical composition and structure. The greatest quantities of water and PG can be found in the NP and inner AF regions, whereas the outer AF has the greatest collagen content. The outer AF is primarily type I collagen whereas the inner AF is predominantly type II. The ratio of type I to type II decreases from outer to inner AF. The CEP collagen composition is almost exclusively type II, similar to that of hyaline cartilage



(Roberts et al. 1989; Setton et al. 1993b). The IVD is well characterized as an inhomogeneous, anisotropic, multiphasic (solid, fluid, ions, uncharged solutes) material.

**Table 2-1:** Percentage of Major Components in the Intervertebral Disc and in the Two Major Regions, Annulus Fibrosus and Nucleus Pulposus

Component	IVD	Annulus Fibrosus	Nucleus Pulposus
Water (% wet weight)	65 – 90%	60 – 70%	70 – 90%
Collagen (% dry weight)	10 – 60%	50 – 70%	15 – 25%
Proteoglycan (% dry weight)	15 – 65%	10 – 20%	~50%

### 2.2.2 CELLS OF THE INTERVERTEBRAL DISC

Although intervertebral disc cells play an integral role in disc health and function, they account for less than 1% of the disc by volume (Urban and Roberts 1995). The cell density of the disc varies by region and has been measured to be an average of approximately 5800 cells/mm<sup>3</sup>. The nucleus pulposus has the sparsest cell population, with only 4000 cells/mm<sup>3</sup>, while the annulus fibrosus has approximately 9000 cells/mm<sup>3</sup> and the cartilaginous end plate has been found to have 15000 cells/mm<sup>3</sup> (Maroudas et al. 1975). This cell density is significantly lower than that in most mammalian tissues, even articular cartilage. Furthermore, the regional variation in cell density is believed to be a result of the differences in nutritional supply to each area of the disc (Maroudas et al. 1975). This explains why cell density is highest closest to the annular edge and endplate, which are both closest to the nutrient supply (Maroudas et al. 1975; Urban et al. 2004).

The cell phenotype also varies by region within the IVD. The nucleus pulposus contains notochordal cells early in life; however, these cells disappear rapidly in the human disc and become undetectable at approximately 4-10 years (Urban and Roberts 1995). The NP is then occupied by cells originally derived from the notochord; these cells are round and chondrocyte-like, often existing in a capsule. The cells in the outer annulus fibrosus are long, thin, and fibroblast-like; these cells run parallel to the collagen fibers in the lamellae (Errington et al. 1998). In the inner annulus region, cells are more rounded. It has been suggested that these differences in cell phenotypes result from the distinct environment within each region, including differences in mechanical and nutritional factors (Maroudas et al. 1975).

The *in vivo* environment for cells in IVD tissues is distinct. Even in healthy tissues, low oxygen and glucose concentrations, as well as high lactic acid concentrations, which result in acidic pH levels, compared with the levels in plasma can be found, particularly at the center of the disc (Bibby et al. 2005). For instance, the oxygen levels at the center of the disc can be as low as 2-5% the values at the periphery, and lactate concentration at the disc center may be 8-10 times that in plasma (Holm et al. 1981; Mirza and White, III 1995). This is due to the avascularity of the tissue, with some cells being as far as 7-8 mm from the nearest blood supply in the case of the human disc (Stairmand et al. 1991; Urban et al. 2004). Local concentrations of nutrients and metabolites have been shown to have a significant effect on cellular activity and survival (Bibby et al. 2002; Horner and Urban 2001; Ishihara and Urban 1999; Ohshima and Urban 1992). Furthermore, these nutrient concentrations are also regulated by cellular demand (Stairmand et al. 1991).

Cells play a vital role in maintaining disc health and function. Not only do IVD cells synthesize the extracellular matrix of the disc, but they also synthesize matrix metalloproteinases (MMPs), which are responsible for matrix breakdown (Bibby 2002). Thus, the composition and turnover of IVD tissue is controlled by the cells. In normal, healthy tissues, there is a delicate balance between the rates of matrix production and degradation; however, if the balance is disrupted, either by an increase in the rate of matrix degradation or a decrease in the rate of production, matrix deterioration results. Hence, changes in disc structure and composition may result in alteration in disc cell metabolism, and vice versa.

### **2.3 INTERVERTEBRAL DISC DEGENERATION**

Degeneration of the intervertebral disc occurs far earlier than in other musculoskeletal tissues (Boos et al. 1993; Miller et al. 1988). About 20% of people in their teens have discs with signs of mild degeneration (Miller et al. 1988). Disc degeneration is characterized as a degradation or deterioration of the structure of the tissue, resulting in a loss of function. As the disc degenerates, changes in disc morphology, biochemistry, function and material properties take place.

During degeneration, the disc morphology changes, with increased disorganization. The nucleus region loses its gel-like properties and becomes more fibrous (Buckwalter 1995). Consequently, the boundary between the nucleus and annulus regions of the disc becomes less apparent. Furthermore, cleft formation and fissures occur frequently in degenerated discs, leading to an in growth of nerves and blood vessels into the tissue (Urban and Roberts 2003). A morphological grading scheme

was previously developed by Thompson et al. (1990), which is used to classify the degenerative grade of intervertebral discs based on a five grade scale, with grade I corresponding to normal, healthy discs, and grade V corresponding to severely degenerate discs (Thompson et al. 1990). A summary of this grading scheme is shown in Table 2-2.

**Table 2-2:** Description of Thompson Morphologic Grading

Grade	Annulus Fibrosus	Nucleus Pulposus
I	Discrete fibrous lamellae	Gelatinous, bulging
II	Mucinous infiltration between lamellae	Fibrous tissue, white
III	Loss of demarcation between AF and NP; extensive mucinous infiltration between lamellae	Consolidated fibrous tissue
IV	Focal disruptions	Clefts running horizontally, parallel to endplate
V	Clefts extending throughout	Clefts extending throughout

*Adapted from Thompson et al, 1990.*

Perhaps the most noteworthy biochemical change occurring in degenerated disc is the loss of proteoglycan (PG) content (Lyons et al. 1981). Aggrecan molecules of the PGs degrade, which allows smaller fragments to leach out of the tissue more easily, resulting in a loss in proteoglycans. The loss of PG is believed to cause a decrease in osmotic pressure and tissue hydration (Urban and McMullin 1988), which leads to a loss of the load support capability of IVD (Adams et al. 1996). Additionally, this can also have a significant effect on the movement of molecules into and out of the disc (Maroudas et al. 1975). Changes in collagen content also take place, although they are not nearly as evident as those for proteoglycan (Urban and Roberts 2003). Though the

total quantity of collagen in degenerated tissue does not change markedly, the types and distributions are altered during degeneration.

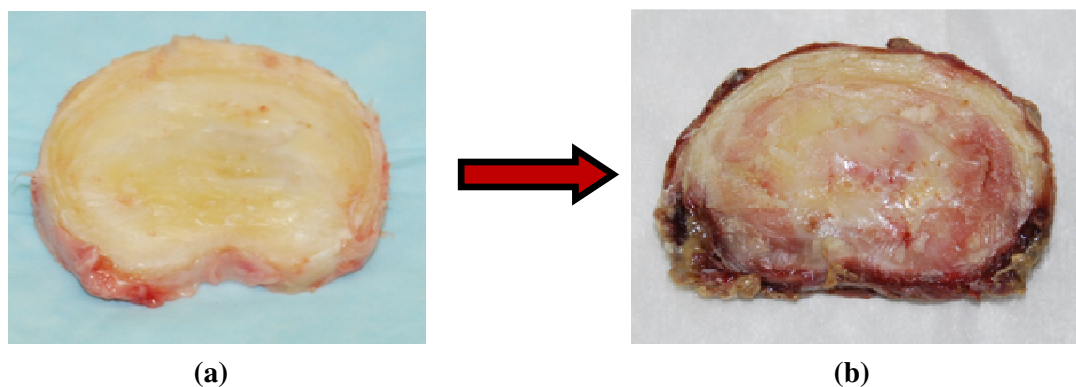


**Figure 2-3:** Photographs showing the visible differences between **(a)** a non-degenerate disc and **(b)** a degenerated disc.

Disc degeneration can have deleterious effects on the biomechanics of the spine and its motion segments. Changes may lead to an increase in spinal flexibility, a loss of fluid pressurization or a decrease in disc height. These changes result in an alteration of the local stress-strain relationship in the disc. Consequently, the disc is no longer able to properly function in load distribution.

Knowledge of the response of tissue transport and metabolic properties to disc degeneration is important in understanding the etiology of disc degeneration because poor nutrition is believed to be one of the main causes of degeneration (Bibby et al. 2002; Holm and Nachemson 1982; Horner and Urban 2001; Nachemson et al. 1970; Urban 2001). It has also been suggested that mechanical factors regulate cellular responses in IVD that may govern the initiation and progression of disc degeneration (Setton and Chen 2006). This dissertation aims to determine the effects of both degeneration and

mechanical strain on important transport properties in IVD tissue, which will aid in further elucidating the causes and mechanisms of disc degeneration.

## 2.4 NUTRITIONAL TRANSPORT IN THE INTERVERTEBRAL DISC

### 2.4.1 PATHWAYS OF TRANSPORT

The lumbar intervertebral disc is the largest avascular structure in the human body. As a result, cells must rely on transport of fluids and solutes through the tissue's extracellular matrix in order to maintain viability; that is, nutrients must be supplied by vasculature at the disc periphery given that there are no blood vessels present in the tissue. There are two possible pathways of transport through the IVD: axially via the cartilage end plate route, or radially through the perianular route, Figure 2-4. In the end plate route, nutrients are supplied by the capillary bed located at the junction of the intervertebral disc and subchondral bone in the vertebral body. In the perianular route, nutrients are supplied by the blood vessels that surround the outer annulus fibrosus.

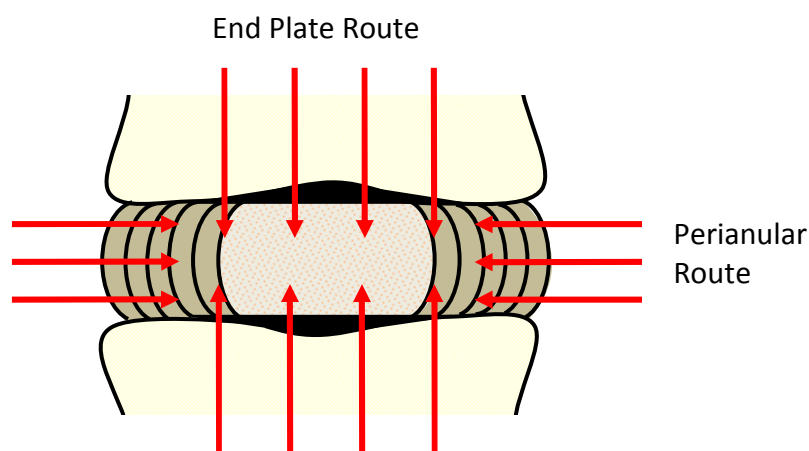


**Figure 2-4:** Sagittal view of the intervertebral disc, highlighting the two main nutritional pathways into the disc from the surrounding vasculature.

The majority of *in vivo* (using animal model) and *in vitro* studies have suggested that the end plate route is the main pathway for exchange of solutes between the NP (and the inner AF) and the surrounding vasculature (Brodin 1955; Brown and Tsaltas 1976; Holm et al. 1981; Maroudas et al. 1975; Nachemson et al. 1970; Ogata and Whiteside 1981; Urban et al. 1982). On the other hand, in an *in vitro* study, Ohshima et al. (1989) showed that the diffusion of water for both uptake and washout in the unloaded disc was approximately 2-3 times larger in the perianular route as compared to the end plate route (Ohshima et al. 1989). However, because of the difficulty in investigating the transport pathways in human subjects *in vivo*, there is little direct evidence that the end plate route is the main transport pathway in human IVD *in vivo*, especially for the discs under mechanical loads or for degenerated discs.

#### 2.4.2 MECHANISMS OF TRANSPORT

Transport of nutrients and waste products through the extracellular matrix of the IVD may occur by diffusion or by convection (i.e., due to fluid flow). It is generally believed that diffusion is the main mechanism of transport for small solutes (Maroudas 1975; Urban et al. 1978; Urban et al. 1982), while convection plays an important role in transport of larger solutes (Bonassar et al. 2001; Garcia et al. 1996; Maroudas 1975; Mauck et al. 2003; O'Hara et al. 1990; Quinn et al. 2002; Urban et al. 1978).

Diffusion is defined as the movement of matter driven by a concentration gradient. A mathematical model for one-dimensional diffusion in fluids was first proposed by Adolf Fick and is known as Fick's law:

$$J = -D \frac{\partial C}{\partial x} , \quad (2-1)$$

where  $J$  is the diffusive flux, defined as the quantity (i.e., moles) passing through per unit area per unit time,  $D$  is the diffusion coefficient (units:  $m^2/s$ ),  $C$  is the concentration of solute in the solution, and  $x$  is the distance along the path of solute transport (Helfferich 1962; Masaro and Zhu 1999). Convection, on the other hand, is a transport process resulting from the bulk motion of fluids.

In order to estimate the relative importance of convective and diffusive effects on transport in cartilaginous tissues, we may use the Peclet (Pe) number. The Peclet number is defined as:

$$Pe = UL/D , \quad (2-2)$$

where  $U$  is the characteristic fluid velocity,  $L$  is the diffusion distance, and  $D$  is the diffusivity of solute (Deen 1998). If the value of the Pe number is much greater than 1, convection is more significant; conversely, if the Pe number is much less than 1, then diffusion is more significant. However, if it is on the order of 1, both convection and diffusion must be considered (Deen 1998).

The partition coefficient is defined as the solute concentration in a porous media relative to the concentration of solute in the surrounding fluid at equilibrium. Knowledge of partition coefficient values is important as they are one of the governing factors in determining the rate of movement of solutes between an external solution and tissue. Therefore, equilibrium partitioning plays an important role in nutritional transport in tissue.



The transport of solutes through the disc is dependent upon several factors related to both the solute and the tissue, including solute size, charge, concentration gradient and pore size; pore size is directly related to tissue hydration and structure (Burstein et al. 1993; Maroudas et al. 1975). The concentration gradient is coupled to both the cellular demand and the supply of solutes. Furthermore, throughout the disc, concentration profiles of important nutrients and metabolites (e.g., oxygen, glucose, and lactate) are steep due to the high rates of cellular metabolism as compared with the low rate of diffusion. Transport of water and solutes in the tissue is governed by several transport properties, including hydraulic permeability (or conductivity) and solute diffusivities.

#### 2.4.3 EXPERIMENTAL STUDIES OF SOLUTE TRANSPORT IN IVD TISSUES

Several studies have investigated the diffusivity of solutes in both human and animal intervertebral disc tissues. A review of these studies can be found in the literature (Jackson and Gu 2009). Solutes investigated include ions ( $\text{Na}^+$  and  $\text{Cl}^-$ ),  $\text{SO}_4^-$ , oxygen, water, glucose, lactate, fluorescein, and various-sized dextran molecules. Diffusion coefficients have been measured by a variety of methods. The most common of these include direct measurement based on Fick's law [Equation (2-1)] (e.g., (Allhands et al. 1984; Jackson et al. 2008; Maroudas 1968; Torzilli et al. 1983; Torzilli et al. 1987; Torzilli et al. 1998)). More recently, imaging techniques such as magnetic resonance imaging (MRI) (Chiu et al. 2001; Drew et al. 2004; Fischer et al. 1995), nuclear magnetic resonance (NMR) (Burstein et al. 1993; Foy and Blake 2001; Ngwa et al. 2002), and fluorescence recovery after photobleaching (FRAP) (Travascio et al. 2009; Travascio and Gu 2007) have been employed to determine solute diffusivities in cartilaginous tissues.

The electrical conductivity method has also been used to determine diffusion coefficients of ions in IVD (Gu et al. 2004).

Several studies have investigated the partition coefficient of solutes in cartilaginous tissues; solutes include both small (glucose, urea, proline, sucrose, and ions) and large (myoglobin, serum albumin, IGG, and dextran) molecules (Fetter N.L. et al. 2006; Maroudas 1976; Nimer et al. 2003; Quinn et al. 2000; Roberts et al. 1996; Torzilli et al. 1998). However, very little is reported in the literature regarding the partitioning of solutes in IVD tissues (Maroudas et al. 1975).

## **2.5 METABOLISM OF DISC CELLS**

It has been found that disc cells obtain their energy primarily through anaerobic glycolysis, even in the presence of oxygen (Holm et al. 1981; Ishihara and Urban 1999). That is, most energy, in the form of adenosine triphosphate (ATP), is produced by the quantitative conversion of glucose to lactic acid, which is almost completely ionized to lactate. Previous studies have shown that there is a threshold level of glucose concentration in order to maintain cell viability; that is, if the glucose concentration falls below around 0.5 mmol/L for more than approximately 3 days, cells begin to die (Horner and Urban 2001). Moreover, acidic conditions (i.e., pH < 6.4), generally resulting from an accumulation of lactic acid in the tissue, have also be shown to lead to cell death (Bibby et al. 2005; Horner and Urban 2001). Further, less acidic conditions, although not leading to cell death, have been shown to be detrimental to the disc matrix (Razaq et al. 2003). This is because the rate of matrix production is reduced, while that of matrix degradation remains unchanged, leading to an imbalance favoring matrix breakdown.

Few studies have been done to investigate the metabolism of disc cells. In particular, four previous studies have measured the oxygen consumption rate of IVD cells (Bibby et al. 2005; Holm et al. 1981; Huang et al. 2007; Ishihara and Urban 1999). Earlier studies using IVD tissue have investigated the effect of oxygen tension levels on the rate of oxygen consumption by IVD cells, showing that oxygen consumption rates decreased as the oxygen tension was decreased (Holm et al. 1981; Ishihara and Urban 1999). A more recent study by Bibby et al (2005) investigated the effect of low oxygen, glucose and pH on the metabolic rates of isolated bovine NP cells and found that the rate of oxygen consumption depends on both oxygen concentration and pH, but not on glucose concentrations over the range of 1 to 5 mmol/L (Bibby et al. 2005). Our recent study showed that the oxygen consumption rate by porcine outer AF cells was significantly lower than that by NP cells at 5% oxygen tension (Huang et al. 2007). Furthermore, the study also demonstrated that, while the oxygen consumption rate by NP cells does not depend on glucose concentration, there was a significant difference in consumption rate between outer AF cells in media containing 1 mM and 25 mM glucose.

Only a small number of studies investigating the glucose consumption rate by IVD cells can be found in the literature. Bibby et al. showed that glucose consumption rates are dependent on both initial glucose concentration as well as value of pH for bovine nucleus pulposus cells (Bibby et al. 2005). However, studies have not come to a consensus on the effect of oxygen tension on cellular activity in IVD cells. On the one hand, one study showed that low oxygen levels result in a diminished rate of glycolysis (i.e., a negative Pasteur effect) (Bibby et al. 2005). In contrast, other studies have shown the opposite: that glycolysis rates rise under low oxygen tension (i.e., a positive Pasteur

effect) (Guehring et al. 2009; Holm et al. 1981; Ishihara and Urban 1999). Because of the very low level of oxygen present in the disc *in vivo*, it is imperative that the effect of oxygen level on the glucose consumption rates of cells be investigated. This is necessary to understanding not only the *in vivo* cellular metabolism in the disc, but also the effects that low nutritional levels seen in degenerating discs have on IVD cells. Furthermore, determining the rate of metabolism by disc cells is an integral part of developing accurate theoretical models to predict nutrient distributions in the disc *in vivo*.

## 2.6 EFFECT OF MECHANICAL LOADING ON THE IVD

The intervertebral disc serves a primarily mechanical function in the spine, offering load support capabilities. During normal daily activity, the IVD is subjected to various loading configurations, such as tension, compression, torsion, or a combination of these. As a result, the intradiscal pressure varies throughout of the day, see Figure 2-5.

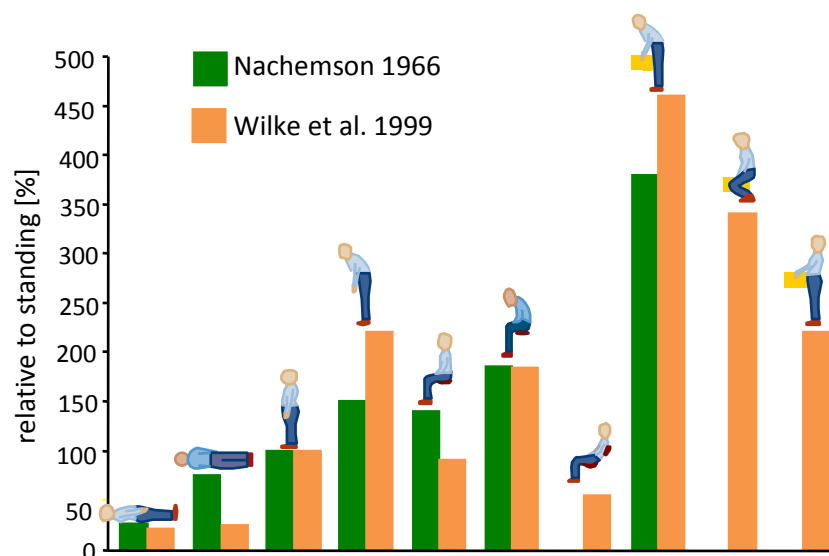


**Figure 2-5:** Intradiscal pressure in common postures and activities normalized to standing posture. For Nachemson study, lifting weight = 10 kg. For Wilke study, lifting weight = 20 kg. (Nachemson 1966; Wilke et al. 1999)

The IVD functions to transfer loads between the two vertebral bodies during compressive loading. When compression is applied to the disc, a hydrostatic pressure develops in the nucleus region. As a result, the surrounding structures, including the cartilage endplates and annulus fibrosus tissues, are pushed away from the disc center, see Figure 2-6. The disc is specially designed to resist these forces; the layered structure of the AF can withstand forces in the radial direction, holding the NP inside the disc, while the gelatinous make-up and high water content of the NP allows for this transfer of load.

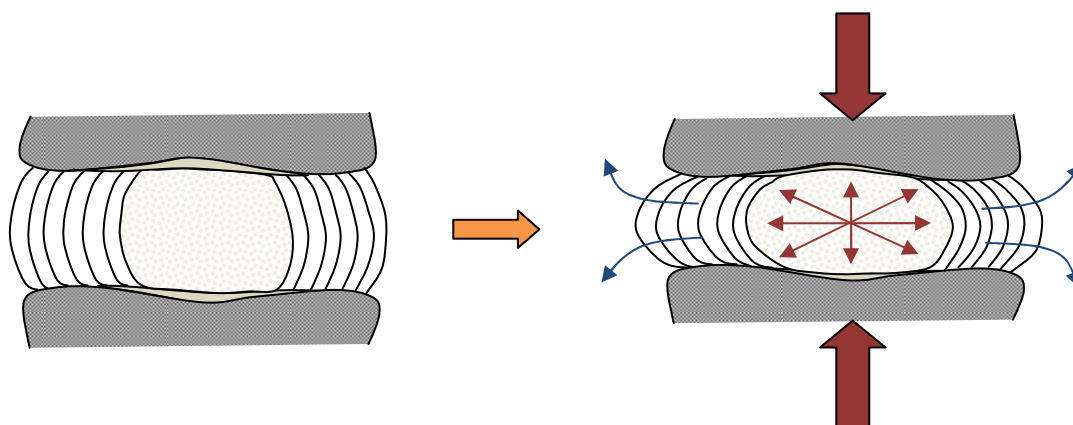


**Figure 2-6:** Pressures created in the disc during compressive loading; adapted from (White and Panjabi 1990).

There are several studies in the literature reporting on the effect of mechanical loading on water content, chemical composition and nutritional levels in the intervertebral disc (Adams and Hutton 1986; Bibby et al. 2002; Holm and Nachemson 1982). In general, it has been found that abnormal loading conditions result in decreased nutrient levels within the disc. In particular, compressive loading conditions have been shown to cause a decrease in water content and water diffusivity in IVD (Adams and

Hutton 1983; Kraemer et al. 1985; Ohshima et al. 1989). Furthermore, it has also been shown that compressive loading leads to an alteration in the matrix components in the disc, including an increase in collagen and other matrix proteins per wet weight (Ohshima et al. 1989). Studies have also shown that tensile mechanical loading causes reduced tissue hydration in AF but not in NP for porcine coccygeal discs *in vitro*. A significant decrease in the diffusion of small solutes in the NP was observed for the same loading conditions (Terahata et al. 1994). Hence, mechanical loading plays an important role in the transport of water and solutes within the disc. It may also affect transport pathways as well as mechanisms of solute transport in the IVD.

Several studies have reported on the effect of mechanical compression on diffusion of water in intervertebral discs using magnetic resonance imaging techniques. Chiu et al. found that the diffusion of water in IVD tissues increased with an increase in compressive load applied (Chiu et al. 2001). Contrary to this finding, Drew et al. reported a decrease in the apparent diffusion coefficient of water in IVD (Drew et al. 2004). The difference in findings in these two studies most likely results from the difference in experimental techniques. Chiu et al. measured diffusion immediately after applying a step load to the IVD, whereas Drew et al. used longer loading times. More recently, Arun et al. (2009) used MRI to show that sustained supine creep loading retards the transport of small solutes into the center of human IVD (Arun et al. 2009). Finally, our recent studies have shown that static mechanical compression results in decreased diffusivity of oxygen and glucose in bovine coccygeal IVDs (Jackson et al. 2008; Yuan et al. 2009).

Few studies have investigated the effect of mechanical loading on the partition coefficient of solutes in cartilage. Quinn et al. found that static compression resulted in a decrease in partition coefficient of several solutes in cartilage, with strongest effects seen in relatively large molecular weight dextran molecules (Quinn et al. 2001). Nimer et al. found that partitioning based on tissue water of  $\text{Na}^+$  ions increased with increasing load, whereas that of  $\text{SO}_4^-$  decreased with increasing load in cartilage under static loading conditions (Nimer et al. 2003). The same study also showed that the partition coefficient of inulin decreased with increasing load. However, to our knowledge, no study has investigated strain-dependent partition coefficients in IVD tissue.

Currently, very little else can be found in the literature regarding the effect of compression on diffusion and partitioning of small solutes in IVD. This information is necessary as the IVD is subjected to a variety of loading conditions during normal daily activity; understanding how this affects transport, and consequently the nutritional supply to disc cells, is essential in elucidating the pathophysiology of disc degeneration.

## **2.7 SIGNIFICANCE AND CLINICAL RELEVANCE**

Low back pain is a major socio-economic dilemma, representing one of the most significant health concerns in the United States (NIH 1997). It is estimated that the annual prevalence of low back pain ranges from 15 to 45 % of the population, with estimates of more than 70% of all individuals experiencing symptoms at some point in their lifetime (Kelsey et al. 1992; NIH 1997). The economic burden of this condition is estimated at between \$50 and \$100 billion annually in medical treatment costs and disability payments (Frymoyer and Cats-Baril 1991).

While back pain does begin early in life, the symptoms and duration increase with increasing age, as does prevalence (Bressler et al. 1999; Woolfe and Pflieger 2003). Although the exact cause of low back pain is unclear, the degenerative changes of IVD have been implicated as a primary etiologic factor (Buckwalter 1995; Eyre et al. 1989; Gruber and Hanley, Jr. 2002; Kelsey et al. 1978; Kelsey et al. 1979; Kelsey et al. 1992; Kelsey and White 1980; Nerlich et al. 1998; White 1981; White and Panjabi 1978). Despite numerous studies investigating disc degeneration, the etiology has not yet been fully delineated. It is generally understood that an imbalance in matrix synthesis (i.e., anabolism) and breakdown (i.e., catabolism) results in tissue degeneration. However, the exact mechanisms and factors triggering this imbalance are not fully understood.

Poor nutritional supply to the disc is believed to be one of the main mechanisms of degeneration (Bibby et al. 2002; Holm and Nachemson 1982; Horner and Urban 2001; Nachemson et al. 1970; Urban 2001), along with genetic factors and abnormal mechanical loading, see Figure 2-7. Cells need nutrients in order to maintain viability and function in maintaining the disc extracellular matrix; nutrients must be transported through the ECM to the cells from the surrounding blood vessels, given the avascularity of the disc.

While it is known that nutrition plays a role in the degeneration cascade, there is a lack of knowledge regarding transport and metabolic properties in IVD. The studies in this work aim to bridge the gap in current knowledge regarding glucose transport and consumption within the disc. Due to the important role of glucose in IVD cell viability, knowledge of these properties is an important step toward further understanding of the pathology of intervertebral discs.



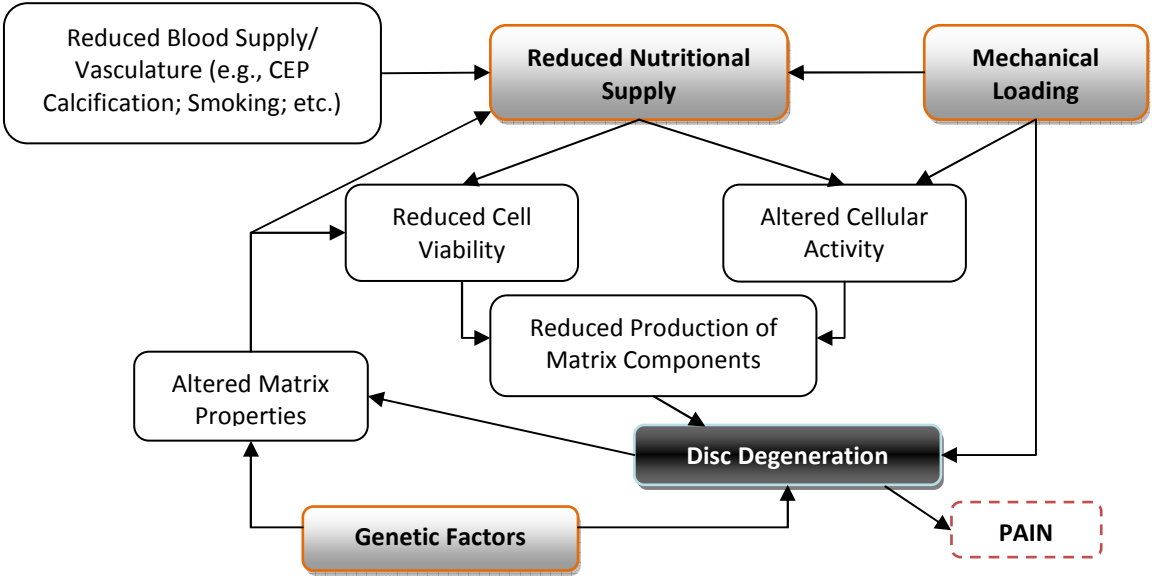


**Figure 2-7:** Schematic showing possible causes and pathways related to disc degeneration. Adapted from (Urban et al. 2004).

## **CHAPTER 3. MEASUREMENT OF STRAIN-DEPENDENT AND ANISOTROPIC DIFFUSION OF GLUCOSE IN HUMAN ANNULUS FIBROSUS**

### **3.1 INTRODUCTORY REMARKS**

The transport of small molecules, such as glucose, through the extracellular matrix of the intervertebral disc has been shown to occur primarily by diffusion (Maroudas 1975; Urban et al. 1978; Urban et al. 1982). Cells throughout the disc require glucose to produce energy through glycolysis and remain viable. Therefore, it is necessary that we better understand the transport pathways and mechanisms of glucose in the disc in order to elucidate nutritional transport and related disc degeneration. Thus, the aim of this study is to measure the strain-dependent and anisotropic (i.e., direction-dependent) diffusivity of glucose in human annulus fibrosus tissues, which is part of Specific Aim #1.

Only few studies can be found in the literature investigating the transport of glucose in IVD tissues. Maroudas et al. (1975) previously measured the diffusion of glucose in human AF, and found that the averaged glucose diffusivity was  $2.5 \times 10^{-6}$  cm<sup>2</sup>/sec at 37°C (Maroudas et al. 1975). In this study, diffusivity was measured under zero compression conditions, and results for diffusion in the axial and radial direction were averaged. Our previous study (2008) investigated the diffusivity of glucose in AF region of bovine coccygeal discs. Our results showed that the diffusion coefficient of glucose decreased with increasing compressive strain and that diffusivity in the axial direction was significantly higher than that in the radial direction (Jackson et al. 2008). However, to our knowledge, no study has measured the strain-dependent and/or anisotropic diffusion coefficient of glucose in human IVD tissues.

### 3.2 THEORETICAL APPROACH

In this study, we employ a one-dimensional steady-state diffusion experiment in order to directly yield values for apparent glucose diffusivity in human AF tissue. Similar methods have been used in the past for determining solute diffusivities in articular cartilage and IVD (Jackson et al. 2008; Maroudas et al. 1968; Maroudas et al. 1975; Yuan et al. 2009). In this approach, a specimen having a known thickness is clamped between the two compartments of a diffusion chamber, see Figure 3-1. A solution containing a high concentration of the solute of interest (here, glucose) is introduced into the upstream chamber, while a solution containing no solute is initially downstream. The solute gradually diffuses through the specimen, from the upstream to the downstream chamber. The concentration in the downstream chamber is monitored and used to calculate the diffusivity of the tissue specimen.

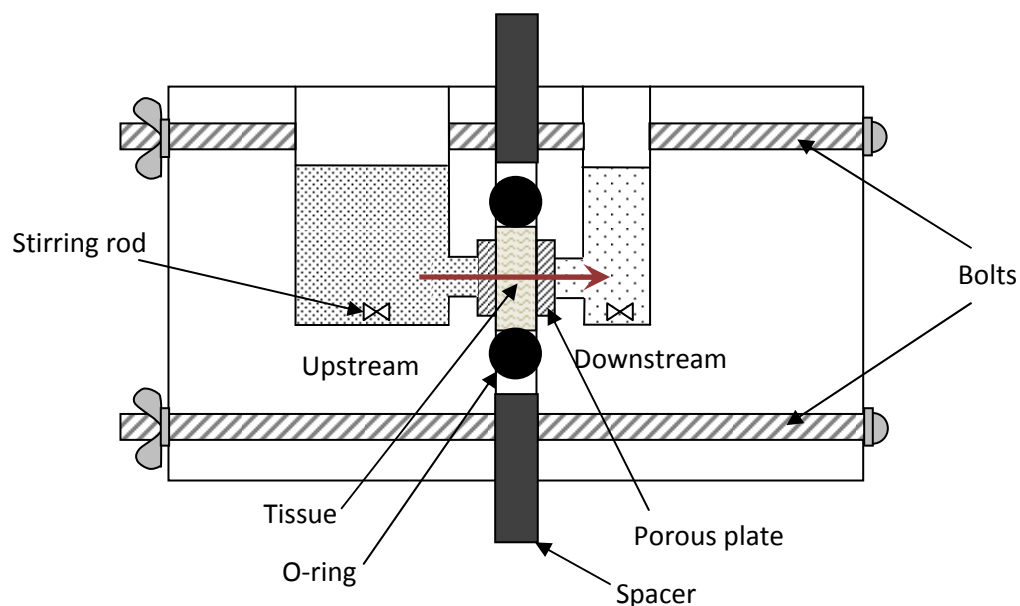


**Figure 3-1:** Schematic of diffusion chamber. Solute diffuses from upstream to downstream chamber (left to right), passing through the tissue specimen.

In this method, the solute in the upstream chamber is assumed to be constant due to the high concentration of the solute and the large volume of solution. Furthermore, because the solution downstream is periodically removed for concentration measurement and replaced with a fresh solution, the concentration in the downstream chamber is always close to zero. The apparent diffusion coefficient,  $D_{app}$  ( $= KD_{eff}$ , where  $K$  is the partition coefficient and  $D_{eff}$  is the effective diffusion coefficient), is derived from Fick's first law of diffusion:

$$J = -D \frac{dC}{dx} = -D_{app} \frac{\Delta C}{h}, \quad (3-1)$$

where  $J$  is the diffusive flux and  $C$  is the concentration. The concentration can be estimated as the concentration difference,  $\Delta C$ , across a tissue of thickness  $h$ . We can assume that, at steady state, the distribution of solute within the tissue is linear (that is,  $-dC/dx = \Delta C/h = (C_{up} - C_{down})/h$ , where  $C_{up}$  is the concentration of solute in the upstream chamber). The diffusive flux is defined as the mass flow rate of solute,  $\Delta Q$ , per unit area,  $A$ :

$$J = \frac{\Delta Q}{A} = \frac{V dC}{A dt}. \quad (3-2)$$

From this relation, we can derive the following:

$$\frac{V_{down} dC_{down}}{A dt} = -D_{app} \frac{\Delta C}{h}, \quad (3-3)$$

where  $C_{down}$  is the concentration of solute in the downstream chamber and  $V_{down}$  is the volume of solution in the downstream chamber.

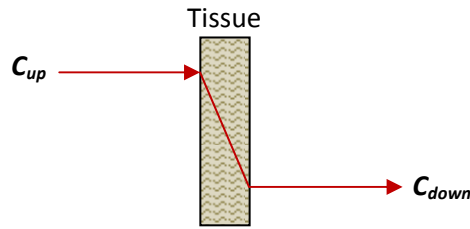


**Figure 3-2:** Schematic illustrating linear distribution of solute in tissue when at equilibrium.

Based on this assumption, we have:

$$\frac{dC_{down}}{dt} = \frac{A D_{app}}{V_{down}} \left[ \frac{(C_{up} - C_{down})}{h} \right], \quad (3-4)$$

$$\frac{dC_{down}}{(C_{up} - C_{down})} = \frac{A D_{app}}{V_{down} h} dt. \quad (3-5)$$

Letting  $C' = C_{up} - C_{down}$  and  $dC' = -dC_{down}$ , we have:

$$-\frac{dC'}{C'} = \frac{A D_{app}}{V_{down} h} dt. \quad (3-6)$$

Integrating, we have:

$$\int_{C_{down}(t_0)}^{C_{down}(t)} \frac{dC'}{C'} = \int_{t_0}^t \frac{A D_{app}}{V_{down} h} dt, \quad (3-7)$$

$$\ln C' \Big|_{C_{down}(t_0)}^{C_{down}(t)} = \frac{A D_{app}}{V_{down} h} \Big|_{t_0}^t, \quad (3-8)$$

$$\ln \frac{C_{up} - C_{down}(t_0)}{C_{up} - C_{down}(t)} = \frac{A D_{app}}{V_{down} h} (t - t_0), \quad (3-9)$$

where  $C_{down}(t_o)$  is the concentration of solute in the downstream chamber at time  $t_o$  (initial time) and  $C_{down}(t)$  is that at time  $t$ . Solving for  $D_{app}$ , we have:

$$D_{app} = \ln \left( \frac{C_{up} - C_{down}(t_o)}{C_{up} - C_{down}(t)} \right) \frac{V_{down} h}{A(t - t_o)}. \quad (3-10)$$

Once the tissue has reached steady-state (i.e., linear distribution of solute across the tissue, see Figure 3-2), the apparent diffusion coefficient can be calculated directly from the concentration measurements in the downstream chamber.

In order to determine the strain-dependent diffusion coefficient of tissues, differing levels of compression must be applied to the tissue specimens. This can be accomplished by changing the size of the spacers between the two chamber halves, see Figure 3-1. Furthermore, the anisotropic behavior of the diffusion coefficient can be investigated by varying the orientation of the tissues specimen during preparation.

### 3.3 MATERIALS AND METHODS

#### 3.3.1 DESIGN OF EXPERIMENTAL APPARATUS

In order to carry out diffusivity experiments, a custom diffusion chamber was designed and constructed. The chamber had to serve several functions in order to successfully carry out the experiments: (1) confine the specimen to inhibit swelling during experimentation; (2) allow for compression of the specimen; and (3) allow for glucose concentrations to be measured in the downstream chamber within a reasonable time period. The custom-designed diffusion cell consists of two solution chambers divided by a specimen holder in the middle. The specimen is secured between two rigid porous plates and sealed radially with an o-ring. The compressive strain on the tissue

sample could be controlled by changing the size of the metal spacer placed between the two chamber halves. For detailed schematic, see Figure 3-1.

An engineering drawing of the chamber can be seen in Figure 3-3. The chamber was machined out of a 2" acrylic rod (Small Parts, Inc., Miami Lakes, FL). The volumes of the two solution chambers were chosen such that a significant quantity of glucose was present downstream after a 15 minute time interval. The upstream chamber was designed to hold 1 mL of solution, while the downstream was designed for 200  $\mu$ L. The difference in chamber diameters, as shown in Figure 3-3, allowed the two volumes to have similar heights of solution, such that gravitational force would not add an additional driving force.

The specimen was sealed between two rigid porous plates made of hydrophilic porous polyethylene (PE) (Small Parts). The PE had a pore size of 50 – 90  $\mu$ m and an open area of 50%. The porous plates were cut to discs of 5 mm in diameter and 0.5 mm in thickness. The 5 mm diameter and 50% open area were used to determine the area of diffusion flux across the tissue specimen, used for calculation of the diffusion coefficient in Equation (3-10). The specimen was also sealed radially using a Buna-N metric o-ring with an inner diameter of 6 mm and a thickness of 2 mm (Small Parts); the o-ring was chosen for its excellent compression set resistance.

The diffusion chamber was assembled using four stainless steel bolts with cap nuts and wing nuts. The wing nuts were tightened sufficiently by hand to the specified sample thickness, based on the size of the metal spacers. Four bolts were used to ensure a uniform compression across the tissue specimen.

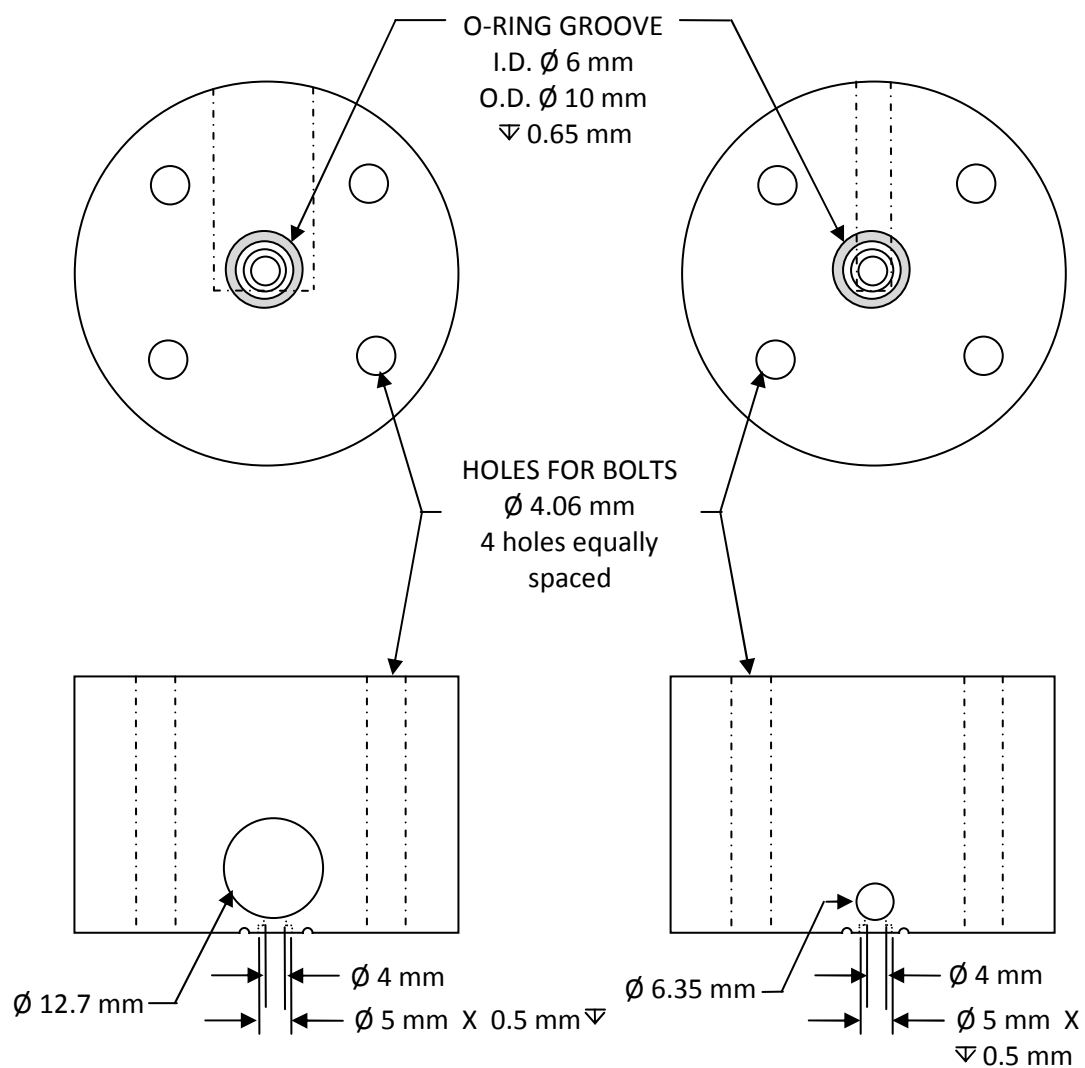


**Figure 3-3:** Engineering drawing showing the front and top views of the diffusion chamber halves.

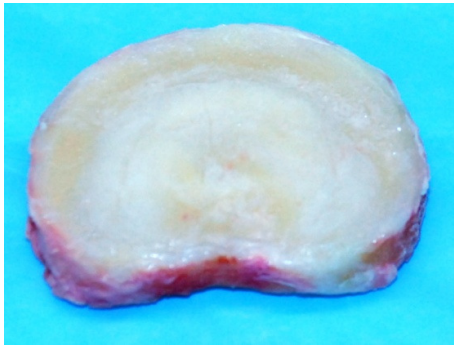
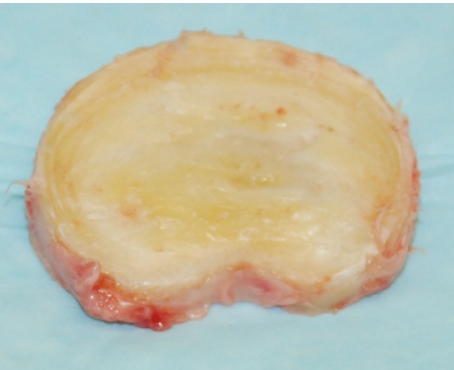
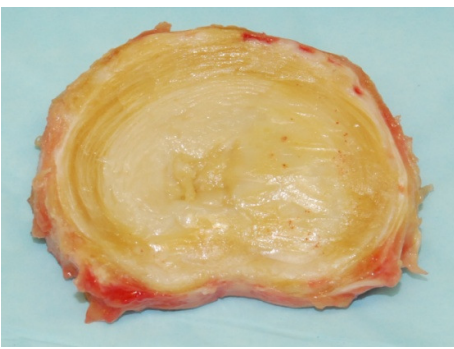
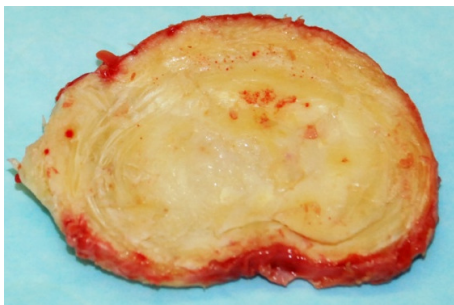


### 3.3.2 SPECIMEN PREPARATION

Human lumbar spines were obtained from cadavers at the University of Miami Miller School of Medicine Tissue Bank. All donors underwent pathological screening prior to receiving the spines; only those with negative results were used for experiments. Lumbar spines were stored at  $-80^{\circ}\text{C}$  until the day of dissection. During dissection, the tissue was removed from around the spinal column using a surgical scalpel until the bone was obviously visible. At that point, a reciprocating (i.e., oscillating) saw was used to remove the facet joints from the spine; this allowed for complete access to the intervertebral discs. Remaining tissues were removed from around the discs using a scalpel.

For these studies, L2-L3 discs were used. In order to harvest the disc from the clean spine, a scalpel was used to make two transverse cuts at the bone-disc interface. Special care was taken to make the cuts as clean as possible, in order to minimize damage to the disc tissue. Once the disc was successfully removed from the spine, the Thompson morphological grade for degeneration was assigned based on the macroscopic examination of the disc, see Table 2-2 in Section 2.3. Photographs were also taken of both surfaces of the disc for later reference, see Table 3-1. These steps were carried out as quickly as possible in order to minimize tissue dehydration. The disc was then wrapped first in plastic wrap, and then in gauze moistened with phosphate buffered saline (PBS) solution, in order to prevent dehydration during storage. The wrapped disc was then stored in a sealed plastic bag at  $-20^{\circ}\text{C}$  until tissue specimen preparation and experimentation.

**Table 3-1:** Photographs of Intervertebral Discs Used in Diffusivity Studies, Along with Patient Information and Degenerative Grades

	<p>5118-2007 41 year old Male Ht: 6'0" Wt: 230 lbs. Cause of death: Hemorrhagic CVA Degenerative grade: I</p>
	<p>5577-2008 40 year old Male Ht: 5'8" Wt: 145 lbs Cause of death: Cardiac Arrest Degenerative grade: I</p>
	<p>5199-2007 63 year old Male Ht: 6'0" Wt: 230 lbs. Cause of death: Cardiac Arrest Degenerative grade: II</p>
	<p>5858-2009 47 year old Male Ht: 6'4" Wt: 260 lbs. Cause of death: Cardioplegic Arrest Degenerative grade: III</p>

For diffusivity measurements, specimens were prepared as previously described in the literature (Jackson et al. 2008; Yuan et al. 2009). Tissue samples were taken from both the anterior and posterior sections of the annulus fibrosus and prepared in the three principal directions – axial, circumferential and radial, see Figure 3-4. Cylindrical specimens with a diameter of 6 mm were cut using a stainless steel corneal trephine (Biomedical Research Instruments, Inc., Silver Spring, MD). A Leica sledge microtome (Model SM2400, Leica Instruments, Nussloch, Germany, minimum slice height capability: 0.001 mm) with freezing stage (Model BFS-30, Physitemp Instruments, Inc., Clifton, NJ) was then used to slice the specimen to a desired thickness of approximately 0.5 mm. The final specimen height was measured using a custom-designed current-sensing micrometer; for each specimen, an average height was taken from three measurements.

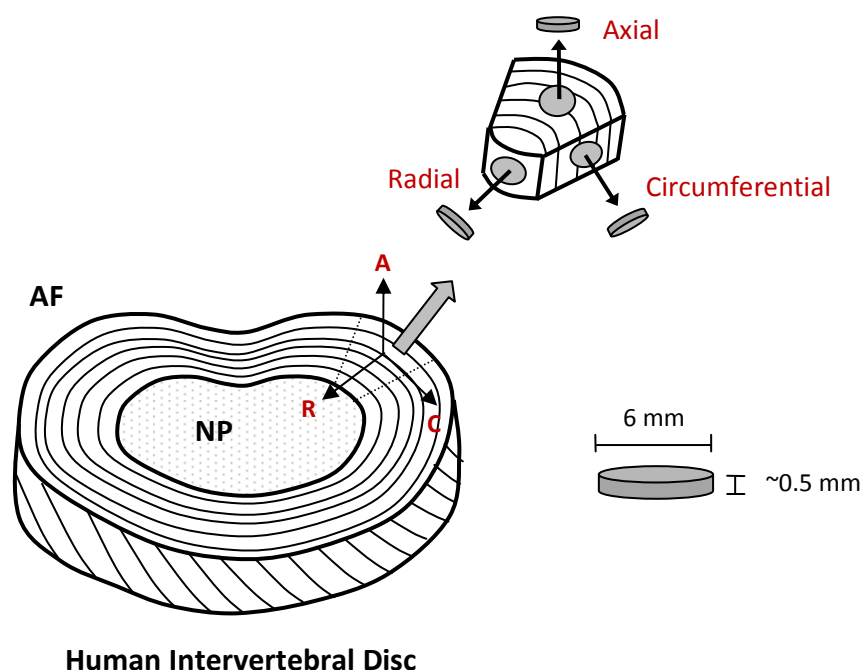


**Figure 3-4:** Schematic showing orientation and size of specimens obtained from human annulus fibrosus (AF).

### 3.3.3 WATER CONTENT MEASUREMENT

Tissue water content, or porosity, was measured in order to correlate with the glucose diffusion coefficient. Water content was determined by a previously developed buoyancy method, based on Archimedes' principle. When an object is completely submerged in fluid having a density of  $\rho_{sol}$ , the volume of the object,  $V$ , is given as:

$$V = \frac{F_b}{\rho_{sol}g} \quad (3-11)$$

where  $F_b$  is the buoyancy force and  $g$  is the acceleration due to gravity. The buoyancy force can be determined from the difference in the weight of the specimen in air,  $W_{air}$ , and the weight of the specimen in solution,  $W_{sol}$ :

$$V = \frac{W_{air} - W_{sol}}{\rho_{sol}g} \quad (3-12)$$

In this case, the solution used is phosphate buffered saline (PBS). The volume of water in the specimen,  $V^w$ , can be determined using mass, density and volume relations:

$$V^w = \frac{W_{air} - W_{dry}}{\rho_w g} \quad (3-13)$$

where  $W_{dry}$  is the dry weight of the specimen and  $\rho_w$  is the density of water. The volume fraction of water, or porosity,  $\phi^w$ , of the tissue specimen can be calculated from the ratio of the water volume in the specimen to the wet tissue volume:

$$\phi^w = \frac{W_{air} - W_{dry} \rho_{sol}}{W_{air} - W_{sol} \rho_w} \quad (3-14)$$

Prior to experiment, the weights of the tissue in air and in solution (PBS) were determined using the density determination kit of a Sartorius analytical balance (Model

LA120S, Sartorius, Goettingen, Germany), see Figure 3-5. In an effort to minimize tissue swelling during measurements, the measurement of the tissue weight in solution was taken in less than 15 seconds. Previous studies have indicated that this short duration produces negligible swelling effects (Gu et al. 2002; Gu and Justiz 2002; Jackson et al. 2008; Yao et al. 2002). Following experimentation, the tissue samples were lyophilized and the dry weights were recorded.

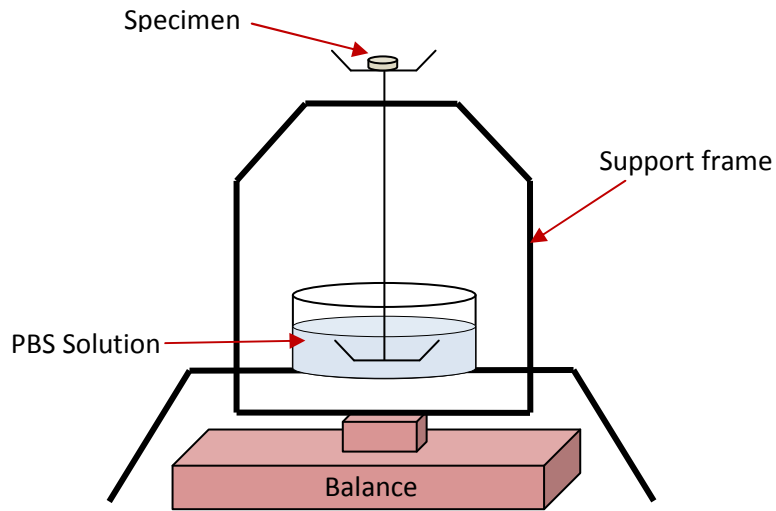


**Figure 3-5:** Schematic showing setup for analytical balance with density determination kit used for measuring tissue water content.

Tissue porosity is related to tissue deformation by:

$$\phi^w = 1 - \frac{\phi_o^s}{J}, \quad \phi^s = \frac{\phi_o^s}{J} \quad (3-15)$$

where  $J$  is the ratio of the deformed tissue volume to the initial (undeformed) tissue volume, and  $\phi_o^s$  is the volume fraction of solid at the undeformed tissue state (i.e., where  $J = 1$ ). Volume fraction of solid is related to tissue porosity by  $\phi_o^s = 1 - \phi_o^w$ . Tissue

dilatation,  $e$ , or relative volume change, is related to deformation by  $e = J - 1$ . Therefore, the water content of deformed tissue can be calculated from the relation:

$$\phi^w = \frac{\phi_o^w + e}{1 + e} \quad (3-16)$$

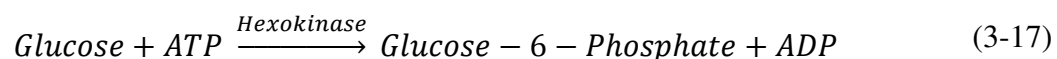
Hence, we can use this relationship to determine the water content of the tissue under compression.

### 3.3.4 MEASUREMENT OF GLUCOSE DIFFUSIVITY

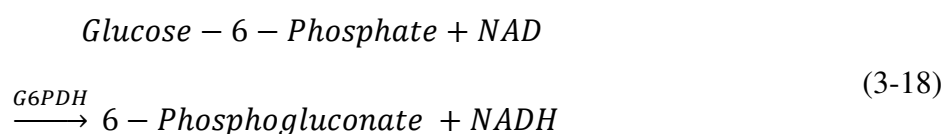
Following specimen preparation and measurement of specimen weight in air and in solution, the diffusion chamber was assembled with the sample for diffusivity measurements. To assemble the chamber, two porous plates were first placed in the designated spaces in each half of the chamber, see Figure 3-1. Then, the prepared specimen was placed centered over the porous plate and the o-ring was placed in the o-ring groove, around the radial edge of the tissue specimen. The other chamber half was then aligned and four bolts were threaded through the holes. The wing nuts were lightly tightened to hold the two halves of the chamber together and the specimen and o-ring in place. Next, spacers of desired thickness, corresponding to 0% nominal compressive strain on the tissue specimen (based on the measured initial height), were inserted in the space between the two chamber halves. The wing nuts were then fully tightened in order to compress the tissue to the appropriate thickness.

Glucose concentrations were measured employing a spectrophotometric technique and using a glucose assay reagent. The basic principal of this technique involves two primary reactions. Glucose is first phosphorylated by adenosine triphosphate (ATP) in a

hexokinase-catalyzed reaction which produces glucose-6-phosphate and adenosine diphosphate (ADP):



Next, the glucose-6-phosphate is oxidized to 6-phosphogluconate in the presence of oxidized nicotinamide adenine dinucleotide (NAD) in a reaction catalyzed by glucose-6-phosphate dehydrogenase (G6PDH):



The latter reaction results in an increase in the spectrophotometric absorbance at 340 nm which is directly proportional to the glucose concentration.

Glucose assay reagent was purchased from Sigma-Aldrich Co. (St. Louis, MO). For each concentration measurement, 100  $\mu\text{L}$  of reagent was mixed with 10  $\mu\text{L}$  of solution to be measured, and then incubated at room temperature for 15 minutes prior to measurement. Absorbance at 340 nm was measured using a SmartSpec<sup>TM</sup> Plus Spectrophotometer (Bio-Rad Laboratories, Inc., Hercules, CA). Prior to each experiment, a new standard calibration curve was constructed for glucose concentrations varying from 0 to 0.5 mg/mL glucose in PBS solution, as experimental samples had glucose concentrations within this range. Calibration curves were curve-fit with a linear trendline passing through zero using Excel Spreadsheet Software (Microsoft Corp., Seattle, WA); all calibration curves had an  $R^2$  value greater than 0.99. The standard curve was then used to calculate the glucose concentrations in experimental samples.

Following assembly of the diffusion chamber, the experiment was started at 0% nominal compressive strain. The chamber was placed on a magnetic stirring rate and magnetic stirring bars (ChemGlass, Inc., Vineland, NJ) were used in each solution chamber. The magnetic stirring plate was set to low speed to minimize convection in the chamber. At the start of the experiment, 200  $\mu$ L of pure PBS solution were dispensed into the downstream solution chamber, while 1 mL of glucose solution containing 20 mg of glucose per mL of PBS was dispensed into the upstream chamber. The chamber was designed such that the solutions in the two chambers had approximately the same height, so as to minimize the pressure difference between upstream and downstream chambers. Upon addition of solution, a timer was set for 15 minutes. During the experiment, the solutions in both chambers were constantly stirred at low speed to maintain uniform solute distribution and minimize stagnant boundary layer formation at the tissue boundary.

At the end of the 15 minute time interval, the solution from the downstream chamber was collected for glucose concentration measurement. The solution in the upstream chamber was removed and discarded. Following removal, both chambers were cleaned with a cotton swab. A new 200  $\mu$ L of PBS and 1 mL of glucose solution were dispensed into the downstream and upstream chambers, respectively, and the experiment was repeated. This was continued until the same concentration measurement (within 5%) was found for 2 to 3 consecutive readings, indicating that steady state had been reached. The average time period of the experiment was 105 minutes (7 intervals of 15 minutes each).



Once the experiment was completed, the spacers between the two chamber halves were changed to apply a 10% nominal compressive strain on the tissue specimen. The experimental procedure was then repeated to determine the diffusion coefficient of glucose at 10% strain level. Following this, the same was done for 20% nominal compressive strain. At the end of experiments, the apparent glucose diffusion coefficient was calculated for each of the strain levels applied using Equation (3-10) and averaged values for glucose concentration at steady state. The tissue specimen was lyophilized for determination of dry weight.

### 3.3.5 STATISTICAL ANALYSES

For each direction of diffusion (i.e., axial, radial or circumferential), sixteen (n=16) specimens were tested; on each specimen, three diffusion tests were performed, corresponding to three levels of compressive strain (0%, 10% and 20% nominal strain). Two-way ANOVA analysis of variance was performed using SPSS 11.5 statistical software (SPSS, Inc., Chicago, IL) to determine if compressive strain and direction affected the diffusion of glucose in human annulus fibrous tissue. Tukey post-hoc analysis was performed to determine among which levels of each factor the differences were significant. Due to differences in sample size for groups of varying degenerative grade, a Student's t-test was used to determine if glucose diffusivity was significantly affected by disc degeneration. For all statistical analyses, the significance level was set to  $p < 0.05$ . All data are given in mean  $\pm$  standard deviation.

### 3.4 RESULTS

The apparent diffusion coefficient of glucose in human annulus fibrosus tissue was determined at three levels of compression and in the three principal directions at room temperature ( $23.4 \pm 0.73^\circ\text{C}$ ). Results are shown in Table 3-2, as well as graphically in Figure 3-6. For each sample, the value of compressive strain was calculated based on the measured initial height of the specimen and the thickness of the spacer. Two-way ANOVA confirmed that apparent glucose diffusivity was significantly affected by both level of compressive strain and direction of diffusion ( $p < 0.05$ ). Post hoc analysis showed that all strain groups were significantly different for all three directions of diffusion (i.e.,  $0\% > 10\% > 20\%$ ). Furthermore, diffusion in the radial direction was significantly lower than that in the axial or circumferential directions, indicating that glucose diffusivity in human annulus fibrosus is anisotropic. Diffusion coefficients in the axial and circumferential directions did not differ significantly at any level of strain.

**Table 3-2:** Results for Apparent Glucose Diffusivity at Varying Levels of Compressive Strain in the Three Principal Directions in Human Annulus Fibrous Tissue

	$n$	$\phi^w$	Strain, $\epsilon$ (%)	$D_{app}$ ( $\times 10^{-7} \text{cm}^2/\text{s}$ )
Axial	16	$0.786 \pm 0.033$	$3.06 \pm 3.09$	$7.56 \pm 0.75$
	16	$0.756 \pm 0.036$	$12.8 \pm 2.78$	$6.52 \pm 0.65$
	16	$0.685 \pm 0.047$	$22.4 \pm 2.47$	$5.74 \pm 0.72$
Circumferential	16	$0.781 \pm 0.043$	$4.97 \pm 4.25$	$7.40 \pm 1.06$
	16	$0.743 \pm 0.049$	$14.5 \pm 3.83$	$6.32 \pm 0.81$
	16	$0.661 \pm 0.068$	$24.0 \pm 3.40$	$5.38 \pm 0.76$
Radial	16	$0.770 \pm 0.034$	$2.43 \pm 2.35$	$5.85 \pm 0.27$
	16	$0.738 \pm 0.039$	$12.2 \pm 2.12$	$5.18 \pm 0.35$
	16	$0.664 \pm 0.053$	$21.9 \pm 1.88$	$4.46 \pm 0.43$

Results for tests on all specimens are shown in Figure 3-7. The decrease in glucose diffusivity with increasing compressive strain is apparent from the figure. Moreover, it is also apparent that the diffusivity in the radial direction, represented by grey triangles, is lower than that in the axial (orange squares) or circumferential (green circles) directions.

The compressive strain for each specimen was calculated based on the size of the spacer and the height of the specimen and was not always exactly 0% initially. Therefore, a linear curve-fit of the experimental data could be used to estimate the value of glucose diffusivity at zero-strain conditions. These curve-fits are shown in Figure 3-8. For axially-oriented specimens, zero-strain diffusivity was found to be  $7.69 \times 10^{-7} \text{ cm}^2/\text{s}$ , compared with  $7.61 \times 10^{-7} \text{ cm}^2/\text{s}$  in the circumferential direction and  $5.96 \times 10^{-7} \text{ cm}^2/\text{s}$  in the radial direction. Again, the anisotropic behavior of glucose diffusivity in human AF tissue is highlighted, with radial diffusivity being lower than both axial and circumferential values.

In order to determine the effect of tissue degeneration on the diffusion of glucose in annulus fibrosus, values for apparent diffusivity at zero-strain were compared for the three degenerative grades used here (i.e., I, II and III). For each specimen, a linear regression was used to estimate the zero-strain diffusion coefficient (data not shown). The values obtained for all specimens were then averaged to determine the mean glucose diffusivity in uncompressed tissue. The results are shown in Table 3-3, as well as graphically in Figure 3-9. Similar to the data described above, diffusion in the axial and circumferential directions was significantly higher than that in the radial direction for discs having a degenerative grade of I or II. However, for grade III tissues, there were no

statistically significant differences between diffusion in the three principal directions. For axial and circumferential directions, diffusion in grade III discs was significantly less than in grades I and II; however, the diffusivities in grades I and II tissues in these two directions did not vary significantly. Furthermore, in the radial direction, diffusivity in grade II tissues was significantly higher than that in either grade I or grade III discs, while diffusivity in grades I and III did not differ significantly.

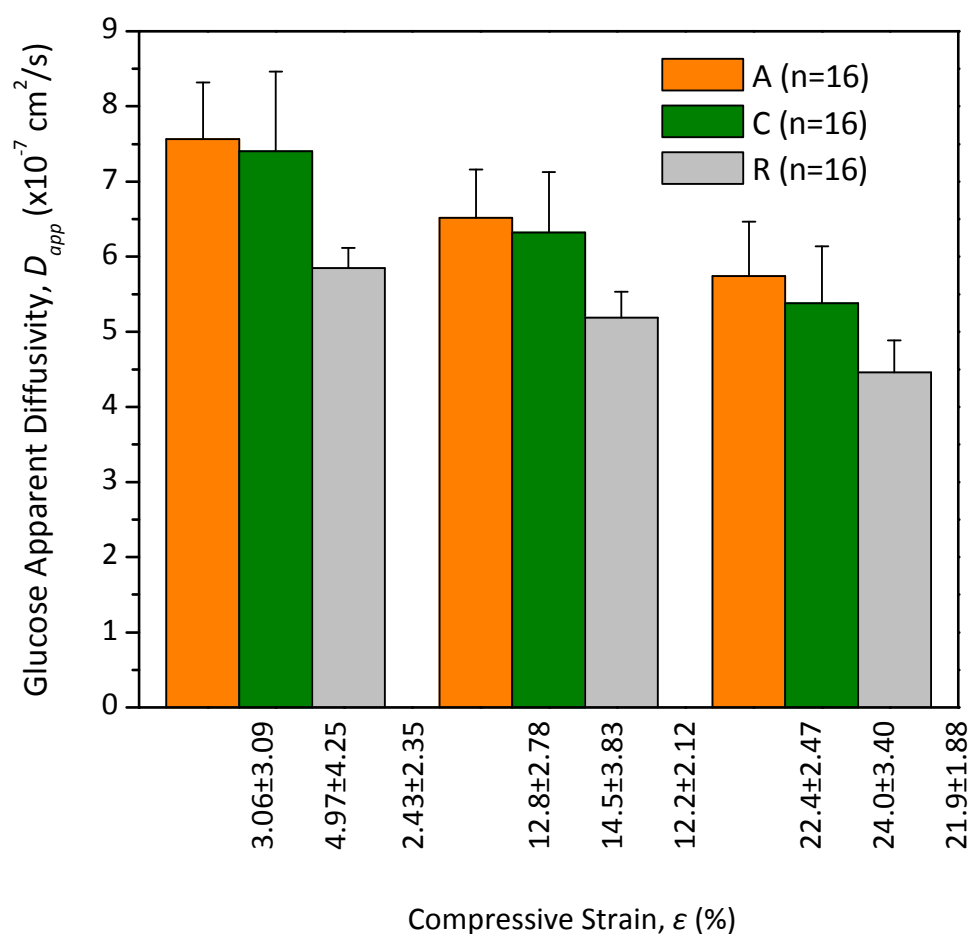


**Figure 3-6:** Results for apparent glucose diffusivity at varying levels of compressive strain in the three principal directions in human annulus fibrous tissue. A: axial, C: circumferential, R: radial.

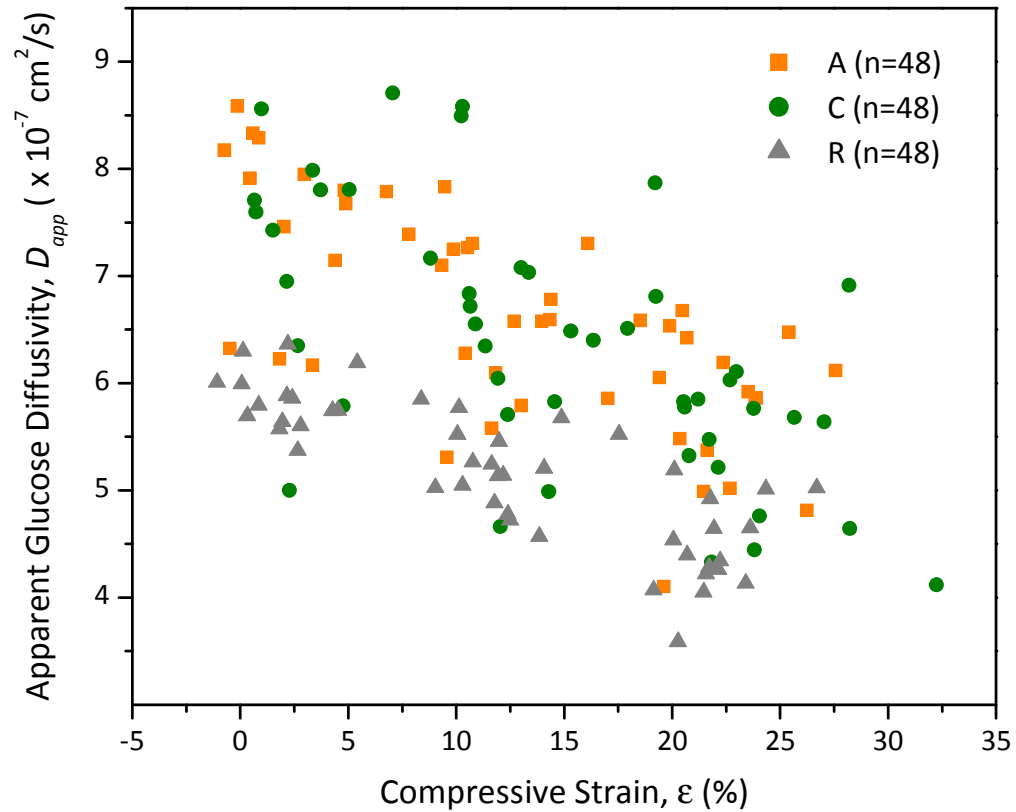


**Figure 3-7:** Variation of apparent glucose diffusivity with compressive strain in the three principal directions in human annulus fibrosus tissue. A: axial, C: circumferential, R: radial.

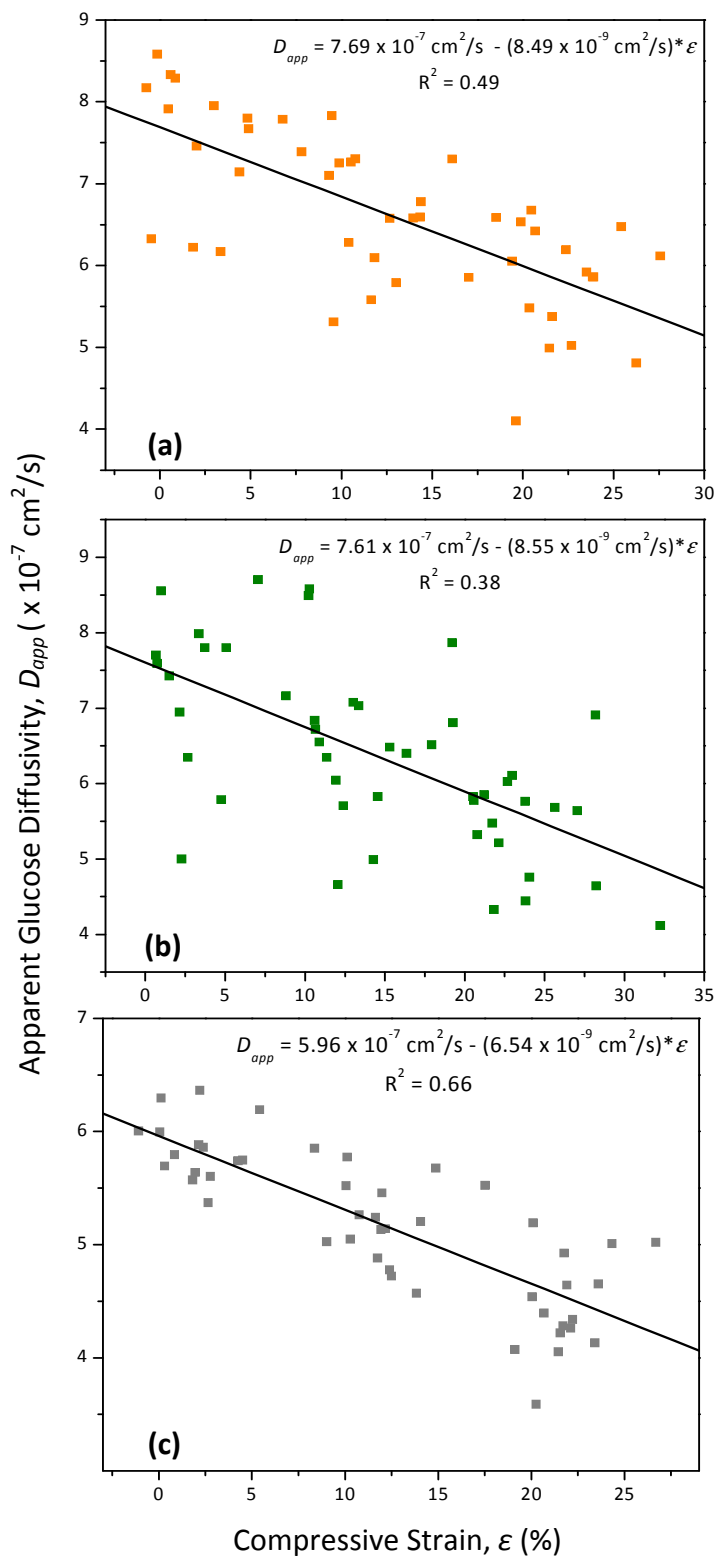


**Figure 3-8:** Graph of apparent glucose diffusivity versus compressive strain for the three principal directions of diffusion: (a) axial, (b) circumferential, and (c) radial. For each, n=48. Linear curve fits for each were used to determine diffusivity at 0% compressive strain level.

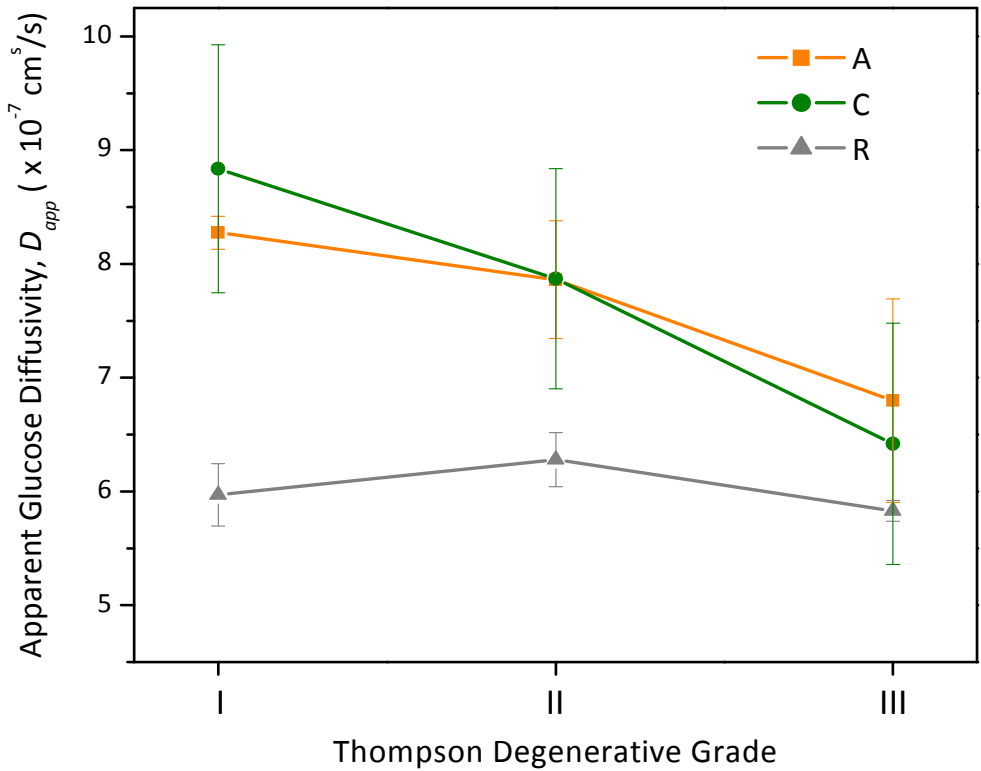


**Figure 3-9:** Variation of apparent glucose diffusivity with Thompson degenerative grade in the three principal directions in human annulus fibrous tissue. A: axial, C: circumferential, R: radial. For Grade I, n=8 for all groups; for Grades II and III, n=4 for all groups.

### 3.5 DISCUSSION

The main objective of this study was to determine the strain-dependent and anisotropic apparent glucose diffusion coefficient in human annulus fibrosus tissues. The findings of this investigation are similar to those found in human IVD, which reported a value of  $1.7 \times 10^{-6} \text{ cm}^2/\text{s}$  at  $37^\circ\text{C}$  (Maroudas et al. 1975). This corresponds to a value of  $1.2 \times 10^{-6} \text{ cm}^2/\text{s}$  at  $23^\circ\text{C}$ , calculated from the Stokes-Einstein equation. Furthermore, our results are also comparable to the results for strain-dependent and anisotropic glucose diffusivity in bovine coccygeal AF, which reported an averaged value of  $1.15 \times 10^{-6} \text{ cm}^2/\text{s}$  at  $23^\circ\text{C}$  and under zero strain conditions (Jackson et al. 2008). The slightly lower values found in this study may be attributed to differences in the micro-organization of the tissue, as well as differences in ages and degeneration of the tissue specimens used.

#### 3.5.1 EFFECT OF COMPRESSION ON THE DIFFUSION OF GLUCOSE

The results of this study suggest that the apparent glucose diffusivity in human annulus fibrosus is affected by the level of compressive strain applied to the tissue specimen. There was a significant decrease in the apparent diffusion coefficient with increase in compressive strain for all directions of diffusion measured. To our knowledge, this is the first reported data showing the effect of compression of the diffusion of glucose in human IVD tissues. Our results are in agreement with previous findings in the literature for strain-dependent diffusion of glucose in bovine coccygeal AF (Jackson et al. 2008).

The decrease in diffusivity caused by compressive strain was anticipated due to the observed changes in water content following compression, when water is exuded from the tissue, see Figure 2-6 in Section 2.6; this relationship is expressed in Equation



(3-16). The diffusion of solutes in cartilaginous tissues, including IVD, has been shown to be dependent upon tissue water content (Gu et al. 2004). Hence, the decrease in water content that is caused by mechanical compression of the tissue was expected to be accompanied by a decrease in the solute diffusivity, as our results indicate. This is similar to previous studies on water diffusivity in the disc.

Few previous studies have investigated the effects of compression on solute diffusivity in IVD tissues (Arun et al. 2009; Chiu et al. 2001; Drew et al. 2004). Three previous studies have used MRI techniques to show the strain-dependent behavior of water diffusion in IVD. Chiu et al. showed an increase in the apparent diffusion coefficient with increasing compressive load (Chiu et al. 2001). On the other hand, Drew et al. reported a decrease in diffusivity with increasing compressive strain in ovine discs (Drew et al. 2004), and Arun et al. recently reported similar findings in human IVD (Arun et al. 2009). Furthermore, our previous studies on oxygen and glucose diffusivity in bovine coccygeal AF, employing a 1-D steady-state diffusion method similar to the one described in this study, showed that solute diffusivity decreases as strain level increases (Jackson et al. 2008; Yuan et al. 2009). Although there is little else in the literature regarding the influence of mechanical compression on solute diffusion in IVD tissues, several studies have reported on this trend of decreased diffusivity with increasing static compressive load in other cartilaginous tissues, such as articular cartilage. Solutes investigated include water,  $\text{Li}^+$  ions, various sized dextran molecules, and  $\text{Na}^+$  ions (Burstein et al. 1993; Ngwa et al. 2002; Quinn et al. 2000; Quinn et al. 2001); all studies demonstrated that increasing compression in bovine articular cartilage results in a decrease in solute diffusion.

The finding of decreased diffusivity with increasing compressive strain has important implications for nutritional supply to disc cells, given the mechanical function of the disc in the spine. The disc provides flexibility in the spine and absorbs loads, often resulting in tissue compression. Decreased rates of diffusion for tissue in the compressed state signify hindered nutritional supply to the cells. Since cells require glucose for survival, prolonged compressive loading of the disc may lead to loss of cell viability as a result of poor nutritional supply, resulting in degenerative changes to the tissue. Hence, these findings provide important insight into the nutrition-related mechanisms of disc degeneration.

### *3.5.2 ANISOTROPIC BEHAVIOR OF GLUCOSE DIFFUSIVITY IN HUMAN IVD*

In this study, we found that diffusion of glucose in human annulus fibrosus is anisotropic. The apparent glucose diffusivity in the radial direction was significantly lower than that in the axial or circumferential directions at all levels of compression. To our knowledge, this is the first study reported on the anisotropic behavior of glucose diffusivity in human IVD tissues.

The anisotropic behavior of glucose diffusivity in AF tissues is believed to be caused by the unique structural organization of the tissue. The annulus fibrosus is made up of 15 to 25 concentric lamellae (Marchand and Ahmed 1990), creating a highly organized, layered structure. Furthermore, recent studies have indicated that a distinct morphology exists in both animal and human AF, with “microtubes” extending along the collagen fiber direction within the lamellae (Iatridis and ap Gwynn 2004; Jackson et al. 2008; Travascio et al. 2009). This unique collagen architecture is believed to play a key

role in the anisotropic behavior of diffusive transport in the tissue (Travascio et al. 2009). As shown in Figure 3-10, microtubes, which run parallel to the direction of collagen fibers, are visible in both axial and circumferential specimens, but not in radial specimens. It is thought that these microtubes may facilitate, or provide a preferred route for, transport in the axial and circumferential directions; that is, solutes may diffuse through the microtubes without significant hindrance by the collagen fiber network of the tissue. In contrast, in radial specimens, the microtubes are not visible, nor do they appear to be contiguous between adjacent lamellae. Therefore, solutes moving in the radial direction must diffuse through the collagen fiber network with greater impediment, thereby resulting in a lower diffusion coefficient in this direction.

Only few studies have investigated the anisotropic transport behavior in IVD tissue. Again, our previous study on glucose diffusivity in bovine coccygeal disc showed a similar trend to results reported here (Jackson et al. 2008), with axial diffusion being significantly greater than that in the radial direction. Furthermore, previous studies using fluorescence recovery after photobleaching (FRAP) methods have shown the anisotropic behavior of the diffusion tensor of fluorescein in both animal and human IVD; results showed a similar trend to those reported here (Travascio et al. 2009; Travascio and Gu 2007).

The ratio of the radial diffusivity to axial diffusivity (i.e, smallest to largest) found here was 0.77. This ratio was similar to those found in the literature for solute transport in IVD tissues. A summary of these results are shown in Table 3-3. Our previous study in bovine coccygeal AF tissue found a ratio of 0.66 for glucose diffusivity (Jackson et al. 2008), while we found a ratio of 0.64 and 0.4 for fluorescein diffusivity in bovine

coccygeal and human lumbar AF tissues, respectively (Travascio et al. 2009; Travascio and Gu 2007). This confirms our previous suggestion that radial hinderance to diffusion caused by collagen fiber organization increases with increasing solute size (Travascio et al. 2009).

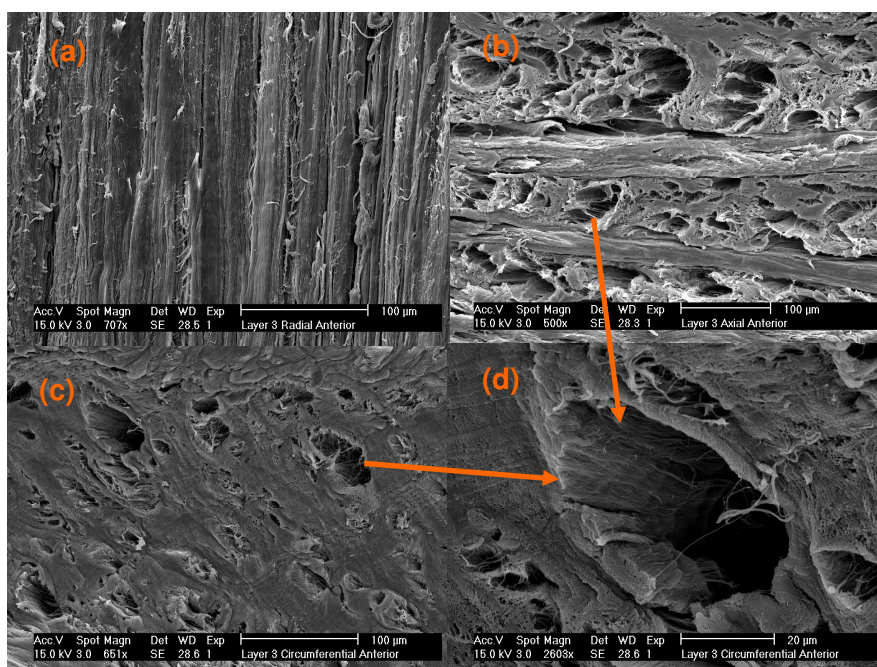


**Figure 3-10:** Scanning electron microscopy (SEM) images showing no obviously visible microtubes in the radial section of human AF (a), the clear presence of microtubes in the axial (b) and circumferential sections (c), along with magnified view of microtube (d).

**Table 3-3:** Summary of Experimental Results for Anisotropic Diffusion in IVD

Solute	Tissue	Anisotropic Ratio	Reference
Na <sup>+</sup>	Bovine coccygeal AF	0.62	(Jackson et al. 2006)
Cl <sup>-</sup>	Bovine coccygeal AF	0.63	(Jackson et al. 2006)
Water	Porcine lumbar AF	0.75	(Hsu and Setton 1999)
	Human lumbar AF	0.84	(Chiu et al. 2001)
	Ovine lumbar AF	0.90	(Drew et al. 2004)
Glucose	Bovine coccygeal AF	0.66	(Jackson et al. 2008)
Fluorescein	Bovine coccygeal AF	0.64	(Travascio and Gu 2007)
	Human lumbar AF	0.40	(Travascio et al. 2009)

*Note: Ratio is of the smallest to largest value of diffusivity reported.*

### 3.5.3 EFFECT OF DISC DEGENERATION ON DIFFUSIVITY OF GLUCOSE

In this study, we investigated the glucose diffusivity in human IVD having Thompson degenerative grades I, II and III. For axial and circumferential sections, there was a trend toward decreasing diffusivity with increasing tissue degenerative grade. This decrease is likely the result of decreasing tissue water content caused by the degenerative process. This is in agreement with several previous studies investigating the diffusivity of water in normal and degenerated IVD, which found that diffusivity decreased with increased degeneration (Beattie et al. 2008; Kealey et al. 2005; Kurunlahti et al. 2001; Niinimäki et al. 2009).

In contrast, unlike axial and circumferential diffusivity, that in the radial direction did not show the same decreasing trend. This difference may result from the specimen preparation for radial tissue specimens. For axial and circumferential specimens, the

layers of AF run perpendicular to the surface of the sample; however, for radial specimens, the lamellae are parallel to the cut surface of the tissue. The thickness of the specimens ( $\sim 500 \mu\text{m}$ ) is larger than the thickness of a single lamella, which varies from 100 to 400  $\mu\text{m}$ , depending on the location (Marchand and Ahmed 1990). Therefore, the arrangement of lamellae may differ from specimen to specimen, see Figure 3-11. This variation may impact the measured rate of diffusion in the radial direction.

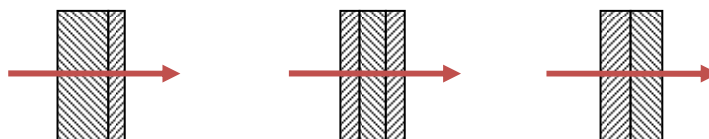


**Figure 3-11:** Various possible arrangements for lamellae in radial specimens which may affect diffusivity measurements in radial direction. Note that diffusion is measured across the specimen, in the direction indicated by the arrows.

These results also show that as the disc becomes more degenerated, the anisotropic nature of diffusivity in the tissue diminishes. This is in agreement with previous studies on fluid transport in the disc, which have shown a trend toward isotropy with increasing degeneration (Gu et al. 1999). This is likely due to a decrease in the organization of the tissue during the degeneration process, which would result in a more disorganized, isotropic material as seen here.

#### 3.5.4 EXPERIMENTAL LIMITATIONS

There are a few limitations to the experimental techniques and study described here. First, porous plates were used to compress and confine the tissue specimen during the experiment. This may result in stagnant layer formation at the tissue boundary,

impacting the measurements for diffusivity. The use of a stirring rod has been shown to minimize boundary layer formation (Maroudas et al. 1968); however, it is likely that it could not be eliminated entirely. Previous studies have shown that porous plate may cause an underestimation of the diffusion coefficient measurement by 7% (Jackson et al. 2008). However, because swelling and proteoglycan leaching is known to occur in IVD tissue in solution, the use of porous plates was necessary in order to carry out the experiments. The use of very thin porous plates and continuous stirring was expected to minimize their effects.

Additionally, only four L2-L3 discs were used in this experiment, resulting in a small sample size. Due to the large variation in tissues from different discs, standard deviations for groups were high. Furthermore, only two degenerated discs – one each of grades II and III – were obtained for this study. To better understand the effects of degeneration on diffusivity of glucose in IVD, the diffusion coefficient should be measured in more discs. This may lead to smaller standard deviation and more statistically significant results.

### **3.6 SUMMARY AND CONCLUSIONS**

In this study, the strain-dependent and anisotropic diffusivity of glucose in human annulus fibrosus tissue was measured using a one-dimensional steady-state diffusion problem and custom-designed chamber. Results indicate that the apparent diffusivity of glucose in human AF is anisotropic (i.e., direction-dependent), being lower in the radial direction as compared with the axial or circumferential directions. We also found that apparent glucose diffusivity in human AF decreases as the level of compressive strain increases. Furthermore, results show that degeneration affects the diffusivity of glucose

in AF tissue. To our knowledge, this is the first study to show how strain, anisotropy, and degeneration affect the transport of glucose in human IVD tissue. The findings of this investigation provide important insight into the pathophysiology of disc degeneration, particularly as it relates to nutrition.



## **CHAPTER 4. MEASUREMENT OF STRAIN-DEPENDENT GLUCOSE PARTITION COEFFICIENT IN HUMAN INTERVERTEBRAL DISC**

### **4.1 INTRODUCTORY REMARKS**

Disc cells require nutrients such as glucose and oxygen in order to survive and properly perform their function. Due to the avascularity of IVD tissues, these nutrients must be supplied by the surrounding blood vessels, and transported through the tissue. The maximum concentration of solute that can enter the IVD tissue is related to properties of the tissue extracellular matrix, as well as to properties of the solute itself. The equilibrium partition coefficient,  $K$ , can be used to describe this maximum concentration.

While partitioning of glucose and several other solutes in articular cartilage has been investigated, little is known regarding the value of the partition coefficient of glucose in IVD tissue. One previous study determined the partition coefficient of glucose in human IVD under zero compression was 0.68 (Maroudas et al. 1975), however little more can be found in the literature. This information is necessary because the partition coefficient is one of the key parameters governing transport properties of a tissue and therefore provides important insight into the mechanisms of transport in the IVD. Furthermore, because our study of glucose diffusivity in the IVD (Chapter 3) is a measure of the apparent glucose diffusion coefficient, information about the partition coefficient is necessary in order to convert apparent diffusivity ( $D_{app}$ ) to effective diffusivity ( $D_{eff}$ ) by the equation:

$$D_{app} = KD_{eff} . \quad (4-2)$$

This information is required for theoretical modeling of nutrient distributions in the disc. Therefore, the aim of this study is to measure the strain-dependent partition coefficient of glucose in human IVD tissues.

#### 4.2 THEORETICAL APPROACH

The partition coefficient is defined as the ratio of the solute concentration in the tissue,  $c$ , to that in the bathing solution,  $c^*$ :

$$c = Kc^*. \quad (4-1)$$

For the case of  $K=1$ , the solute is evenly distributed between the tissue and the bathing solution; this is generally only the case for small, uncharged solutes. For  $K < 1$ , the solute is excluded from the tissue; this may be due to the size of the solute or the charge of the solute. For the intervertebral disc, which has negative fixed charges on the matrix,  $K > 1$  for small cations, such as  $\text{Na}^+$  and  $\text{Ca}^{2+}$ .

The partition coefficient of glucose in intervertebral disc tissue can be measured by equilibrating the tissue in a series of baths and measuring the equilibrium concentrations. That is, the tissue sample is initially equilibrated in a solution containing glucose and the final (equilibrium) concentration of solution is measured. This is then repeated for a bath containing no glucose and the equilibrium concentration is measured.

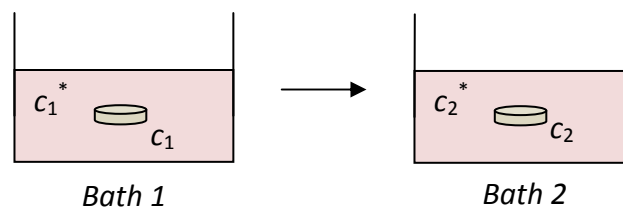


**Figure 4-1:** Schematic showing the procedure for determining the partition coefficient in a tissue specimen.

Using the relationship in Equation (4-1), the concentration of solute in bath 1,  $c_1^*$ , is related to the concentration of the solute in the tissue equilibrated in bath 1,  $c_1$ , by:

$$c_1 = Kc_1^*. \quad (4-3)$$

Likewise, the same relationship holds for bath 2:

$$c_2 = Kc_2^*. \quad (4-4)$$

By conservation of solute mass after transfer from the first to second equilibration bath, we have:

$$\phi^w V(c_1 - c_2) = V_2 c_2^*, \quad (4-5)$$

where  $V$  is the tissue specimen volume,  $\phi^w$  is the porosity, or water volume fraction, of the tissue, and  $V_2$  is the volume of equilibrium bath 2. Using the relationship in Equations (4-3) and (4-4), we have:

$$\phi^w V(Kc_1^* - Kc_2^*) = V_2 c_2^*. \quad (4-6)$$

Therefore, the partition coefficient can be calculated from (Fetter N.L. et al. 2006; Quinn et al. 2001):

$$K = \frac{V_2 c_2^*}{\phi^w V(c_1^* - c_2^*)}. \quad (4-7)$$

This method has been previously used to measure the partition coefficient of solutes in articular cartilage.

In order to determine the strain-dependent partition coefficient, the tissue must first be compressed to the desired height; equilibrations take place while the tissue is confined, in order to maintain the proper strain-level. By varying the level of

compression, a relationship for the strain-dependent partition coefficient of glucose in IVD tissues can be determined.

### **4.3 MATERIALS AND METHODS**

#### *4.3.1 DESIGN OF EXPERIMENTAL APPARATUS*

Due to the nature of the disc tissue, which tends to swell and break down when immersed in solution, it is necessary to confine the specimen during equilibration. This will limit tissue swelling as well as proteoglycan leaching, both of which lead to changes in the composition and structure of the tissue. Therefore, a chamber that accomplishes this while allowing for the measurement of the partition coefficient of glucose in IVD tissues was specially-designed to carry out this experiment.

The custom-designed chamber, designed in order to allow for confined compression of a specimen during equilibration in a given solution, is shown in Figure 4-2 and 4-4b. The chamber consists of a specimen well having the same dimensions as the compressed tissue, a porous plate and o-ring used to seal and confine the specimen, and a chamber for the equilibration solution. The solution chamber is sealed with a custom-fit cap.

The chamber was machined out of a 2" acrylic rod (Small Parts). The optimal specimen size was determined in preliminary experiments in order to maximize tissue volume and surface area, while minimizing the diffusion distance (i.e., relatively small height compared with surface area). The specimen size chosen was a height of 2 mm and a diameter of 8 mm. Therefore, the well for holding the specimen during equilibration

had the same dimensions. The solution chamber was designed to hold 100  $\mu\text{L}$  of solution, in addition to a magnetic stirring bar.

The specimen was sealed using an o-ring and a metal screen (Small Parts). The stainless steel screen was chosen over the polyethelene plates, as were used in diffusion measurements, because it could confine the specimen without absorbing any of the bathing solution. The o-ring was used to seal the chamber and confine the equilibrating solution to the chamber above the tissue specimen.

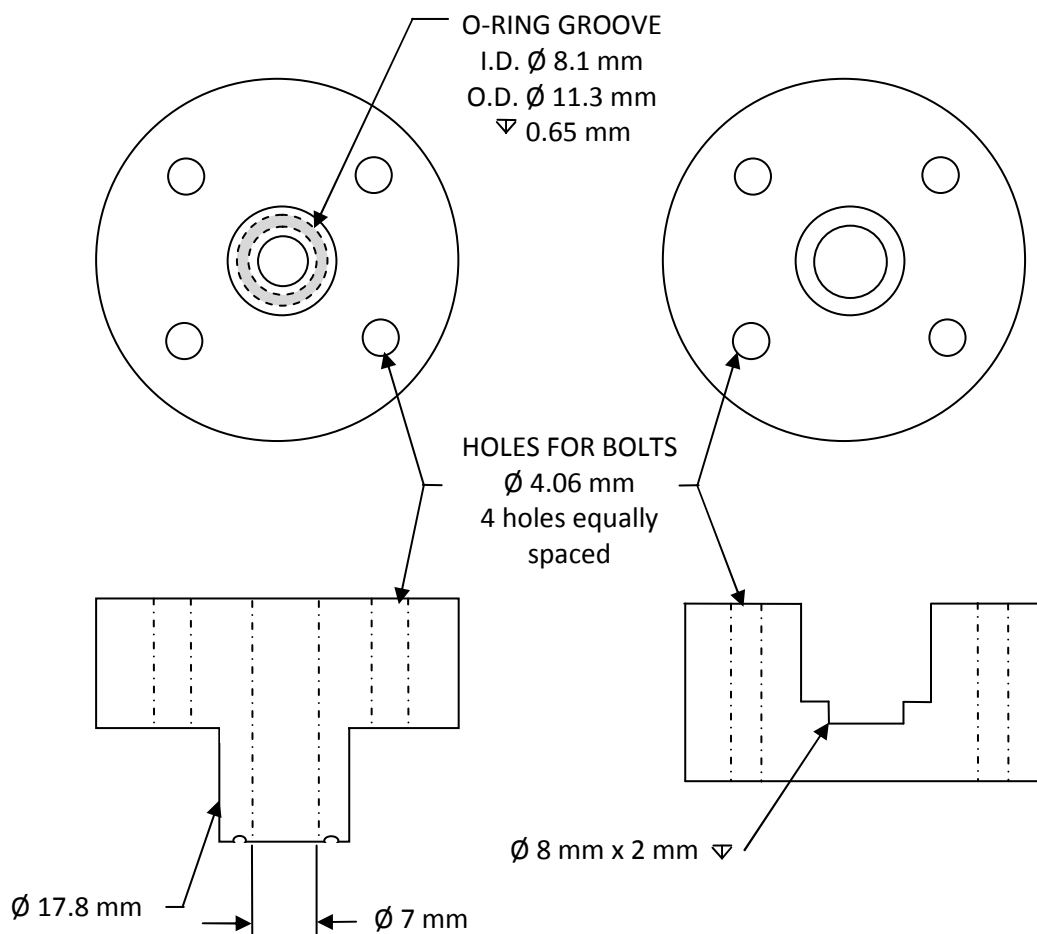


**Figure 4-2:** Engineering drawing showing the top and front views of the two halves of the custom partition coefficient chamber. See Figure 4-4 for schematic of assembled apparatus.

#### 4.3.2 SPECIMEN PREPARATION

Intervertebral discs used for partition coefficient experiments were the same as those used for diffusivity experiments; therefore, methods for harvesting of discs is the same as those described in Section 3.2.1. For details on the donor information and degenerative grades of discs used, see Table 3-1 in Section 3.2.1.

For partition coefficient experiments, specimens were prepared with either axial or circumferential orientation, based on tissue availability. Specimens were not prepared having radial orientation due to the lower diffusion coefficient of glucose in this direction, as described in Section 3.4. The equilibration period,  $t$ , for a tissue specimen can be estimated by the equation:

$$t = \frac{h^2}{D}, \quad (4-8)$$

where  $h$  is the specimen thickness and  $D$  is the diffusivity. Therefore, in order to minimize equilibration times, only axial and circumferential specimens were used.

Axial or circumferential blocks of tissue were harvested from the IVD, see Figure 4-3. From each block, cylindrical specimens were prepared using a corneal trephine ( $d = 8$  mm), as described previously. A microtome with freezing stage was then used to slice specimens to the desired thickness of approximately 2.0 – 2.5 mm, depending on the desired level of compression. The final height of the specimen was measured using a current-sensing micrometer; as in diffusivity studies, the averaged height was taken from three measurements.

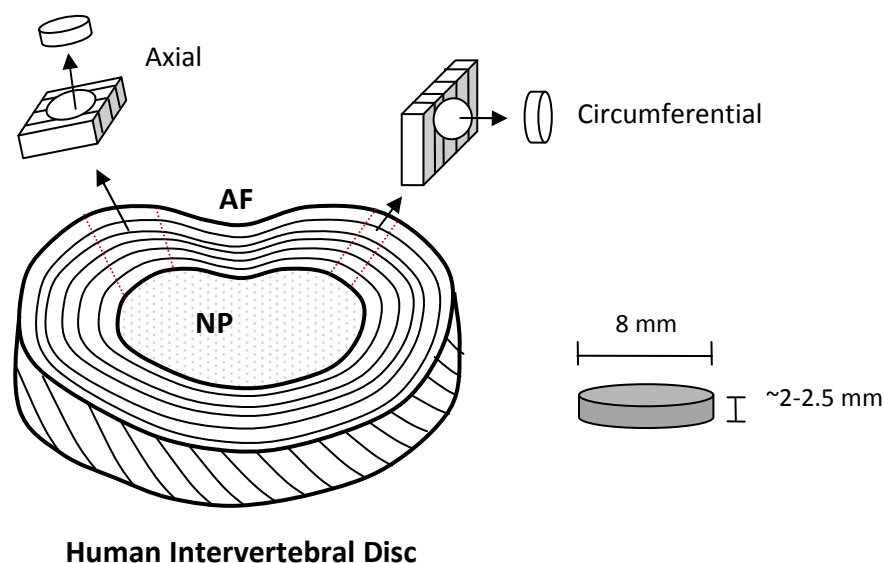


**Figure 4-3:** Schematic showing orientation and size of specimens obtained from human annulus fibrosus (AF).

#### 4.3.3 WATER CONTENT MEASUREMENT

Tissue water content for partition coefficient specimens was measured using the buoyancy method described in Section 3.3.3. Following equilibration in two baths, the weights of the tissue in air and in solution (PBS) were determined using the Sartorius analytical balance. Again, the measurement of the tissue weight in solution was taken in less than 15 seconds to minimize swelling and PG leaching. Then, the tissue samples were lyophilized and the dry weights were recorded. Water contents of compressed tissues were measured directly, since tissue specimens were equilibrated in the compressed state.

#### 4.3.4 MEASUREMENT OF PARTITION COEFFICIENT

Following specimen preparation, samples were first compressed in a separate compression apparatus, see Figure 4-4, prior to loading into the measurement chamber. All specimens were compressed to a final height of 2 mm, and the level of compressive strain was calculated based on the initial height measured during specimen preparation. Because even the specimens used for 0% nominal compressive strain were not exactly 2.0 mm in height, all specimens were compressed prior to loading in the chamber.

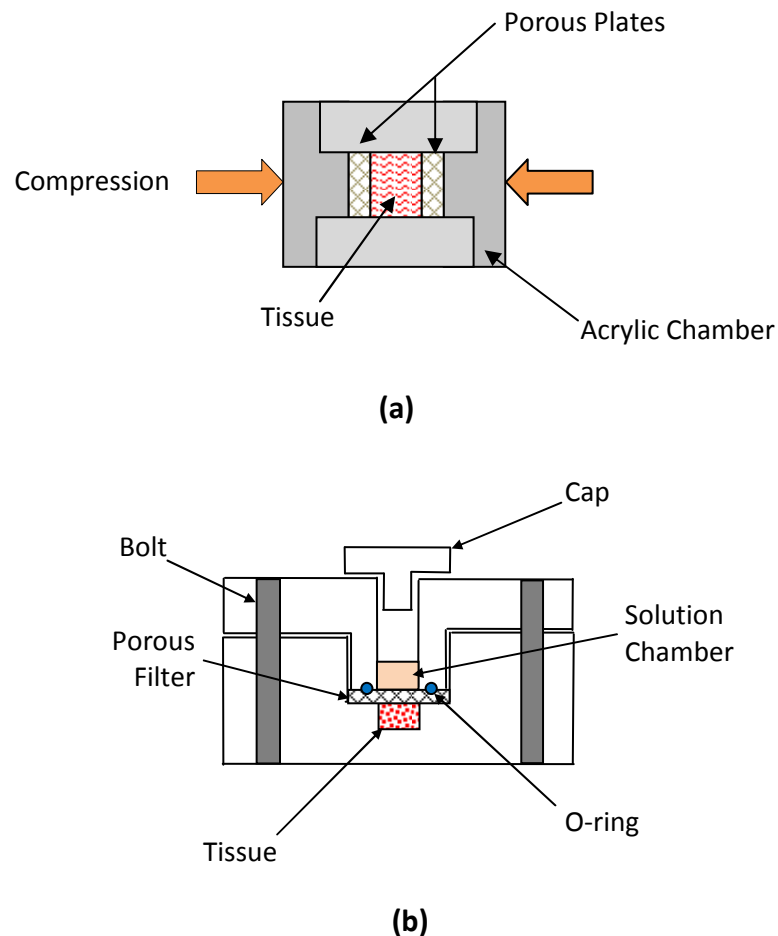


**Figure 4-4:** Schematic of (a) the compression apparatus and (b) the custom chamber for measuring the partition coefficient of a compressed IVD tissue sample.



Once loaded into the experimental chamber, the tissue was sealed in place with the stainless steel filter and o-ring, and the chamber was tightly closed using four bolts and wing nuts. Next, 100  $\mu\text{L}$  of high glucose Dulbecco's Modified Eagle Medium [DMEM, concentration = 5 g/L ( $\sim 25$  mM) glucose in solution] was dispensed into the solution chamber. A magnetic micro-stirring rod was also inserted, and the custom cap was used to seal the chamber. The apparatus was placed on a magnetic stirring plate inside a refrigerator ( $T = \sim 2^\circ\text{C}$ ). The experiment was carried out at lower temperature in order to minimize the production of bacteria in the bathing solution. The initial equilibration period was 24 hours.

At the end of the first equilibration period, the concentration of glucose in the bathing solution was measured. Concentration measurements were carried out using a commercially-available blood glucose meter (Accu-Check Aviva, Roche Diagnostics, Indianapolis, IN). The meter uses an electrochemical method to measure glucose concentrations in solution (for more details, see Section 6.3.5). Using a micro-pipet, 1  $\mu\text{L}$  of solution was extracted from the solution chamber and the concentration measured.

Following concentration measurement, the solution was removed and the chamber dried using a cotton swab. Then, 100  $\mu\text{L}$  of DMEM containing no glucose was dispensed into the solution chamber. The chamber was again placed on a magnetic stirring plate at  $2^\circ\text{C}$  and allowed to equilibrate for 8 hours. Following this period, the solution was collected and a fresh 100  $\mu\text{L}$  of no glucose DMEM was dispensed into the chamber for an additional 8 hour equilibration. This was then repeated a third time, for a total of 24 hours of equilibration. At the end of this period, the concentration of the collected bathing solution (a total of 300  $\mu\text{L}$  combined from three equilibrations) was measured by

the same method. The consecutive equilibrations in three solutions were carried out in order to facilitate the diffusion of glucose out of the tissue sample and into solution; that is, but replacing the equilibrating solution with a fresh, blank solution, the concentration gradient remained steep, therefore allowing for a faster equilibration. Following the final equilibration, the specimen was removed for water content measurement.

Using the concentration and water content measurements, the partition coefficient was calculated using Equation (4-7). The volume of the tissue specimen was calculated based on weight measurements, see Equation (3-12) in Section 3.3.3.

#### 4.3.5 STATISTICAL ANALYSES

A total of 12 specimens ( $n=12$ ) were measured for each of three levels of nominal compressive strain (0%, 10% and 20%), for a total of 36 specimens. A one-way ANOVA analysis of variance was performed to determine if differences between groups were statistically significant. Tukey post-hoc analysis was performed to determine among which levels of each factor the differences were significant. A two-way ANOVA was used to determine if partitioning was significantly affected by both disc degeneration and compressive strain, followed by Tukey post-hoc analysis. For all statistical analyses, the significance level was set to  $p<0.05$ . All data are given in mean  $\pm$  standard deviation.

## 4.4 RESULTS

The partition coefficient of glucose in human annulus fibrosus was determined at three levels of compressive strain. Results are shown in Table 4-1. The value of compressive strain was calculated based on the initial height of the specimen and the

compressed height (2 mm for all specimens). One-way ANOVA confirmed that there was a significant decrease in the partition coefficient with increase in compressive strain ( $p < 0.05$ ). Post-hoc analysis showed that only the partition coefficients determined at 0% and 20% nominal strain levels differed significantly.

The effect of degenerative grade on the partition coefficient was also investigated in this study. Tissues having three different degenerative grades (I, II and III) were used. Due to the small number of specimens, the tissue was divided into normal (grade I) and degenerated (grades II and III), with each group having six specimens ( $n=6$ ) for each level of compression, for a total of 18 specimens for each degeneration group. The dependence of the glucose partition coefficient on the tissue degenerative grade is shown in Figure 4-6. A two-way ANOVA showed that there was a significant decrease in the partition coefficient as both the compressive strain and degenerative grade increased ( $p < 0.05$ ). However, post-hoc analysis showed that only the difference between normal and degenerated tissue at ~0% strain was significantly different, while there was no significant difference at ~10% and ~20% strain levels.

**Table 4-1:** Results for Glucose Partition Coefficient at Varying Levels of Compressive Strain in Human Annulus Fibrous Tissue

$n$	$\phi^w$	Strain, $\epsilon$ (%)	$K$
12	$0.77 \pm 0.03$	$1.45 \pm 0.90$	$0.82 \pm 0.05$
12	$0.75 \pm 0.03$	$13.2 \pm 1.18$	$0.76 \pm 0.04$
12	$0.73 \pm 0.04$	$26.4 \pm 1.87$	$0.71 \pm 0.08$

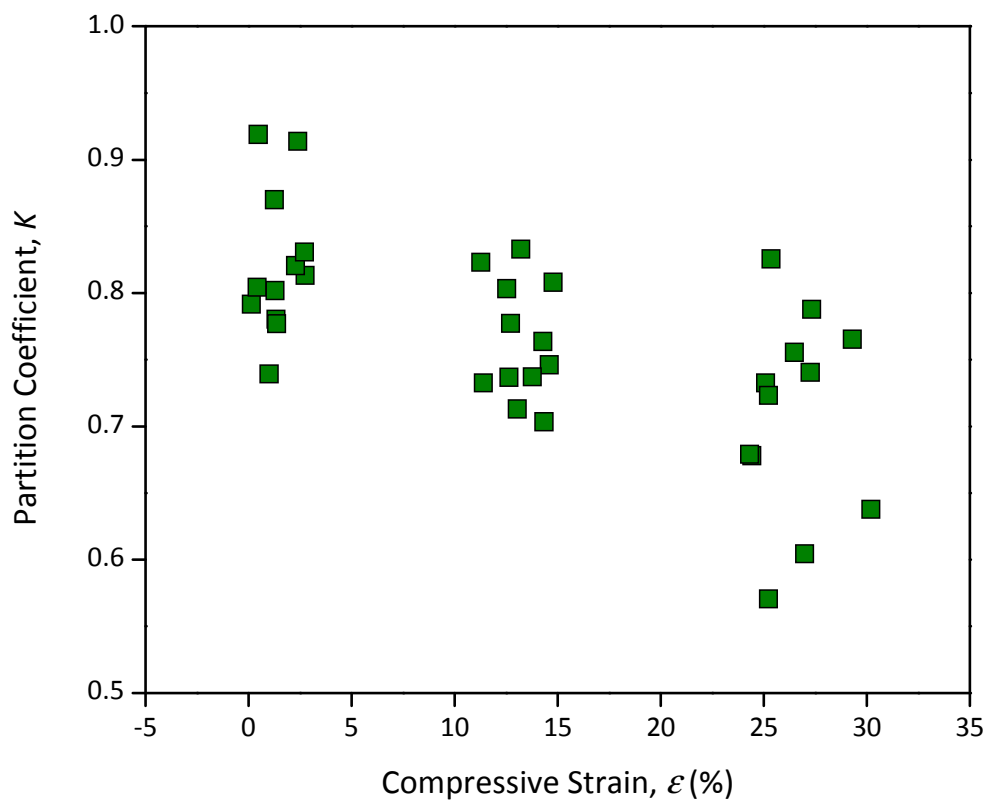


**Figure 4-5:** Results for glucose partition coefficient in human annulus fibrosus tissue at varying levels of compressive strain.

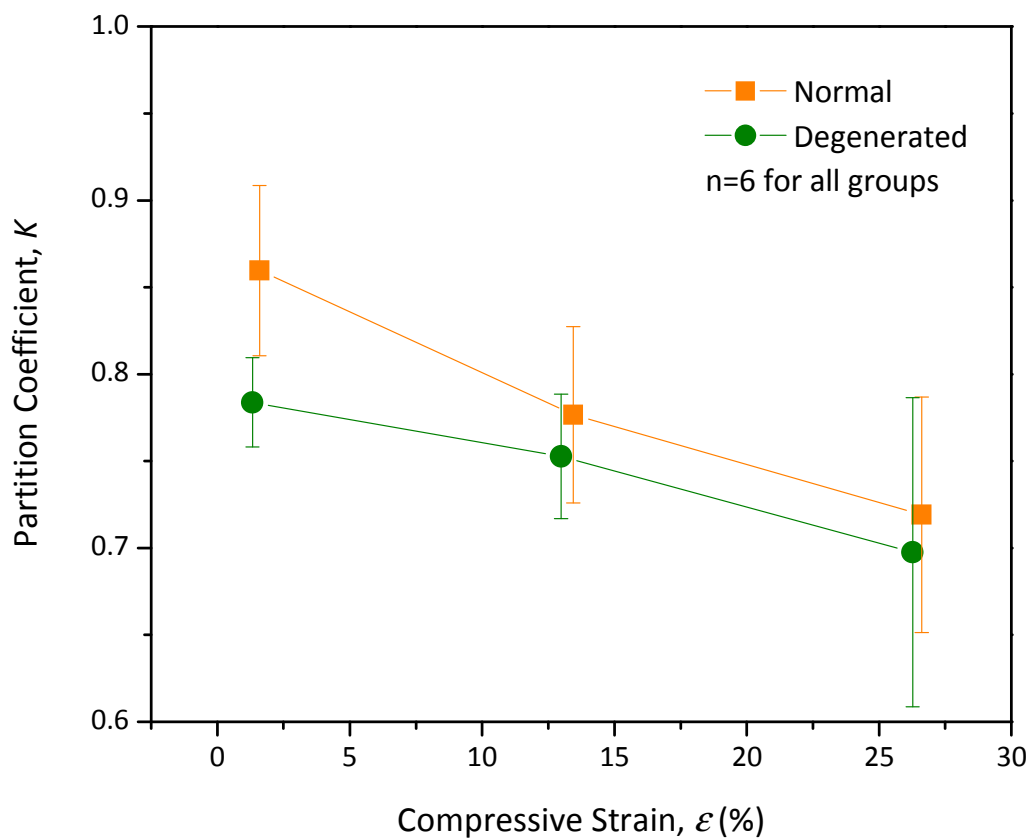


**Figure 4-6:** Relationship between partition coefficient and compressive strain for normal and degenerated human annulus fibrosus tissue. Note that normal tissue signifies Thompson Grade I, while degenerated tissue is for Grades II and III.

## 4.5 DISCUSSION

The primary aim of this study was to determine how mechanical strain affects the partitioning of glucose in human annulus fibrosus tissue. The results found here are similar to those for glucose partitioning (or distribution) in human AF at zero-strain, measured as  $0.68 \pm 0.05$  using a radiotracer method (Maroudas et al. 1975). Additionally, our results are similar to those in the literature for articular cartilage, ranging from 0.666 to 0.9 (Maroudas 1976; Torzilli et al. 1998).

### 4.5.1 EFFECT OF COMPRESSION ON GLUCOSE PARTITIONING IN HUMAN IVD

Our results indicate that compression significantly affects the partitioning, or solubility, of glucose in human AF tissue. To our knowledge, this is the first study investigating the effect of compression on partitioning in intervertebral disc tissues. The results found here are similar to those for partitioning of solutes in articular cartilage under compressive strain found in the literature. Previous studies have shown that compression causes decreased solubility of solutes in cartilaginous tissues (Nimer et al. 2003; Quinn et al. 2000; Quinn et al. 2001).

A plot of the partition coefficient versus compressive strain is shown in Figure 4-5. The decrease in partitioning with increasing strain is apparent. Compression causes exudation of water from the tissue, resulting in decreased tissue water content, as expressed in Equation (3-16) in Section 3.3.3. Since transport of solutes in cartilaginous tissues is dependent upon tissue porosity, the trend found here was expected. This is similar to the trend found for diffusion of glucose in human AF tissue (Chapter 3).

The relationship between tissue porosity and glucose partition coefficient was also investigated, and is shown in Figure 4-7. A linear relationship was found to exist. The

large scatter of data is likely the result of tissue variation between discs; we would expect to find a stronger correlation with a greater number of tissue specimens. Nonetheless, this provides the first quantitative relationship between tissue porosity (or water content) and glucose partitioning in IVD tissue. The decrease in the partition coefficient with decreasing porosity was expected, as transport of solutes in cartilaginous tissues is dependent upon the tissue water content.

The effect of compression on the partitioning of glucose in IVD tissue is significant because of the mechanical role of the disc in the spine. The IVD is subjected to a variety of loading conditions throughout the day, often in compression. This may have a deleterious effect on disc cells, which need nutrition for survival. Decreased solubility of glucose in compressed tissue decreases its availability to disc cells, which may lead to loss of viability or functioning.

#### *4.5.2 EFFECT OF DEGENERATION ON GLUCOSE PARTITIONING IN HUMAN IVD*

In this study, it was found that degeneration of intervertebral disc tissue affects the partitioning of glucose in the tissue. Although results were not significant for all groups, this trend is apparent, as seen in Figure 4-6. To our knowledge, this is the first study to investigate how degeneration affects the solubility of solute in disc tissue. The decreased partition coefficient of glucose in degenerated tissue is likely the result of lower water content in the tissue, as it is known that disc degeneration results in loss of tissue porosity.

The finding of decreased solubility of glucose in degenerated tissue provides important insight into the nutrition-related causes of disc degeneration. In order to

survive, disc cells require glucose, which must be transported through the extracellular matrix of the tissue from the surrounding blood vessels, given that the tissue is avascular. Therefore, determining how glucose transport is affected by degenerative changes to the tissue is important for understanding disc pathophysiology. A decrease in the partition coefficient with increasing degeneration signifies that less glucose is able to enter degenerated tissue. As a result, the nutritional supply to disc cells will be diminished, leading to loss of cell viability and further degenerative changes.

#### *4.5.3 EXPERIMENTAL LIMITATIONS*

The methods for determining the partition coefficient of glucose in IVD developed here have few limitations. For instance, it is difficult to determine if the tissue specimens were confined to exactly 2.0 mm using the metal screens. That is, there is a possibility that the screens could have allowed for some tissue swelling during the equilibration period. In this case, the value for strain-level, calculated based on the measured height and the final, 2.0 mm height, would have error. However, since the tissue porosity was measured directly from the compressed tissue, the relationship shown in Figure 4-7 is believed to be accurate.

Additionally, the commercially-available glucose sensor used to measure glucose concentrations did not have a high resolution. This may have allowed for some error in the accuracy of glucose concentration measurements. This may have been corrected by using an alternate source for current measurements, as described in Section 6.3.5. However, the resolution was deemed sufficient for this application.



Finally, as for the diffusivity measurements, only four IVDs were harvested for partition coefficient measurements. Due to low tissue availability, only a small number of specimens were prepared for this study. There was a large scatter in experimental data due to differences in the tissues from different discs and regional variation. Furthermore, no significant differences could be found for normal and degenerative groups at 10% and 20% nominal compressive strains, despite an apparent trend. Therefore, more discs should be used in order to further investigate the significance of the results found here.

#### **4.6 SUMMARY AND CONCLUSIONS**

In this study, we investigated the effect of compression and degeneration on the partitioning of glucose in human annulus fibrosus. Our results indicate that both factors lead to lower partition coefficients, although not all trends were statistically significant. To our knowledge, this is the first study to determine the strain-dependent partition coefficient of glucose in human IVD, as well as the first to investigate the effects of tissue degeneration on glucose partitioning in human IVD. The results provide insight for better understanding the nutritional supply to disc cells and related disc degeneration and low back pain.

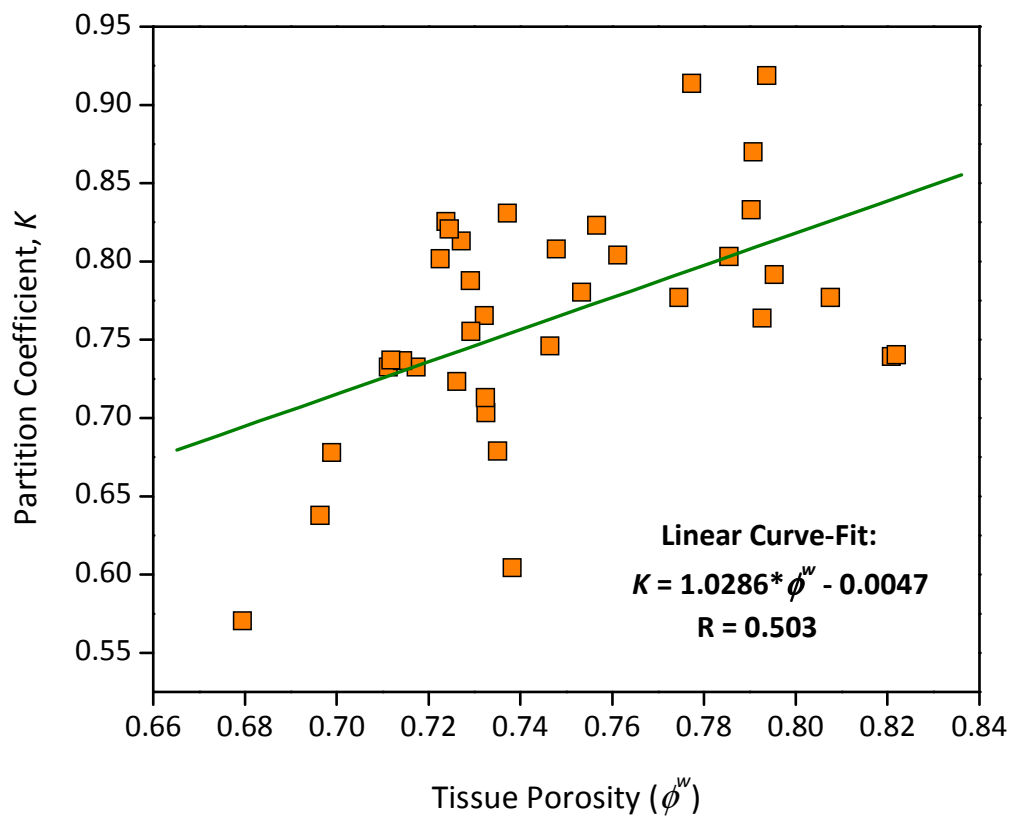


**Figure 4-7:** Relationship between partition coefficient and tissue porosity for human annulus fibrosus tissue. A linear curve-fit was performed using Origin 6.1.

## **CHAPTER 5. EFFECTIVE DIFFUSIVITY OF GLUCOSE IN HUMAN ANNULUS FIBROSUS**

### **5.1 INTRODUCTORY REMARKS**

In Chapter 3 of this dissertation, we determined the apparent diffusion coefficient of glucose in human annulus fibrosus in the three principal directions. However, the effective diffusivity is the quantity most commonly expressed in the literature. Furthermore, theoretical modeling of transport in IVD requires knowledge of effective diffusion coefficients to predict solute concentrations in the tissue. As has been mentioned, the apparent diffusivity is related to the effective diffusivity by the partition coefficient. Hence, our results for apparent diffusivity of glucose in human IVD, detailed in Chapter 3, can be converted to effective diffusion coefficients using our measured values for the partition coefficient (Chapter 4).

In this chapter, we combine our results in Chapters 3 and 4 in order to determine the effective diffusivity of glucose in human AF. Results are then compared with those in the literature for other solutes in IVD tissues.

### **5.2 COMBINATION OF DIFFUSIVITY AND PARTITIONING RESULTS**

In order to calculate the effective diffusion coefficient, the partition coefficient was first calculated based on its relationship with tissue porosity, determined from curve-fitting data in Chapter 4:

$$K = 1.0286 * \phi^w - 0.0047. \quad (5-1)$$

For each measurement of apparent diffusion coefficient, the partition coefficient was calculated based on the porosity of the tissue. The effective diffusivity was then calculated from:

$$D_{eff} = \frac{D_{app}}{K}. \quad (5-2)$$

The results for the effective diffusion coefficient of glucose in human AF in the three principal directions, as related to tissue porosity, are shown in Figure 5-1, and are also listed in Table 5-1. The data show significant variability, as can be seen in Figure 5-1. This is likely the result of variation between specimens from different discs. Human tissue harvested from discs of different spines shows wide variation.

Diffusion coefficients of solutes in cartilaginous tissues are often expressed relative to the diffusivity of the solute in aqueous solution, called the relative diffusivity. The diffusivity of glucose in aqueous solution,  $D_o$ , at 23°C is  $6.382 \times 10^{-6} \text{ cm}^2/\text{s}$ , calculated based on the value at 25°C (Longworth 1953) using Stokes-Einstein equation:

$$D_o = \frac{k_B T}{6\pi\eta r_s}, \quad (5-3)$$

where  $k_B$  is Boltzmann's constant,  $T$  is absolute temperature,  $\eta$  is the solvent viscosity, and  $r_s$  is the hydrodynamic radius of the solute.

The relative diffusivities of glucose in human AF tissue at 0% nominal compressive strain are shown in Table 5-1. The average relative diffusivity for all strain levels was  $0.14 \pm 0.02$  for axial specimens, and ranged from 0.088 to 0.17. For circumferential specimens, the relative diffusivity was  $0.13 \pm 0.02$  at 0% nominal strain, ranging from 0.099 to 0.16. And finally, for radial specimens, the relative diffusivity at 0% nominal strain calculated was  $0.11 \pm 0.01$ , and ranged from 0.084 to 0.14.

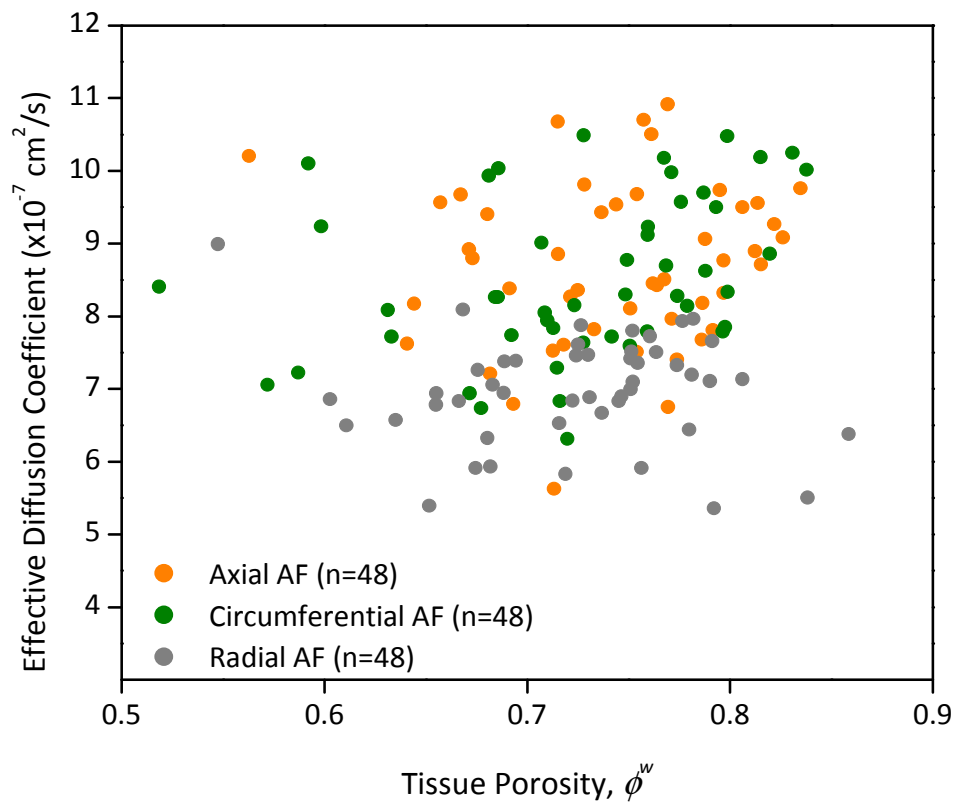


**Figure 5-1:** Relationship between effective diffusivity and tissue porosity for human AF in the three principal directions (axial, circumferential, and radial).

**Table 5-1:** Results for Effective Diffusion Coefficient and Relative Diffusivity for Human AF in the Three Principal Directions

	Strain (%)	Effective Diffusivity ( $\times 10^{-7} \text{ cm}^2/\text{s}$ )	Relative Diffusivity
Axial	$3.06 \pm 3.09\%$	$9.41 \pm 1.00$	$0.15 \pm 0.01$
Circumferential	$4.97 \pm 4.25\%$	$9.29 \pm 1.04$	$0.14 \pm 0.02$
Radial	$2.43 \pm 2.35\%$	$7.44 \pm 0.42$	$0.12 \pm 0.01$

### 5.3 COMPARISON WITH PREVIOUS STUDIES

Many studies have investigated the transport of solutes in IVD tissues. These studies are summarized in Table 5-2; note that results were found using a variety of techniques and at varying temperatures. In general, the diffusivities of small solutes in cartilaginous tissues, such as IVD, have been found to be smaller than their diffusivity in aqueous solution, as was found here (Bonassar et al. 2001; Burstein et al. 1993; Garcia et al. 1996; Gu et al. 2004; Jackson et al. 2008; Jackson et al. 2006; Leddy and Guilak 2003; Maroudas 1975; Quinn et al. 2000; Torzilli et al. 1987; Travascio et al. 2009; Travascio and Gu 2007; Urban et al. 1978; Yuan et al. 2009). Moreover, for small solutes, the relative diffusivities have been found to be in the range of 0.35 to 0.6 (Burstein et al. 1993; Gu et al. 2004; Jackson et al. 2006; Urban 1977).

The results from our study are lower than this reported range. By comparison, a previous study investigating glucose diffusivity in human AF tissue determined the relative diffusivity was approximately 0.28 (Maroudas et al. 1975), which is also below the range reported in the literature, but above the value determined in this study. The differences in findings may result from different measurement techniques. The previous study used a radiotracer method to measure glucose diffusivity using a method similar to

our one-dimensional steady-state diffusion technique. This method for measuring glucose concentrations may differ in precision with our measurements using a glucose assay and spectrophotometer. Furthermore, although the tissues in both studies were from human spines, the study by Maroudas et al. does not provide information regarding the degenerative grade or porosity of the tissue specimens used; this may also account for differences in results.

In general, solute diffusivity decreases as the size of the solute increases; this is apparent from results in Table 5-2. Our results follow this trend; as expected, glucose diffusivity is lower than values reported for smaller molecules, such as lactate, oxygen, water, and ions, and higher than the diffusivity of large molecules such as dextrans. Furthermore, the results found here are similar to those for fluorescein, which is of comparable size to glucose (Travascio et al. 2009; Travascio and Gu 2007).

#### **5.4 SUMMARY**

The results for apparent diffusivity and partitioning of glucose in human annulus fibrosus were combined to calculate the effective diffusivity. Our results are below the range stated in the literature for relative diffusivity of small solutes in cartilaginous tissues. However, they are comparable with previous studies on glucose and similarly-sized molecules (Jackson et al. 2008; Maroudas et al. 1975; Travascio et al. 2009; Travascio and Gu 2007). Additionally, our results fit within the trend of decreasing diffusivity with increased solute size or molecular weight. The results for effective diffusivity of glucose in human AF are necessary for theoretical modeling of nutrient transport in the IVD.

**Table 5-2:** Summary of Experimental Results for Diffusion Coefficient,  $D$ , in IVD from the Literature

Solute	Tissue	$D$ ( $\times 10^{-6}$ cm <sup>2</sup> /s)	Reference
Na <sup>+</sup>	Human lumbar IVD	7.4	(Urban 1977)
	Bovine coccygeal AF	2.75 – 4.4	(Jackson et al. 2006)
Cl <sup>-</sup>	Human lumbar IVD	11.4	(Urban 1977)
	Bovine coccygeal AF	4.25 – 6.75	(Jackson et al. 2006)
Oxygen	Bovine lumbar AF	14.3	(Yuan et al. 2009)
	Porcine lumbar IVD	25	(O'Hare et al. 1991)
Water	Porcine lumbar AF	10.6 – 13.6	(Hsu and Setton 1999)
	Ovine lumbar AF	10.3 – 11.4	(Drew et al. 2004)
	Human lumbar IVD	20.6 – 22.7	(Kealey et al. 2005)
	Human lumbar NP	15.0 – 19.2	(Beattie et al. 2008)
	Human lumbar IVD	10.9 – 16.0	(Kerttula et al. 2001)
	Human lumbar IVD	19.1 – 21.8	(Niinimäki et al. 2009)
SO <sub>4</sub> <sup>-</sup>	Canine IVD	2.78 – 3.89	(Urban et al. 1978)
Lactate	Human lumbar AF	4.86	(Selard et al. 2003)
	Bovine AF	3.4	(Boubriak and Urban 2002)
	Bovine caudal IVD	2.73 – 5.12	(Das et al. 2009)
Glucose	Human lumbar AF	2.5	(Maroudas et al. 1975)
	Bovine coccygeal AF	0.917 – 1.38	(Jackson et al. 2008)
	Human lumbar AF	0.744 – 0.941	Present Study
Fluorescein (332Da)	Bovine coccygeal AF	0.814 – 1.26	(Travascio and Gu 2007)
	Human lumbar AF	0.38 – 2.68	(Travascio et al. 2009)
Dextran (3kDa)	Bovine caudal IVD	0.247	(Das et al. 2009)
Dextran (10kDa)	Bovine caudal IVD	0.171 – 0.173	(Das et al. 2009)
Dextran (40kDa)	Bovine caudal IVD	0.159 – 0.164	(Das et al. 2009)
Dextran (70kDa)	Bovine AF	0.14	(Boubriak and Urban 2002)
	Bovine caudal IVD	0.113 – 0.161	(Das et al. 2009)



## **CHAPTER 6. DEVELOPMENT OF NOVEL METHOD FOR MEASURING OXYGEN-TENSION-DEPENDENT RATE OF GLUCOSE CONSUMPTION BY IVD CELLS**

### **6.1 INTRODUCTORY REMARKS**

Intervertebral disc cells require nutrients to maintain viability and function in the tissue. Although the cell density in the tissue is low, cells require large quantities of energy in order to maintain the extracellular matrix. It has been found that disc cells rely mainly on glycolysis (i.e., anaerobic respiration) in order to produce energy in the form of adenosine triphosphate (ATP) (Holm et al. 1981; Ishihara and Urban 1999). That is, disc cells consume glucose, which is then converted to ATP and lactate through the process of glycolysis; there is a net yield of 2 moles of lactate and 2 moles of ATP per mole of glucose. Hence, it has been found that glucose is the main nutrient necessary for disc cell survival (Bibby et al. 2002; Bibby and Urban 2004; Horner and Urban 2001; Shirazi-Adl et al. 2010).

Despite this, there remains a lack of knowledge regarding the rate of glucose consumption by IVD cells. Several studies have investigated this (see Section 2.5), however, there is a no consensus in the literature as to the effects of oxygen tension levels on glucose consumption rates. This knowledge is necessary in order to better understand the relationship between disc cell functioning and nutrient levels in the IVD. Furthermore, determining the functional relationship between oxygen tension level and glucose consumption rates is necessary for theoretical modeling of the intervertebral disc and accurate prediction of nutritional levels. Therefore, the objective of this study is to develop a new method for measuring the rate of glucose consumption by IVD cells, and

to validate this method by determining the glucose consumption rate by porcine annulus fibrosus and nucleus pulposus cells under various oxygen tension levels.

## 6.2 THEORETICAL APPROACH

In order to determine the rate of glucose consumption by IVD cells, a diffusional uptake problem was used. The Michaelis-Menten equation can be used to describe the relationship between the glucose consumption rate and glucose concentration in the medium (Huang et al. 2007):

$$\frac{dC}{dt} = -R_{glu} = -\frac{V_{max}C}{K_m + C}\rho \quad (6-1)$$

where  $R_{glu}$  is the glucose consumption rate,  $t$  is time,  $C$  is the glucose concentration in culture medium,  $K_m$  is the Michaelis-Menten constant,  $V_{max}$  is the maximum consumption rate per cell and  $\rho$  is the number of cells per volume of solution in the chamber.

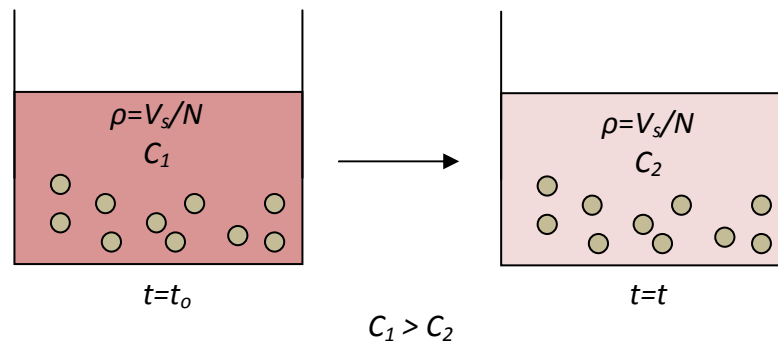


**Figure 6-1:** Schematic showing how consumption rate is measured. Cells are placed in culture media with cell density  $\rho(=V_s/N$ , where  $V_s$  is the volume of media in the chamber, and  $N$  is the number of cells) and initial concentration  $C_1$ ; as cells consume glucose, the concentration in the media decreases to  $C_2$ . The rate is calculated based the change in concentration over time.

Based on this relationship, an analytical solution to the equation can be determined:

$$(K_m + C)dC = -(V_{max}C)\rho dt, \quad (6-2)$$

$$\left(\frac{K_m + C}{C}\right)dC = -(V_{max})\rho dt, \quad (6-3)$$

$$\left(\frac{K_m}{C} + 1\right)dC = -(V_{max})\rho dt. \quad (6-4)$$

Assuming that at  $t = t_o$ ,  $C = C_o$ , and integrating, we have:

$$\int_{C_o}^C \left(\frac{K_m}{C} + 1\right)dC = -\rho \int_{t_o}^t (V_{max})dt, \quad (6-5)$$

$$K_m[\ln(C) - \ln(C_o) + (C - C_o)] = -\rho V_{max}(t - t_o), \quad (6-6)$$

$$\ln\left(\frac{C_o}{C}\right) = \frac{\rho V_{max}}{K_m}(t - t_o) - \frac{(C_o - C)}{K_m}, \quad (6-7)$$

$$t = \frac{K_m}{\rho V_{max}} \ln\left(\frac{C_o}{C}\right) + \frac{C_o - C}{\rho V_{max}} + t_o. \quad (6-8)$$

Hence, by measuring the change in glucose concentration over time and curve-fitting to the analytical solution, we can determine the values of the Michaelis-Menten constants,  $V_{max}$  and  $K_m$ , and calculate the glucose consumption rate from Equation (6-1). Furthermore, by taking measurements at various levels of oxygen tension, we can determine the dependence of the glucose consumption rate by IVD cells on the oxygen levels present.

The above method, curve-fitting the Michaelis-Menten equation, was used to determine the glucose consumption rate by NP cells. However, for AF cells, the

consumption rate was estimated based on a linear curve-fit of glucose concentration change over time. This was due to slower consumption by AF cells, and resulting small change in glucose concentration over the time course of the experiment.

## 6.3 MATERIALS AND METHODS

### 6.3.1 CELL ISOLATION

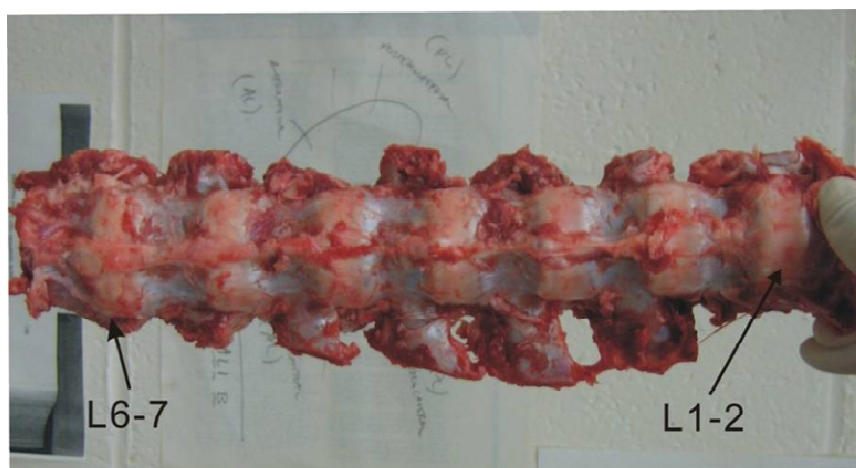
Porcine IVD cells were used in this investigation. Pigs, aged approximately 6 months and weighing ~200 lbs., were obtained from a local slaughterhouse within 1 hour of death. Cell isolation was carried out within 6 hours of death, during which time cells remained viable.

The spine was first isolated from the porcine body using a reciprocating saw and bone-cutting forceps. Excess tissue and ligaments were removed from around the disc tissues. The facet joints were also removed in order to make the IVD easily accessible, see Figure 6-2a. The isolated spine was then washed with PBS solution containing 1% antibiotic-antimycotic (Invitrogen, Corp., Carlsbad, CA) three to four times for 15 minutes each. Following wash, the spine was placed inside a biological safety hood and wiped with 70% isopropyl alcohol in order to minimize contamination.

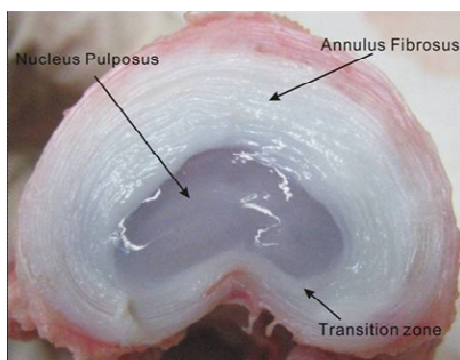
Each disc was opened by making a circular transverse cut through the IVD using a surgical scalpel, see Figure 6-2b. The outer AF and NP regions were extracted, independently, using a scalpel and tweezers. The NP tissue was placed directly into enzyme solution, while the AF tissue was first finely chopped, in order to facilitate tissue digestion, and then placed in enzyme solution. The enzyme solution was made from high glucose (5 g/L) Dulbecco's Modified Eagle's Medium (DMEM, Invitrogen),

supplemented with 15% fetal bovine serum (FBS; Invitrogen) and 1% antibiotic-antimycotic, and containing 1 mg/mL collagenase (Worthington Biochemical Corp., Lakewood, NJ), and 0.6 mg/mL protease (Sigma Chemical, St. Louis, MO). Digestion was carried out for 24 hours on a plate shaker at 37°C, 5% CO<sub>2</sub> and 21% O<sub>2</sub> within an incubator.

Following digestion, media containing released cells were filtered using a 70 µm cell strainer (BD Biosciences, San Jose, CA) in order to isolate cells. Cells were then collected by centrifugation and re-suspended in high glucose DMEM.



(a)



(b)

**Figure 6-2:** (a) Porcine lumbar spine harvested from 3-6 month old pig; (b) transverse view of porcine IVD showing AF, NP and transition zone.

### 6.3.2 CELL – GEL CONSTRUCT PREPARATION

Following release from porcine IVD tissues, cells were encapsulated in a 2% agarose gel construct. This was done in order to maintain cell phenotype for the remainder of the culture period. To prepare constructs, cells were first suspended in DMEM. Suspensions were adjusted to a density of 20 million cells per milliliter of DMEM. A 4% agarose solution was prepared using sterile PBS solution and low melting agarose (Sigma). The isolated cells, suspended in DMEM, were then mixed in a 1:1 volume ratio with agarose gel at 37°C, giving a final concentration of 10 million cells per milliliter in 2% agarose gel. Molds having a diameter of 8 mm and a thickness of 1.5 mm were then used to prepare agarose discs using 100 µL of cell-agarose mixture, see Figure 6-3; each disc contained approximately 1 million cells.

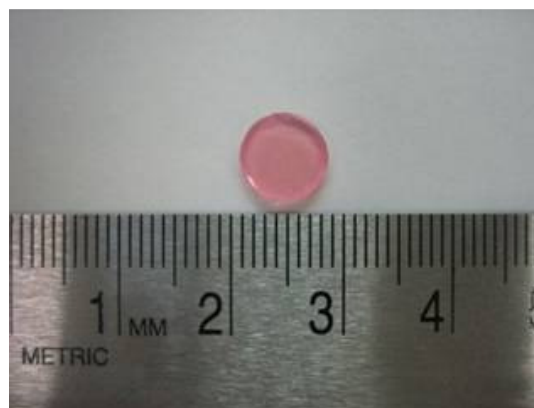


**Figure 6-3:** Cell-gel construct having a diameter of 8 mm and containing approximately 1 million cells in 2% agarose gel.

Once the agarose disc cooled to room temperature, constructs were removed from molds and placed in culture dish. Constructs were cultured with low glucose DMEM (1 g/L glucose) for at least 24 hours at 37°C, 5% CO<sub>2</sub> and 21% O<sub>2</sub>. Culturing the cells at

low glucose concentrations for 24 hours allows the cellular glycogen levels to adjust to low extracellular glucose levels (Bibby 2002). Prior to the start of the experiment, cells were allowed to adjust to oxygen tension levels (for experiments at 5% and 2.5% oxygen tension) overnight (~15 hours).

### *6.3.3 ASSESSMENT OF CELL VIABILITY*

The viability of the cells in the agarose constructs was assessed in order to ensure that cells could remain viable during the timeframe of the experiment. Additional cell-gel constructs were prepared for this purpose using the same protocols as for experimental samples. Constructs were cultured at the same conditions as experimental constructs (i.e., low glucose DMEM solution at 21% O<sub>2</sub>, 5% CO<sub>2</sub>, 37°C). On the day of each experiment, one construct was used to assess viability using a LIVE/DEAD® Viability / Cytotoxicity Assay Kit (Invitrogen). Results showed that cells maintained viability during the experimental time period (data not shown).

### *6.3.4 EXPERIMENTAL SETUP*

Following the pre-incubation period, gels were removed from culture media. Each agarose construct was cut into 4 pieces and placed into a well of a 96-well culture plate. Gels were cut in order to minimize the concentration gradient of both glucose and oxygen across the specimen. Although the size of gel pieces was still on the order of several millimeters, due to the small thickness (~1.5 mm) and fast rate of diffusion of nutrients in 2% agarose gel compared with the relatively slow rate of consumption by disc cells, effects of concentration gradients on metabolic rates were believed to be

negligible. A magnetic micro-stir bar was also placed in the well along with the gels, in order to allow for continuous stirring throughout the experiment for uniform concentration distribution. At the start of the experiment, 200  $\mu\text{L}$  of low glucose DMEM were dispensed into the well. The 96-well plate was then placed on a magnetic stirring plate inside the incubator set to the appropriate oxygen tension level.

At one hour intervals, the culture plate was removed from the incubator and 1.1  $\mu\text{L}$  of solution was collected for glucose concentration measurements, carried out as described in Section 6.3.5. The experiment was continued until the glucose concentration

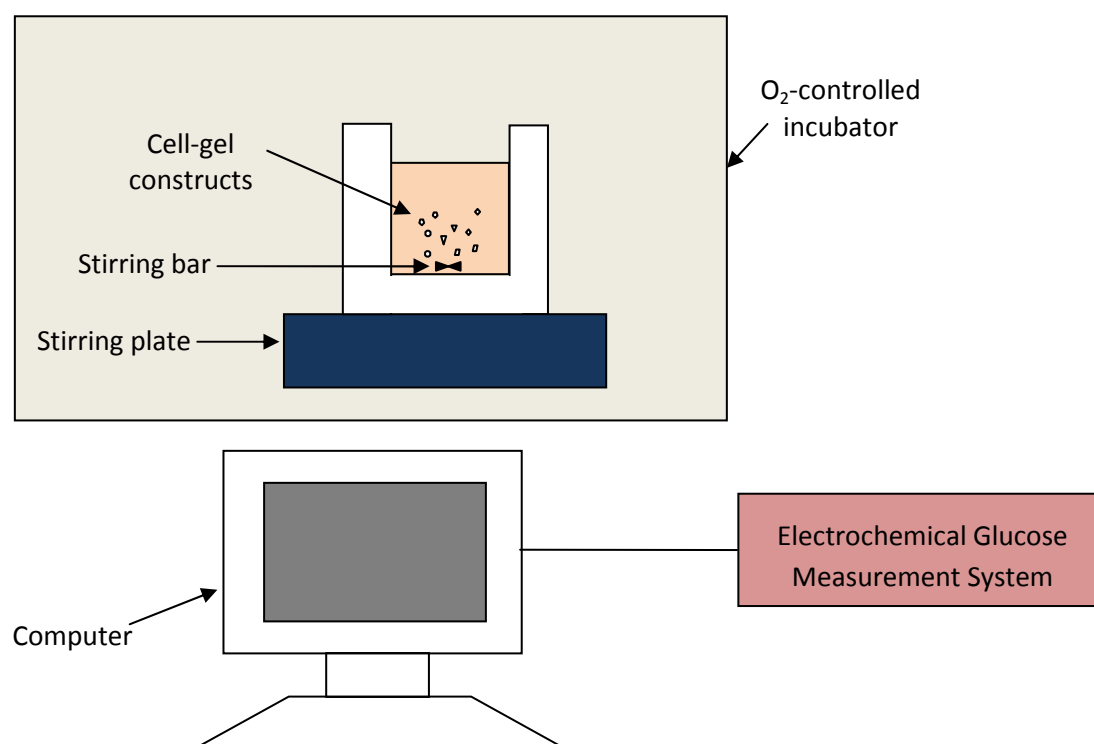


**Figure 6-4:** Schematic showing the basic experimental setup. The chamber was housed in a controlled environment in order to maintain constant oxygen tension, humidity and temperature. There was a free exchange of gas between the culture medium and the inner controlled environment. Glucose concentrations were measured outside the incubator using an electrochemical method connected to data acquisition.



in the chamber was depleted (i.e., less than 0.5 mM). At the end of the experiment, the gels were removed and collected for measurement of DNA content.

#### 6.3.5 MEASUREMENT OF GLUCOSE CONCENTRATION

Glucose concentrations were measured using a modified blood glucose meter (Accu-Chek Aviva, Roche Diagnostics, Indianapolis, IN). The Accu-Chek Aviva system employs an electrochemical method for measuring glucose concentration in solution. The meter and test strips act as a small electrochemical cell that produces an electrical current proportional to the glucose concentration.

Details regarding electrochemical glucose meters and fundamentals of the measurement technique are described in the literature (Heller and Feldman 2008). The electrical current is produced by the oxidation of glucose in the measured solution; this reaction is catalyzed by an enzyme and a mediator molecule that are coated onto the strip. In the case of the Accu-Chek Aviva strips, the enzyme used is pyrrole quinoline quinine glucose dehydrogenase (PQQ-GDH), while the mediator molecule is not disclosed due to proprietary reasons. The enzyme reacts directly with the glucose molecule to remove two available electrons. The mediator molecule accepts the electrons from the enzyme and transports them to the working electrode for measurement. This chain of transfer is illustrated in Figure 6-5.

Each strip contains several elements that allow it to work as a miniature electrochemical cell. Within the solution chamber, strips contain (1) a working electrode, (2) a reference/counter electrode, and (3) chemical reagents necessary for the reaction. The working electrode is generally constructed from an inert material, such as carbon,

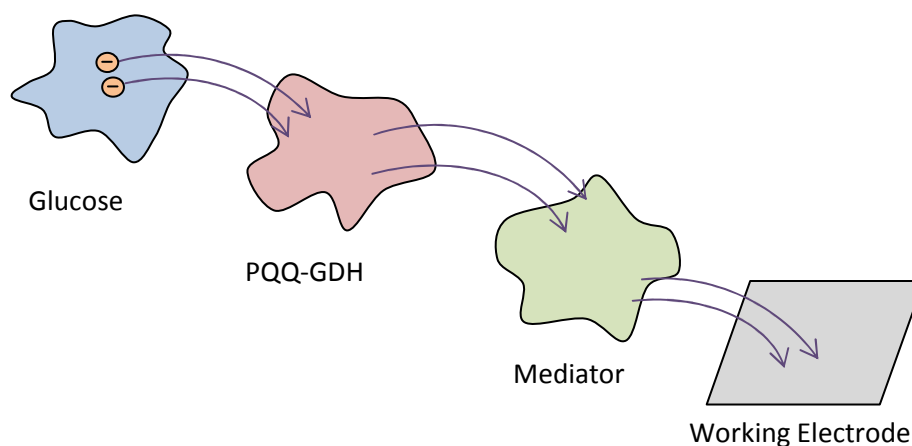


**Figure 6-5:** Schematic illustrating the chain of transport of electrons from the glucose molecule, to the enzyme (here, PQQ-GDH), to the mediator, and finally to the working electrode.

gold or platinum, and serves as the portal through which electrons exit the solution sample and enter the meter for measurement. The reference/counter electrode, generally constructed from Ag/AgCl or an inert material, acts as the portal through which electrons derived from glucose exit the meter and return to the solution sample. The working and reference/counter electrodes are generally minimized, which allows for a smaller sample volume; the configuration of electrodes in the Accu-Chek Aviva test strips is shown in Figure 6-6b. The chemical reagents are deposited, in dry form, over the working electrode. Chemicals include the enzyme and mediator molecules, as well as other reagents that may help to stabilize the enzyme or aid in the solution filling.

The Accu-Chek Aviva strips used here employ an amperometric analysis method for measuring glucose concentrations. Since the concentration can be determined from the peak current value, which can be measured over a short period (5 – 15 seconds), we can quickly obtain results for concentrations measurements. The current level is directly proportional to the glucose concentration in the sample.

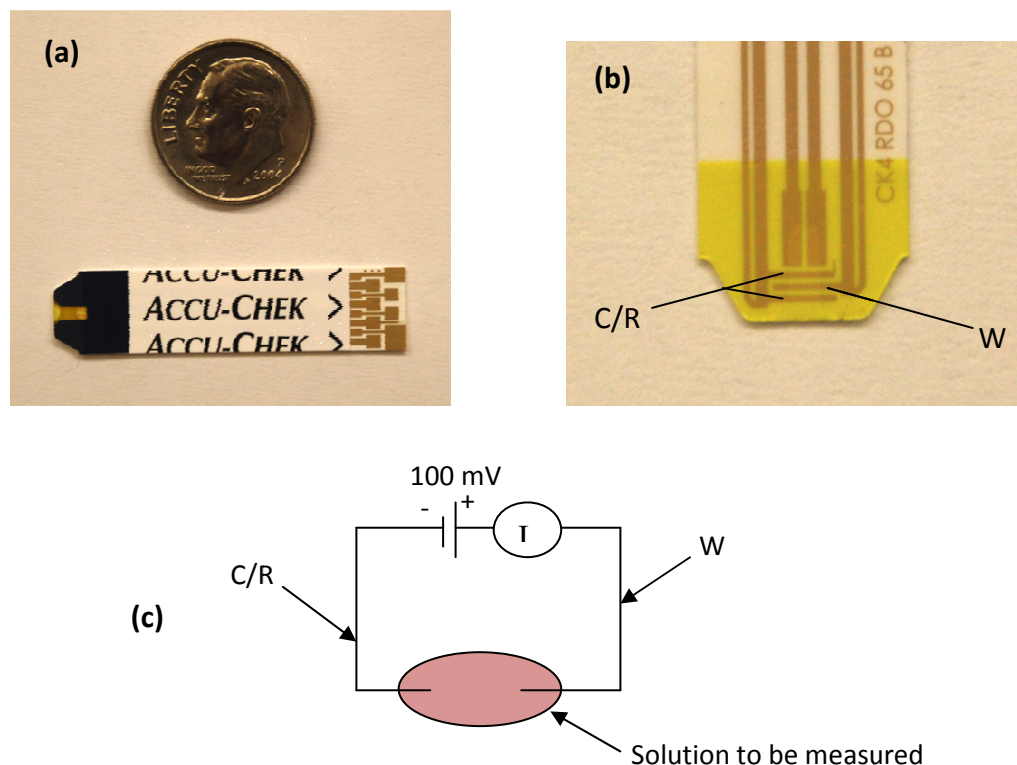


**Figure 6-6:** Photographs showing (a) the Accu-Chek Aviva test strip and relative size; (b) the electrode configuration of the test strip, with working electrode (W) and counter/reference electrode (C/R) labeled; and (c) schematic of electrical circuit, with the working electrode connected to the positive terminal and the counter/reference electrode connected to the negative terminal; a constant 100 mV was applied and the current generated was measured.

In this experiment, we used the Accu-Chek Aviva test strips in combination with a Keithley SourceMeter (Model 2400, Keithley Instruments Inc., Cleveland, OH) in order to measure the current produced. This method was employed due to the need for measurement of very low glucose concentrations. The commercially available Aviva meter has a range of 25 – 345 mg/dl (i.e., 1.4 – 19 mM); however, for measurement of

glucose consumption rates by IVD cells, measurements for concentrations of 0.5 mM or lower are necessary. The lower limit of 1.4 mM was deemed to be a limitation of the meter itself, rather than of the test strips; therefore, the Keithley SourceMeter was used to measure current values produced. The SourceMeter, which has a measurement resolution in the pA range, was capable of measuring currents in the nA range as was the case for glucose concentration measurements.

The SourceMeter was connected to a computer via data acquisition and LabView software (National Instruments Corp., Austin, TX). The working electrode and counter/reference electrodes were connected to the positive and negative terminals of the SourceMeter, respectively. To measure the current, a test strip was placed into the holder (with electrodes connected), and a 100 mV voltage was applied. The peak current produced after 1  $\mu$ L of solution was applied to the test strip was measured.

A calibration curve was used to determine the relationship between glucose concentrations and measured current. Glucose solutions, prepared from DMEM and ranging from 0 to 1 g/L (i.e., 0 to 5.56 mM), were used for calibration. A linear curve-fit was performed using Excel software (Microsoft). An example of a calibration curve is shown in Figure 6-7. A new calibration curve was prepared for each box of glucose strips used, unless strips were manufactured in the same batch (as indicated on the packaging). The linear relationship was then used to calculate glucose concentrations based on current measurements for each experimental sample.

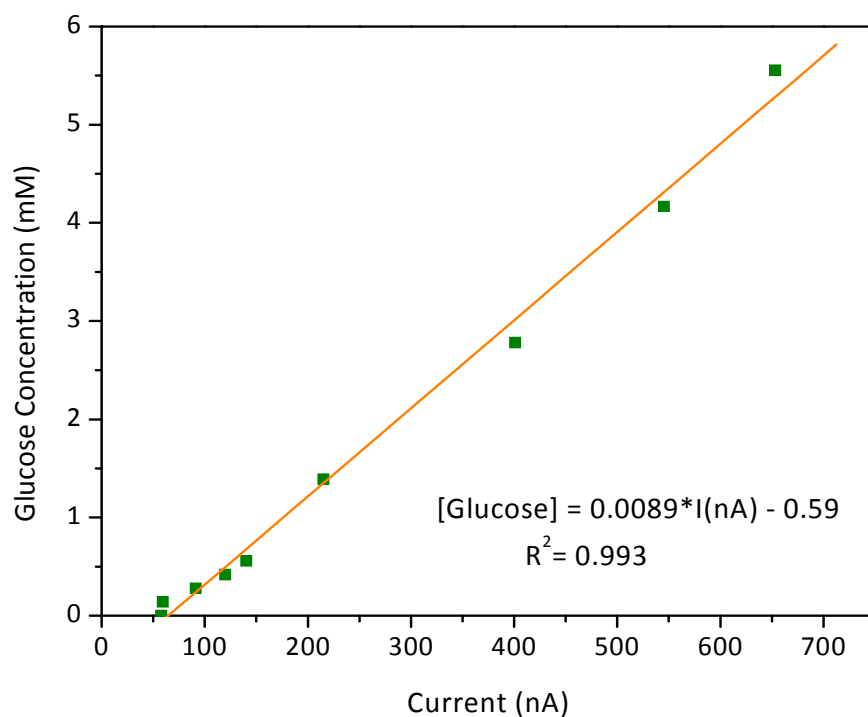


**Figure 6-7:** Example of calibration curve used for calculating glucose concentration from current measurements measured with a constant 100 mV applied voltage.

### 6.3.6 MEASUREMENT OF DNA CONTENT

DNA content was used to normalize experimental results. Cells were first lysed using a lysis buffer containing 15% 1.5 M NaCl, 15% 50 mM EDTA, 1% Triton-X 100 and 10% 100 mM TRIS-Cl at pH 7.4 in distilled, deionized water. Samples with buffer were heated at 65°C for 10 minutes, vortexed to promote breakdown of agarose and cell release, and then heated for an additional 10 min at 65°C. Samples were then centrifuged at 9000 rpm for 15 minutes and the supernatant was collected. The DNA content was measured using a fluorometric assay (Quant-it, Invitrogen).

### 6.3.7 DETERMINATION OF EVAPORATION EFFECT

During incubation throughout the experiment, which lasted for 6 hours or more, evaporation of culture media from the experimental samples occurred. This results in an increase in the concentration of glucose in the media, due to the loss of fluid volume. Quantifying this loss was necessary for accurately determining the glucose consumption rate by cells, based on the change in glucose concentration in the media.

In order to determine the evaporation effect, three (n=3) control wells were included for each experiment. In each well, there was a micro-stir bar, a 2% agarose gel having the same volume as the cell-gel constructs, but without cells, and 200  $\mu$ L of DMEM. The same procedure was followed for the control wells as described in Section 6.3.4 above. The change in glucose concentration over time was monitored to determine a quantitative relationship for the effect of evaporation on measurements. This was incorporated into the glucose concentration measurements for experimental samples, in order to correct for the evaporation.

### 6.3.8 CALCULATION OF GLUCOSE CONSUMPTION RATE

Following completion of the experiment, data for change in glucose concentration versus time were used to determine the rate of glucose consumption by IVD cells. For AF cells, a linear curve-fit of glucose concentration measurements over time was performed using Excel software; the consumption rate was determined from the slope of the line. For NP cells, the data was curve-fit to Equation (6-8) using MATLAB 6.5 (MathWorks, Natick, MA) to determine values for  $V_{max}$  and  $K_m$ . The consumption rate could then be calculated based on Equation (6-1).

### 6.3.9 STATISTICAL ANALYSES

A total of 5 gel constructs (n=5) were used to measure the glucose consumption rate of IVD cells for each of six groups (i.e., 2 cell groups [AF and NP] and 3 levels of oxygen tension [2.5%, 5% and 21%]), for a total of 30 tests. For each NP sample, the values of  $K_m$  and  $V_{max}$  were determined via curve-fitting, while the rate of consumption was determined by linear curve-fit for AF samples, see Section 6.3.8. A one-way ANOVA analysis of variance was performed to determine if differences between  $K_m$  and  $V_{max}$  for the different NP groups were statistically significant. Post-hoc analysis (Tukey test) was performed to determine between which groups differences were significant. The same analysis was performed to determine if the difference between consumption rates for AF cells of different groups were significant. Two-way ANOVA was performed to determine if differences in the consumption rates of AF and NP cells at various oxygen tension levels were significant; rate of consumption for NP cells was calculated based on Equation (6-1). A student's t-test was used to determine if rates of consumption for AF and NP cells varied significantly (2 groups of n=15 each). All analyses were performed using SPSS 11.5 statistical software. For all statistical analyses, the significance level was set to  $p < 0.05$ . All data are given in mean  $\pm$  standard deviation.

## 6.4 RESULTS

The glucose consumption rate by porcine AF and NP cells was determined at three different levels of oxygen tension (2.5%, 5%, and 21%). For NP cells, the values of the Michaelis-Menten constants,  $K_m$  and  $V_{max}$ , were determined by curve-fitting experimental data. Results are shown in Table 6-1 and in Figure 6-8. Values for  $V_{max}$

have been normalized by DNA content and are expressed in nmol/hr/ $\mu$ g DNA. One-way ANOVA analysis did not show significance differences for values of  $V_{max}$  ( $p=0.078$ ) or  $K_m$  ( $p=0.39$ ) for different levels of oxygen tension. Post-hoc analysis showed that there were no statistically significant differences between any groups for either  $V_{max}$  or  $K_m$  values.

For AF groups, the consumption rates determined are shown in Figure 6-9. Values have been normalized by DNA content and are expressed in nmol/hr/ $\mu$ g DNA. One-way ANOVA showed that the consumption rate of glucose by porcine AF cells is significantly affected by the oxygen tension level. Furthermore, post-hoc analysis showed that the consumption rates at 2.5% and 5% oxygen tension were significantly lower than that at 21% oxygen tension, but did not differ significantly from each other.

Using values determined for  $V_{max}$  and  $K_m$  for NP cells, the consumption rate at 5 mM glucose was calculated based on Equation (6-1) and used to compare with the results for consumption rate of AF cells. These results are shown in Figure 6-9. Two-way ANOVA showed that both oxygen tension level and cell type significantly affected the consumption rate of cells. Student's t-test analysis showed that the consumption rate for NP cells was significantly higher than that for AF cells.

**Table 6-1:** Results for  $V_{max}$  and  $K_m$  for Porcine NP Cells at Varying Oxygen Levels

O <sub>2</sub> Level	$V_{max}$ (nmol/hr/ $\mu$ g DNA)	$K_m$ (mM)
2.5%	482.4 $\pm$ 212.9	0.46 $\pm$ 0.23
5%	425.9 $\pm$ 98.1	0.70 $\pm$ 0.54
21%	269.6 $\pm$ 47.5	0.36 $\pm$ 0.39



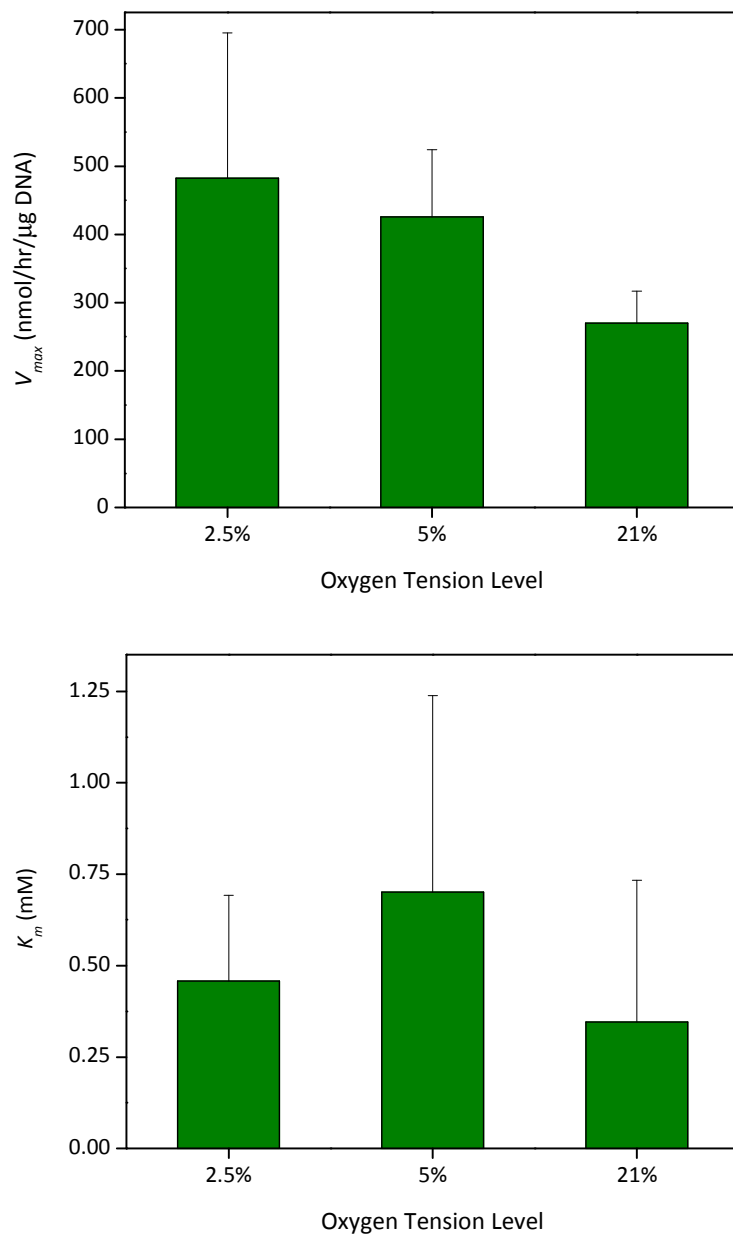


**Figure 6-8:** Results for  $V_{max}$  and  $K_m$  for porcine NP cells at three oxygen tension levels: 2.5%, 5%, and 21%.

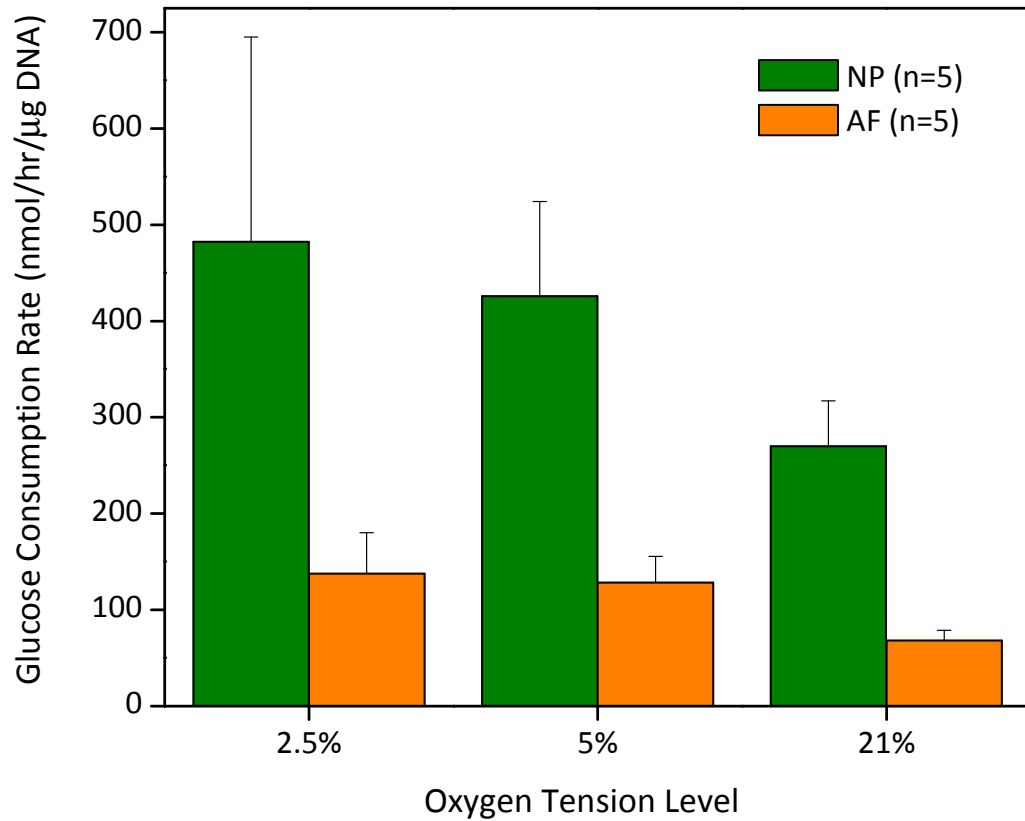


**Figure 6-9:** Comparison of glucose consumption rates for porcine AF and NP cells at varying oxygen tension levels. For NP cells, consumption rates were calculated at 5 mM glucose concentrations based on values for  $V_{max}$  and  $K_m$  determined and Equation (6-8).

## 6.5 DISCUSSION

The major objective of this study was to develop a new method for determining the rate of glucose consumption by IVD cells. This method was then employed to measure the oxygen-tension dependence of the glucose consumption rate by porcine AF and NP cells. Our results for consumption rate by porcine AF and NP cells are discussed in detail below, including comparisons with previous studies in the literature.

### 6.5.1 COMPARISON OF CONSUMPTION RATES WITH STUDIES IN THE LITERATURE

The findings of this investigation for the rate of glucose consumption by IVD cells are comparable with previous findings in the literature for IVD cells. A previous study by Guehring et al. found that the glucose consumption rate by notochordal NP cells was 205 nmoles/million cells/hr at 21% oxygen tension (Guehring et al. 2009). These results are similar to those found in this study. For each experiment, approximately one million cells were used; converting our results, we find an averaged maximum consumption rate of approximately 216 nmoles/million cells/hr at 21% oxygen tension. Furthermore, Bibby found that glucose consumption by bovine NP cells ranged from approximately 20 to 120 nmols/million cells/hr, depending on the glucose concentration (Bibby 2002). Comparison with our results for other studies in the literature for IVD cells is difficult due to the lack of knowledge on cell density used in experiments (Holm et al. 1982; Ishihara and Urban 1999); however, the trends found in these studies are discussed in more detail below.

Only few studies have used the Michaelis-Menten relationship to describe glucose consumption by IVD cells and chondrocytes. Guehring et al. found that the value of  $K_m$

for notochordal NP cells was 0.199 mM, compared with our averaged value of 0.51 mM (Guehring et al. 2009). Alternatively, a study of articular chondrocytes found the value of  $K_m$  to be 0.35 mM, which similar to our results (Windhaber et al. 2003). Differences in values determined for  $K_m$  may be due to the techniques used. For the method described here, concentration values are measured every sixty minutes; however, in order to accurately detect the value for  $K_m$ , more frequent measurements may be necessary.

#### 6.5.2 EFFECT OF OXYGEN TENSION LEVEL ON GLUCOSE CONSUMPTION RATE

In this study, we found that the rate of glucose consumption by IVD cells increases as the oxygen level decreases; hence, there was a positive Pasteur effect (i.e., an increase in the glycolysis rate under low oxygen tension). The dependence of the glucose consumption rate on oxygen tension can be seen in Figure 6-10. Our findings are in agreement with a recent study, which reported that the rate of lactate production increased at low level of oxygen for notochordal NP cells (i.e., porcine NP cells) (Guehring et al. 2009). Note that the rate of glucose consumption is related to the lactate production rate by a ratio of 1:2. Additionally, two other previous studies have also reported similar results for NP cells (Holm et al. 1981; Ishihara and Urban 1999). However, one study in the literature found a negative Pasteur effect for bovine NP cells (Bibby et al. 2005). It should be noted, however, that the bovine NP cells used in the study by Bibby et al. were more mature than the porcine cells used here. Notochordal cells in the nucleus disappear with age, and NP cells become more chondrocyte-like with maturation. This difference in cell phenotype may account for the varied behavior of the cells in these two studies. Additionally, differences in experimental conditions may also

account for differences. A negative Pasteur effect has also been shown to exist for articular chondrocytes (Lee and Urban 1997).

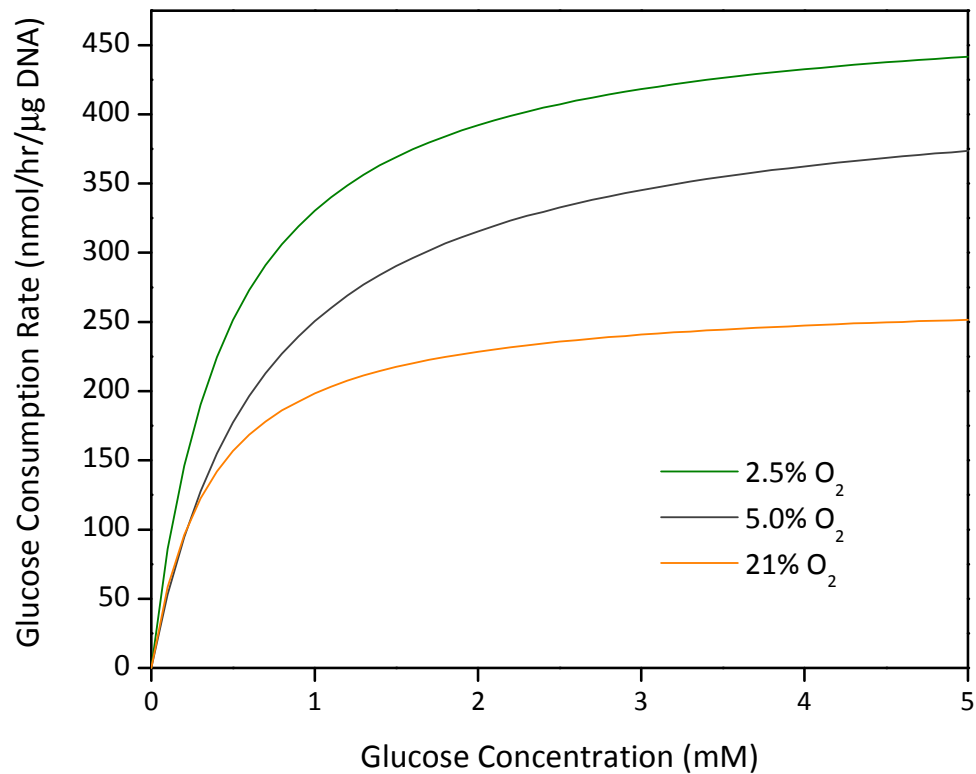


**Figure 6-10:** Comparison of glucose consumption rates for porcine NP cells at varying oxygen tension levels, calculated based on values for  $V_{max}$  and  $K_m$  determined and Equation (6-8).

Our finding of a positive Pasteur effect for porcine AF cells is in agreement with previous studies in the literature, which found that, as oxygen tension levels decreased, the rate of lactate production by bovine (Ishihara and Urban 1999) and canine (Holm et al. 1982) AF cells increased. One previous study showed that lactate production at high oxygen tension (i.e., 10% to 21%) was lower than that at low oxygen tension (1% to 5%), while no difference was found between the lactate production rates for oxygen tension levels below 5% (Ishihara and Urban 1999). This is in agreement with the findings of this study.

The positive Pasteur effect found in this study suggests that the IVD cells are able to adapt themselves to local nutrient concentrations in order to maintain energy production. At higher levels of oxygen, the cells may go through aerobic oxidation in order to produce the energy necessary to maintain the disc extracellular matrix. On the other hand, in the absence of oxygen, cells may “switch” to glycolysis, or anaerobic respiration, to meet energy demand. Indeed, our previous study showed that the rate of oxygen consumption by porcine IVD cells decreases as the oxygen tension level decreases (Huang et al. 2007), which is similar to earlier studies in the literature (Bibby et al. 2005; Holm et al. 1981; Ishihara and Urban 1999).

Our findings have important implications for better understanding the metabolism of disc cells. Disc cells are in a hypoxic environment *in vivo*, and cells likely rely on glycolysis for energy production since oxygen tension levels are very low. This validates the finding that cells require glucose to survive (Bibby and Urban 2004; Guehring et al. 2009; Horner and Urban 2001). As the disc ages, supply of glucose to disc cells becomes hindered. Therefore, since disc cells rely on glucose, they may not receive an adequate

supply to produce the energy necessary to maintain and repair the extracellular matrix of the disc via anaerobic metabolism. This, in turn, would result in degenerative changes to the tissue, and a subsequent loss of functioning.

### *6.5.3 DIFFERENCE IN GLUCOSE CONSUMPTION RATE FOR NP AND AF CELLS*

In this study, we found that the rate of glucose consumption by porcine AF cells was significantly lower than that by NP cells for all oxygen tension levels investigated. Only a few studies in the literature have investigated the metabolic rate of AF cells (Guehring et al. 2009; Holm et al. 1981; Holm et al. 1982), with mixed results. Guehring et al. showed that the rate of lactate production by both mature (bovine) and notochordal (porcine) AF cells was higher than that of NP cells (Guehring et al. 2009). In contrast, Holm et al. found the opposite trend, with the lactate production rate by NP cells from canine lumbar discs being higher than that of AF cells (Holm et al. 1982). Finally, Ishihara and Urban found that lactate production by bovine outer AF cells was higher than that by NP cells at low oxygen tensions, but lower at high oxygen tension levels (Ishihara and Urban 1999). The varied findings of these studies may result from differing experimental conditions, as well as the use of cells from different animal discs and at different stages of maturation. Our results are in agreement with those of Holm et al.

The difference in glucose consumption rates by AF and NP cells may be attributed to differences in cell phenotypes. NP cells are notochordal-derived, while AF cells are derived from the mesenchyme. As a result, these cells exhibit differences in cell morphology, phenotypic expression, and matrix production (Chelberg et al. 1995; Chen

et al. 2006; Chiba et al. 1997; Flagler et al. 2009; Horner et al. 2002; Maldonado and Oegema, Jr. 1992; Melrose et al. 2001; Urban et al. 2000; Wang et al. 2001). In this study, we used porcine IVDs from young pigs, in which the NP cells are notochordal (as opposed to more mature tissue, in which notochordal cells have disappeared). Therefore, the differences between metabolic rates of the two cell types likely result from differences in cell types. Indeed, our previous study found that the oxygen consumption rate by porcine NP cells was significantly higher than that by AF cells (Huang et al. 2007). These results suggest that notochordal NP cells are more metabolically active than AF cells.

The findings of this investigation provide important information necessary for understanding and predicting nutrient distributions in the IVD *in vivo*. Since IVD cells receive nutrients from the surrounding vasculature, concentration gradients across the tissue exist, with the concentration of glucose and oxygen falling moving away from the supply at the periphery. These gradients are coupled to the rate of nutrient consumption by disc cells; that is, the faster cells consume nutrients, the steeper the concentration gradient. Therefore, understanding how cells in different regions of the disc (i.e., AF and NP) consume nutrients is important for predicting the distributions in the tissue. Furthermore, this knowledge provides important insight into nutritional pathways in the IVD.

#### 6.5.4 EXPERIMENTAL LIMITATIONS

In this study, we investigated the rate of glucose consumption by porcine IVD cells. As has been mentioned, porcine NP cells are notochordal, and therefore differ from



adult human IVD cells. This difference in phenotype likely influences the metabolism of the two cells types. Therefore, it is expected that the rate of glucose consumption by human NP cells would differ from that of porcine NP cells, and thus should be investigated further.

The consumption rate of AF cells in this study was measured over a relatively small range of glucose concentrations. As a result, values for  $V_{max}$  and  $K_m$  could not be determined for AF cells. Therefore, we have not determined a relationship between the rate of glucose consumption by AF cells and the concentration of glucose (i.e., a Michaelis-Menten relationship). Better understanding of this relationship is necessary for more accurate prediction of nutrient distributions in the disc, as discussed later in Chapter 7. Hence, the glucose consumption rate by AF cells should be further studied to determine this functional relationship.

In the experimental setup developed for this study, cells had to be removed from the oxygen-controlled incubator periodically in order to collect samples for glucose concentration measurements. As a result, the oxygen environment changed during the experiment. However, due to the very low solubility of oxygen in solution, it is not likely that the dissolved oxygen concentration in the media was significantly altered during the approximately 1-2 minutes that the cells were removed from the incubator for measurement. Nonetheless, the use of a glove box, or other closed environment, would allow for constant oxygen tension environment throughout the experiment, and may lead to more accurate results; conversely, the development of a continuous, online probe to measure glucose concentrations over the course of the experiment may also provide increased accuracy. Furthermore, the use of either of these experimental methods would

allow for more frequent measurement of glucose concentrations, thereby providing greater accuracy in curve-fitting and determination of Michaelis-Menten constants.

Furthermore, during the experiment some media was lost due to evaporation, as discussed in Section 6.3.7. In addition to this, the volume of solution in the chamber decreased during the experiment due to solution extraction for concentration measurements. We have determined that evaporation results in an approximate 1% decrease in media volume for each hour of the experiment ( $\sim 3\mu\text{L}$ ). And, as mentioned,  $1.1\ \mu\text{L}$  of media was extracted each hour for concentration measurement. We have corrected for the evaporation effect in the calculation of the consumption rate by the cells; however, the change in volume due to solution extraction has not been accounted for. Since the original volume of media in the chamber ( $300\ \mu\text{L}$ ) was comparatively large, this change in volume is expected to have negligible effects on calculated values for the consumption rate of IVD cells. Nonetheless, in future experiments, this factor should be taken into account for more accurate calculations.

Due to low cell density in IVD tissue coupled with the large number of cells needed to carry out the experiment, only five samples were investigated for each experimental group. Because of large sample variation, trends found here, although apparent, were not always statistically significant. Therefore, more studies should be conducted in order to better understand the trends for glucose metabolism by IVD cells.

Finally, it should be noted that the cells used for these experiments were isolated from the AF and NP tissue for measurements. Cells were cultured in three-dimensional agarose constructs, which has been shown to maintain phenotype (Gruber et al. 1997; Gruber et al. 2004). However, by isolating cells, the cell-matrix interactions are

disrupted, and the extracellular environment is markedly changed (Bibby 2002). This may alter the behavior of disc cells, thereby changing their metabolic activity. Hence, actual *in vivo* rates of glucose metabolism by AF and NP cells may differ from those described here. However, in order to minimize nutrient gradients and determine consumption rates at the cellular level (rather than at the tissue level), cell isolation was necessary. Additional studies should be conducted to further investigate IVD cellular metabolism for cells within the native disc extracellular matrix.

## 6.6 SUMMARY AND CONCLUSIONS

In this study, we developed a new technique for determining the rate of glucose consumption by IVD cells. We validated this technique by measuring the oxygen tension-dependent rate of glucose consumption by porcine annulus fibrosus and nucleus pulposus cells. Our results show a positive Pasteur effect in both AF and NP cells, indicating that the glucose consumption rate increases as the oxygen tension level is lowered. This finding is in agreement with several studies in the literature (Guehring et al. 2009; Holm et al. 1982; Ishihara and Urban 1999). Furthermore, we also determined that the rate of glucose consumption by AF cells is significantly lower than that by NP cells, which is similar to a previous study in canine discs (Holm et al. 1982). These findings provide important insight into better understanding the metabolism and nutrition by IVD cells, and its relationship to disc degeneration.

## CHAPTER 7. INVESTIGATION OF GLUCOSE DISTRIBUTIONS IN THE INTERVERTEBRAL DISC USING THREE-DIMENSIONAL FINITE ELEMENT ANALYSIS

### 7.1 INTRODUCTORY REMARKS

The intervertebral disc is a complex, highly organized structure that functions to support loads and allows flexibility in the spine. Due to the difficulty in investigating the distribution of important nutrients, such as glucose, *in vivo*, theoretical modeling can be a helpful tool to supplement *in vitro* studies in order to better understand the *in vivo* conditions in the disc. Several investigators have presented theoretical models of the disc in order to investigate the mechanical behavior of the tissue, without the inclusion of cellular metabolism, see review in (Yao and Gu 2006). More recent models of the IVD have incorporated nutrient concentrations coupled to metabolic rates, but have either presented an axisymmetric disc geometry, or have not included mechanical loading configurations (Huang and Gu 2008; Magnier et al. 2009; Selard et al. 2003; Shirazi-Adl et al. 2010; Soukane et al. 2005; Soukane et al. 2007; Soukane et al. 2009).

In order to accurately predict the nutrient distributions in the IVD, theoretical models must incorporate each of three main elements: (1) three-dimensional (3D) anatomical disc geometry; (2) nutrient concentrations coupled to cellular metabolic rates; and (3) *in vivo* mechanical loading conditions along with strain-dependent tissue properties. The aim of this study is to develop a finite element model of the disc which includes all of these aspects. Using this newly developed model, we will investigate the effects of endplate calcification, simulated by reduced endplate permeability, and *in vivo* mechanical loading conditions on the glucose distributions in the IVD. Furthermore, we also incorporate cell viability criteria into the model, based on threshold glucose levels in

the tissue; we then analyze the effect of disc degeneration and static compression on the glucose distributions and cell viability in the IVD.

## 7.2 THEORETICAL MODEL

The theoretical framework based on the triphasic theory has been extended to a new formulation (Gu et al. 1998; Huang and Gu 2008; Lai et al. 1991; Yao and Gu 2004). The following governing equations were based on the balance of linear momentum for the mixture and the conservation of mass for each of the phases or solute species:

$$\nabla \cdot \sigma = 0, \quad (7-1)$$

$$\nabla \cdot (v^s + J^w) = 0, \quad (7-2)$$

$$\frac{\partial(\phi^w c^\alpha)}{\partial t} + \nabla \cdot (J^\alpha + \phi^w c^\alpha v^s) = Q^\alpha, \quad (7-3)$$

where  $\sigma$  is the total stress of the mixture,  $v^s$  is the velocity of the solid phase,  $J^w$  and  $J^\alpha$  are the molar fluxes of the water and solute  $\alpha$  phases, respectively, relative to the solid phase,  $\phi^w$  is the tissue porosity (water volume fraction),  $c^\alpha$  is the concentration (per unit water volume) of solute  $\alpha$ , and  $Q^\alpha$  is the cellular metabolic rate of solute  $\alpha$  per unit tissue volume. Note that, in Equation (7-3), nutrient concentrations are coupled to cellular metabolic rates.

In this study, three neutral solutes (glucose, oxygen (O<sub>2</sub>), and lactate), sodium ion (+) and chloride ion (-) were considered. Charged ions were included as a necessary balance to the fixed negative charges on the solid matrix. Therefore, Equation (7-3) above expands to Equations (7-4) – (7-6) for the solutes (i.e.,  $\alpha = +, -, O_2, \text{glu}, \text{and lac}$ ):

$$\frac{\partial(\phi^w c^+)}{\partial t} + \nabla \cdot (J^+ + \phi^w c^+ v^s) = 0, \quad (7-4)$$

$$\frac{\partial(\phi^w c^-)}{\partial t} + \nabla \cdot (J^- + \phi^w c^- v^s) = 0, \quad (7-5)$$

$$\frac{\partial(\phi^w c^{O_2})}{\partial t} + \nabla \cdot (J^{O_2} + \phi^w c^{O_2} v^s) = Q^{O_2}, \quad (7-6)$$

$$\frac{\partial(\phi^w c^{glu})}{\partial t} + \nabla \cdot (J^{glu} + \phi^w c^{glu} v^s) = Q^{glu}, \quad (7-7)$$

$$\frac{\partial(\phi^w c^{lac})}{\partial t} + \nabla \cdot (J^{lac} + \phi^w c^{lac} v^s) = Q^{lac}. \quad (7-8)$$

The pH-dependent (Bibby et al. 2005) consumption rate of oxygen ( $Q^{O_2}$ ) was based on the literature (Huang et al. 2007) :

$$Q^{O_2} = -\frac{V'_{max}(pH - 4.95)c^{O_2}}{K'_m(pH - 4.95) + c^{O_2}}\rho^{cell}, \quad (7-9)$$

where  $c^{O_2}$  is expressed in  $\mu\text{M}$ ,  $V'_{max} = 5.27$  nmol/million cells-hr for NP cells and 3.64 nmol/million cells-hr for AF cells,  $K'_m = 3.4$   $\mu\text{M}$  for NP cells and 12.3  $\mu\text{M}$  for AF cells, and  $\rho^{cell}$  is the cell density. The rate of production of lactate ( $Q^{lac}$ ) was based on that of NP cells in the literature (Bibby et al. 2005):

$$Q^{lac} = \exp\left(-2.47 + 0.93 \times pH + 0.16 \times c^{O_2} - 0.0058 \times c^{O_2^2}\right)\rho^{cell}, \quad (7-10)$$

where  $c^{O_2}$  is expressed in kPa. The oxygen concentration can be converted between kPa and  $\mu\text{M}$  using the solubility of oxygen in water (i.e.,  $1.0268 \times 10^{-6}$  mol/kPa – 100 mL) (Huang and Gu 2008; Soukane et al. 2005). For sodium and chloride ions, the metabolic rates were assumed to be zero. The rate of glucose consumption is based on the

assumption that glucose is primarily consumed through the process of glycolysis, in which one molecule of glucose is broken down into two lactic acid molecules; therefore, the rate of glucose consumption ( $Q^{glu}$ ) was:

$$Q^{glu} = -0.5 * Q^{lac}. \quad (7-11)$$

An approximate linear relationship between pH and lactate was used to calculate the pH within the IVD (Bibby et al. 2005; Soukane et al. 2005):

$$pH = (-0.1 \text{ mM}^{-1})c^{lac} + 7.5 \quad (0 < c^{lac} < 30\text{mM}). \quad (7-12)$$

In this model, strain-dependent tissue properties were taken into consideration. The tissue porosity, or water volume fraction, is related to the tissue dilatation,  $e$ , and the tissue porosity at reference configuration (i.e.,  $e = 0$ ) by (Lai et al. 1991):

$$\phi^w = \frac{\phi_o^w + e}{1 + e}. \quad (7-13)$$

The hydraulic permeability,  $k$ , of the tissue was calculated based on the constitutive equation (Gu et al. 2003):

$$k = a \left( \frac{\phi^w}{1 - \phi^w} \right)^n, \quad (7-14)$$

where  $a$  and  $n$  are material constants previously determined for gels and cartilaginous tissues. The diffusivity of solute  $\alpha$ ,  $D^\alpha$ , was estimated based on the constitutive relationship (Gu et al. 2004):

$$\frac{D^\alpha}{D_o^\alpha} = \exp \left[ -A \left( \frac{r^\alpha}{\sqrt{k}} \right)^B \right], \quad (7-15)$$

where  $D_o^\alpha$  is the diffusivity of solute  $\alpha$  in aqueous solution,  $r^\alpha$  is the hydrodynamic radius of solute  $\alpha$ , and  $A$  and  $B$  are material constants previously determined for agarose gel and IVD tissues. Values for  $D_o^\alpha$  and  $r^\alpha$  for solutes included are shown in Table 7-1 (Huang and Gu 2008).

**Table 7-1:** Diffusivity in Aqueous Solution and Hydrodynamic Radius of Solutes Used in Model

	$D_o^\alpha$ (m <sup>2</sup> /s)	$r^\alpha$ (nm)
Glucose	$9.2 \times 10^{-10}$	0.3
Oxygen	$3.0 \times 10^{-9}$	0.1
Lactate	$1.28 \times 10^{-9}$	0.255

The averaged glucose concentration,  $\bar{c}^{glu}$ , in AF and NP regions was determined by:

$$\bar{c}^{glu} = \frac{\int_V c^{glu} dV}{V} \quad (7-16)$$

where  $V$  is the volume of the disc region (i.e., AF or NP).

### 7.3 FINITE ELEMENT FORMULATION

In this study, we considered a 3-D anatomical geometry based on that of an L2-L3 IVD (Thompson degenerative grade I) harvested from the lumbar spine of a 41 year-old male (Figure 7-1a). The IVD was modeled as an inhomogeneous material consisting of



three distinct regions: AF, NP and CEP. The AF and NP regions were considered to have a uniform thickness of  $h = 10$  mm. The CEP had a thickness of  $h = 0.6$  mm and was considered to be permeable above the NP region only (i.e., completely calcified, or impermeable, above the AF). Due to symmetry with respect to the plane  $x = 0$  and the plane  $z = 0$ , only the upper right quadrant of the disc was modeled (Figure 7-1d).

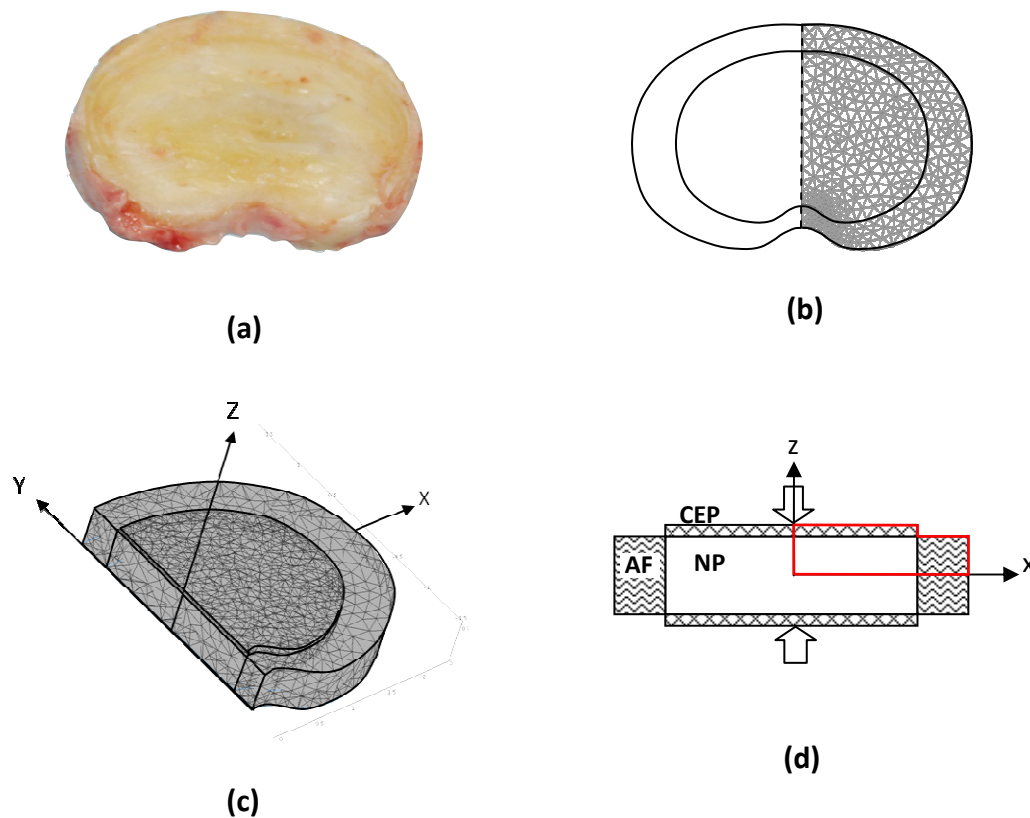


**Figure 7-1:** (a) Photograph of L2-L3 IVD used for determining disc geometry; (b) disc geometry; (c) disc mesh; (d) test configuration.

The FEM formulation was based on the work by Sun et al. (1999) (Sun et al. 1999). The standard Galerkin weight residual method was used to construct the finite element formulation. The weak form is given by:

$$\int_{\Omega} \mathbf{w} \cdot \nabla \cdot \boldsymbol{\sigma} d\Omega = 0 \quad (7-17)$$

$$\int_{\Omega} w^{(1)} [\nabla \cdot (\mathbf{v}^s + \mathbf{J}^w)] d\Omega = 0 \quad (7-18)$$

$$\int_{\Omega} w^{(2)} \left[ \frac{\partial(\phi^w c^+)}{\partial t} + \nabla \cdot (J^+ + \phi^w c^+ v^s) \right] d\Omega = 0 \quad (7-19)$$

$$\int_{\Omega} w^{(3)} \left[ \frac{\partial(\phi^w c^-)}{\partial t} + \nabla \cdot (J^- + \phi^w c^- v^s) \right] d\Omega = 0 \quad (7-20)$$

$$\int_{\Omega} w^{(4)} \left[ \frac{\partial(\phi^w c^{o_2})}{\partial t} + \nabla \cdot (J^{o_2} + \phi^w c^{o_2} v^s) - Q^{o_2} \right] d\Omega = 0 \quad (7-21)$$

$$\int_{\Omega} w^{(5)} \left[ \frac{\partial(\phi^w c^{glu})}{\partial t} + \nabla \cdot (J^{glu} + \phi^w c^{glu} v^s) - Q^{glu} \right] d\Omega = 0 \quad (7-22)$$

$$\int_{\Omega} w^{(6)} \left[ \frac{\partial(\phi^w c^{lac})}{\partial t} + \nabla \cdot (J^{lac} + \phi^w c^{lac} v^s) - Q^{lac} \right] d\Omega = 0 \quad (7-23)$$

where vector  $\mathbf{w}$  and six scalar functions  $w^{(1)}$ ,  $w^{(2)}$ ,  $w^{(3)}$ ,  $w^{(4)}$ ,  $w^{(5)}$  and  $w^{(6)}$  are arbitrary admissible weighting functions for the seven governing equations. Applying the divergence theorem, we obtain:

$$\int_{\Omega} \text{tr}[(\nabla \mathbf{w})^T \cdot \boldsymbol{\sigma}] d\Omega = \int_{\Gamma_t} \mathbf{w} \cdot \mathbf{t}^* d\Gamma \quad (7-24)$$

$$\int_{\Omega} w^{(1)} \nabla \cdot \mathbf{v}^s d\Omega - \int_{\Omega} \mathbf{J}^w \cdot \nabla w^{(1)} d\Omega = - \int_{\Gamma_{J^w}} w^{(1)} \mathbf{J}^{w*} \cdot \mathbf{n} d\Gamma \quad (7-25)$$

$$\begin{aligned} \int_{\Omega} w^{(2)} \frac{\partial(\phi^w c^+)}{\partial t} d\Omega - \int_{\Omega} \mathbf{J}^+ \cdot \nabla w^{(2)} d\Omega + \int_{\Omega} w^{(2)} \nabla \cdot (\phi^w c^+ \mathbf{v}^s) d\Omega = \\ - \int_{\Gamma_{J^+}} w^{(2)} \mathbf{J}^{+*} \cdot \mathbf{n} d\Gamma \end{aligned} \quad (7-26)$$

$$\begin{aligned} \int_{\Omega} w^{(3)} \frac{\partial(\phi^w c^-)}{\partial t} d\Omega - \int_{\Omega} \mathbf{J}^- \cdot \nabla w^{(3)} d\Omega + \int_{\Omega} w^{(3)} \nabla \cdot (\phi^w c^- \mathbf{v}^s) d\Omega = \\ - \int_{\Gamma_{J^-}} w^{(3)} \mathbf{J}^{-*} \cdot \mathbf{n} d\Gamma \end{aligned} \quad (7-27)$$

$$\begin{aligned} \int_{\Omega} w^{(4)} \frac{\partial(\phi^w c^{o_2})}{\partial t} d\Omega - \int_{\Omega} \mathbf{J}^{o_2} \cdot \nabla w^{(4)} d\Omega + \int_{\Omega} w^{(4)} \nabla \cdot (\phi^w c^{o_2} \mathbf{v}^s) d\Omega \\ - \int_{\Omega} w^{(4)} Q^{o_2} d\Omega = - \int_{\Gamma_{J^{o_2}}} w^{(4)} \mathbf{J}^{o_2*} \cdot \mathbf{n} d\Gamma \end{aligned} \quad (7-28)$$

$$\begin{aligned} \int_{\Omega} w^{(5)} \frac{\partial(\phi^w c^{glu})}{\partial t} d\Omega - \int_{\Omega} \mathbf{J}^{glu} \cdot \nabla w^{(5)} d\Omega + \int_{\Omega} w^{(5)} \nabla \cdot (\phi^w c^{glu} \mathbf{v}^s) d\Omega \\ - \int_{\Omega} w^{(5)} Q^{glu} d\Omega = - \int_{\Gamma_{J^{glu}}} w^{(5)} \mathbf{J}^{glu*} \cdot \mathbf{n} d\Gamma \end{aligned} \quad (7-29)$$

$$\begin{aligned}
& \int_{\Omega} w^{(6)} \frac{\partial(\phi^w c^{lac})}{\partial t} d\Omega - \int_{\Omega} \mathbf{J}^{lac} \cdot \nabla w^{(6)} d\Omega + \int_{\Omega} w^{(6)} \nabla \cdot (\phi^w c^{lac} \mathbf{v}^s) d\Omega \\
& - \int_{\Omega} w^{(6)} Q^{lac} d\Omega = - \int_{\Gamma_{J^{lac}}} w^{(6)} \mathbf{J}^{lac*} \cdot \mathbf{n} d\Gamma
\end{aligned} \tag{7-30}$$

where  $\mathbf{t}^* = \boldsymbol{\sigma}^* \cdot \mathbf{n}$  is the traction on the boundary of the tissue and \* stands for the quantities on the tissue boundary.

The model was solved using COMSOL software (Comsol 3.2, COMSOL, Inc., Burlington, MA). The upper right quadrant of the disc was modeled with a mesh of 6927 second-order, tetrahedral Langrange elements (Figure 7-1c). The relative tolerance for convergence was  $1 \times 10^{-6}$ .

Initial solute concentrations at the tissue boundaries were the same as those used in our previous model (Huang and Gu 2008), see Table 7-2. Note that ‘AF edge’ signifies the lateral surface of the AF; the axial AF edge (i.e., at  $z = 0.5$ ) is impermeable. Tissue properties used in the model are shown in Table 7-3.

**Table 7-2:** Solute Concentrations at the AF Edge and CEP edge of the IVD

	AF edge	CEP edge
Glucose	5 mM	4 mM
Oxygen	5.8 kPa	5.1 kPa
Lactate	0.9 mM	0.8 mM
Na <sup>+</sup>	0.15 M	0.15 M
Cl <sup>-</sup>	0.15 M	0.15 M

**Table 7-3:** Tissue Properties Incorporated Into Finite Element Model of the Intervertebral Disc

	AF	NP	CEP
$\phi_o^w$	0.75 <sup>a</sup>	0.86 <sup>a</sup>	0.60 <sup>b</sup>
$\rho^{\text{cell}}$ (cells/mm <sup>3</sup> ) <sup>c</sup>	9000	4000	15000
$c^f$ (mol/m <sup>3</sup> )	150	250	90
Parameters for diffusivity <sup>d</sup>	A = 1.29 B = 0.372	A = 1.25 B = 0.681	A = 1.29 B = 0.372
Parameters for hydraulic permeability	a = 0.00044 nm <sup>2</sup> <sup>e</sup> n = 7.193 <sup>e</sup>	a = 0.00339 nm <sup>2</sup> <sup>f</sup> n = 3.24 <sup>f</sup>	a = 0.0248 nm <sup>2</sup> <sup>g</sup> n = 2.154 <sup>g</sup>
Lamé constants	$\lambda = 0.30$ MPa <sup>h</sup> $\mu = 0.10$ MPa <sup>h</sup>	$\lambda = 15.6$ kPa <sup>i</sup> $\mu = 0.18$ kPa <sup>i</sup>	$\lambda = 0.10$ MPa <sup>j</sup> $\mu = 0.20$ MPa <sup>j</sup>

<sup>a</sup>(Yao and Gu 2007)

<sup>b</sup>(Roberts et al. 1989) and (Setton et al. 1993a)

<sup>c</sup>(Maroudas et al. 1975)

<sup>d</sup>Values for porcine AF tissue (AF and CEP) and agarose gels (NP) (Gu et al. 2004)

<sup>e</sup>Values for porcine AF tissue (AF) (Gu and Yao 2003)

<sup>f</sup> Values for agarose gels (NP) (Gu et al. 2003)

<sup>g</sup>From (Yao and Gu 2004), curve-fit from Figure 9 of (Maroudas 1975)

<sup>h</sup>(Iatridis et al. 1999)

<sup>i</sup>Calculated from results in (Iatridis et al. 1997) and (Johannessen and Elliot 2005)

<sup>j</sup>(Yao and Gu 2004)

#### 7.4 CASE 1: EFFECT OF ENDPLATE CALCIFICATION AND MECHANICAL LOADING ON GLUCOSE DISTRIBUTIONS IN IVD

The cartilage endplate is known to become calcified during aging and degeneration (Bernick and Cailliet 1982; Nachemson et al. 1970; Roberts et al. 1993), resulting in a decrease in the nutrient exchange between the disc and the capillary bed in the adjacent vertebrae (Nguyen-minh et al. 1998; Urban et al. 2001). Consequently, the nutrient distributions in the disc are altered due to the hindered transport. Additionally, the disc undergoes a variety of loading configurations throughout daily activity. This loading can affect the transport of solutes into and out of the disc, thereby altering the distribution of nutrients in the IVD. In this study, we investigated the affect of *in vivo* mechanical loading conditions and endplate calcification on the distribution of glucose in the disc.

##### 7.4.1 BOUNDARY CONDITIONS

In this investigation, we analyzed the distribution of glucose in the IVD under three loading configurations: (1) supine, (2) standing, and (3) weight-bearing standing. Strain was applied to the disc using a displacement boundary condition. In the supine configuration, no strains were applied to the disc (i.e., initial, or reference, geometry). The standing configuration was based on a recent *in vivo* study investigating the change in disc geometry associated with the transition from supine to standing positions (Wang et al. 2009). This transition was found to result in 16% compression in the posterior region of the disc, while the anterior region is 19% in tension (Figure 7-2). In order to investigate a weight-bearing standing configuration, we considered the same tension/compression configuration described for the standing condition, plus an

additional 10% static compressive strain (i.e., the anterior region was in 9% tension, while the posterior region was 26% in compression). These configurations are illustrated in Figure 7-2.

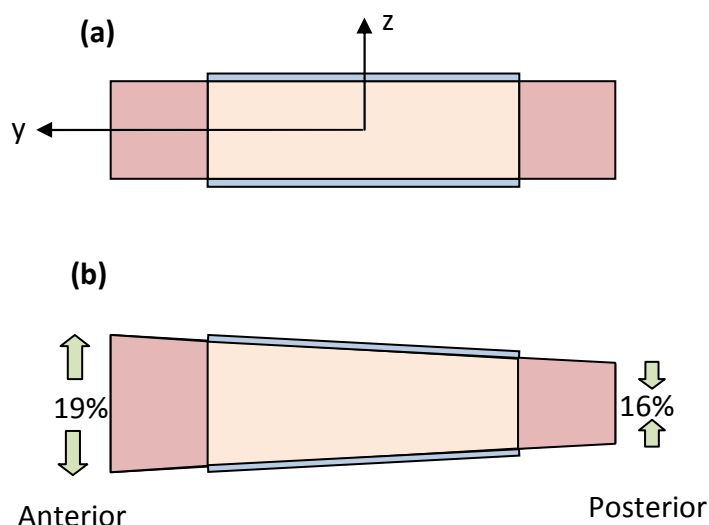


**Figure 7-2:** Loading on the disc for (a) supine and (b) standing configurations.

The effects of endplate calcification on the distribution of nutrients in the disc were also considered by reducing the permeability of the endplate tissue. Since the permeability of the endplate tissue is related to the tissue water content, see Equation (7-14), the water content of the CEP was reduced to simulate endplate calcification; the water content of the normal CEP was considered as 0.6, while that in the ‘calcified’ case was 0.42 (i.e., a 30% reduction). Based on the constitutive model for hydraulic permeability (Gu et al. 2003) incorporated into the model, this reduction in tissue porosity results in ~79% decrease in the hydraulic permeability (from  $5.94 \times 10^{-17} \text{ m}^4 /$

N·s to  $1.24 \times 10^{-17} \text{ m}^4 / \text{N}\cdot\text{s}$ ). Furthermore, the solute diffusivity is also reduced due to the decreased permeability of the tissue, see Equation (7-15) (Gu et al. 2004). The degree to which diffusivity is reduced varies based on the size of the solute; for instance, for glucose, the 30% reduction in CEP water content results in a ~38% decrease in glucose diffusivity in CEP tissue.

#### 7.4.2 RESULTS

The main objective of this study was to investigate the effects of mechanical loading and endplate calcification on the distribution of glucose in the disc using a 3-D finite element model of the IVD. Although only the results for glucose and pH distributions are reported here, our model is capable of simultaneously predicting stress and strain distributions in the disc, as well as the concentration distributions of other solutes (e.g., oxygen, lactate, ions).

In general, our results showed that glucose concentrations decrease moving away from the blood supply at the disc periphery and cartilaginous endplates. Minimum glucose concentrations were found at the interface between the AF and NP regions of the disc and varied according to strain configurations (Figures 7-3, 7-4 and 7-6). The values for minimum glucose concentration determined here (i.e., 0.41 – 0.75 mM for supine configuration) are in agreement with those measured in the AF of scoliotic discs, which were the range of 0.5 – 2.5 mM (Bibby et al. 2002). Typical results for glucose concentrations in the disc for both the normal (left column) and ‘calcified’ endplate (right column) cases are shown in Figure 7-3.



Our results indicate that there is a 17% decrease in the minimum glucose concentration in the IVD for the ‘calcified’ CEP case, for which the permeability of the CEP tissue was reduced. Additionally, our results show that the NP region is more strongly affected by endplate calcification as compared with the AF region of the disc. This effect is shown in Figures 7-5 and 7-6. In fact, there was a 30.6% decrease in the averaged glucose concentration, calculated using Equation (7-16), in the NP region for the ‘calcified’ case compared with normal CEP, in contrast to the 6.4% decrease in the averaged glucose concentration in the AF region.

In this study, we also investigated the effects of mechanical compression on the glucose concentrations in the IVD. The *in vivo* strain conditions associated with the transition from lying to standing configuration resulted in a 4.8% decrease in the minimum glucose concentration in the disc for the normal endplate case, as compared with the supine configuration. In contrast, this standing configuration led to a 14% decrease in the minimum glucose concentration in the disc for the ‘calcified’ case. The standing configuration also led to an alteration in the glucose distribution in the IVD, resulting in an increase in the glucose concentration in the anterior region while that in the posterior region of the disc decreased (Figure 7-5).

Furthermore, deformation associated with weight-bearing standing conditions (i.e., an additional 10% static compressive strain added to that in standing configuration) led to a 21% decrease in the minimum glucose concentration in the disc, as compared with the standing configuration, for the normal endplate case. By comparison, the same loading led to a 57% decrease in the minimum glucose concentration for the ‘calcified’ endplate case.

The change in pH distribution in the disc with varying endplate permeability and strain configurations was also investigated. The pH profile in the IVD for the normal and 'calcified' endplate conditions (in supine configuration) are shown in Figure 7-7. Similar to results for glucose, minimum pH values were found near the interface between the AF and NP, at the mid-plane of the disc (i.e.,  $z = 0$ ). Our results indicate that the minimum pH value in the disc decreases when the permeability of the endplate is reduced, from 6.899 in the normal CEP case, to 6.854 in the 'calcified' case. Additionally, both the standing and weight-bearing standing configurations resulted in small decreases in the minimum pH value for both CEP conditions. The minimum pH value decreased to 6.894 and 6.875 for standing and weight-bearing standing, respectively, in the normal endplate case, as compared with decreases to 6.846 and 6.821 for the 'calcified' endplate cases.

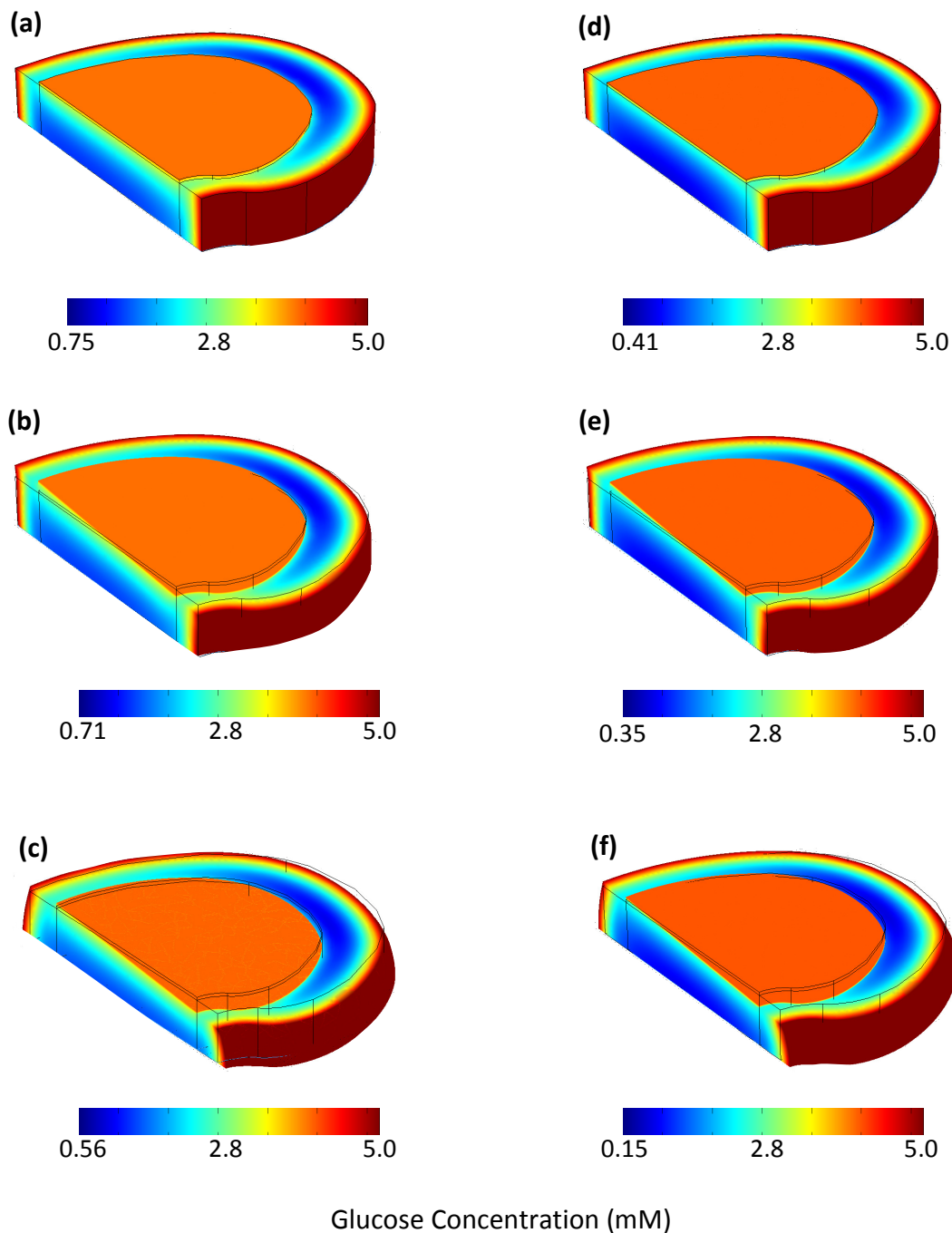


**Figure 7-3:** Typical glucose concentrations in the IVD for the six cases investigated: **(a)** normal CEP, supine; **(b)** normal CEP, standing; **(c)** normal CEP, weight-bearing standing; **(d)** 'calcified' CEP, supine; **(e)** 'calcified' CEP, standing; and **(f)** 'calcified' CEP, weight-bearing standing. Note in (b)-(c) and (e)-(f), the deformed shape is shown, while the black outline signifies the original geometry.

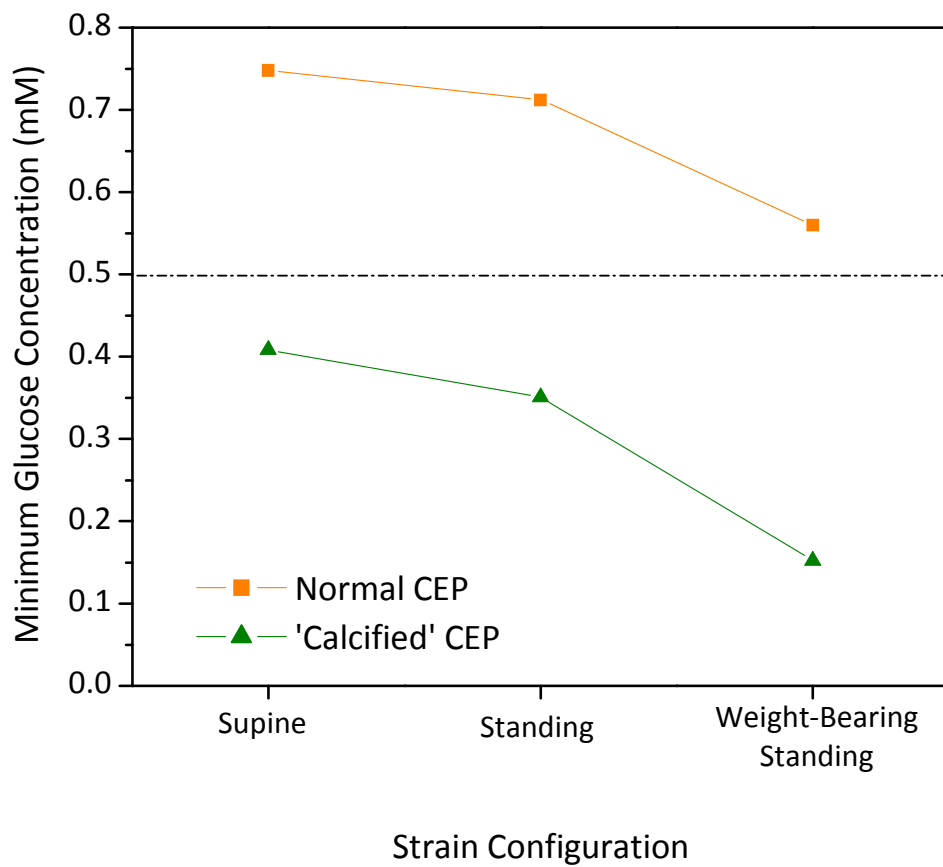


**Figure 7-4:** Minimum glucose concentration in the disc for the three loading configurations (supine, standing, and weight-bearing standing) and for normal (orange) and 'calcified' (green) endplate cases. Note the dashed line at 0.5 mM, which denotes the glucose concentration below which cells begin to die (Horner and Urban 2001).

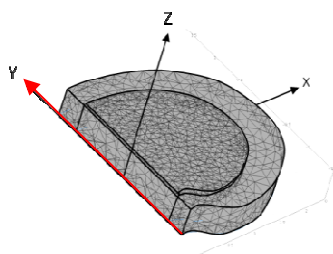
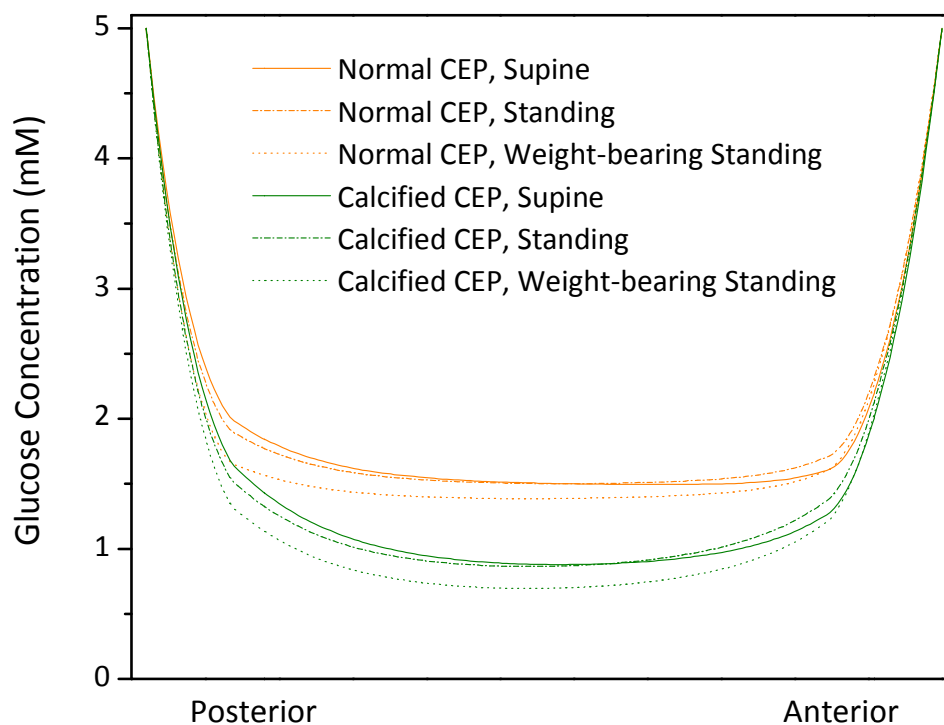


**Figure 7-5:** Distribution of glucose in the IVD under three loading conditions (supine, standing, and weight-bearing standing) and for normal (orange) and 'calcified' (green) endplate cases along the y axis at  $x = z = 0$  (from posterior to anterior, see figure).

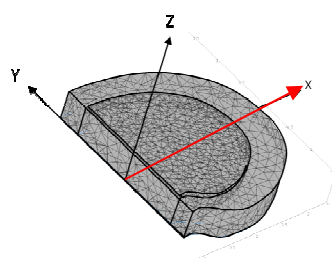
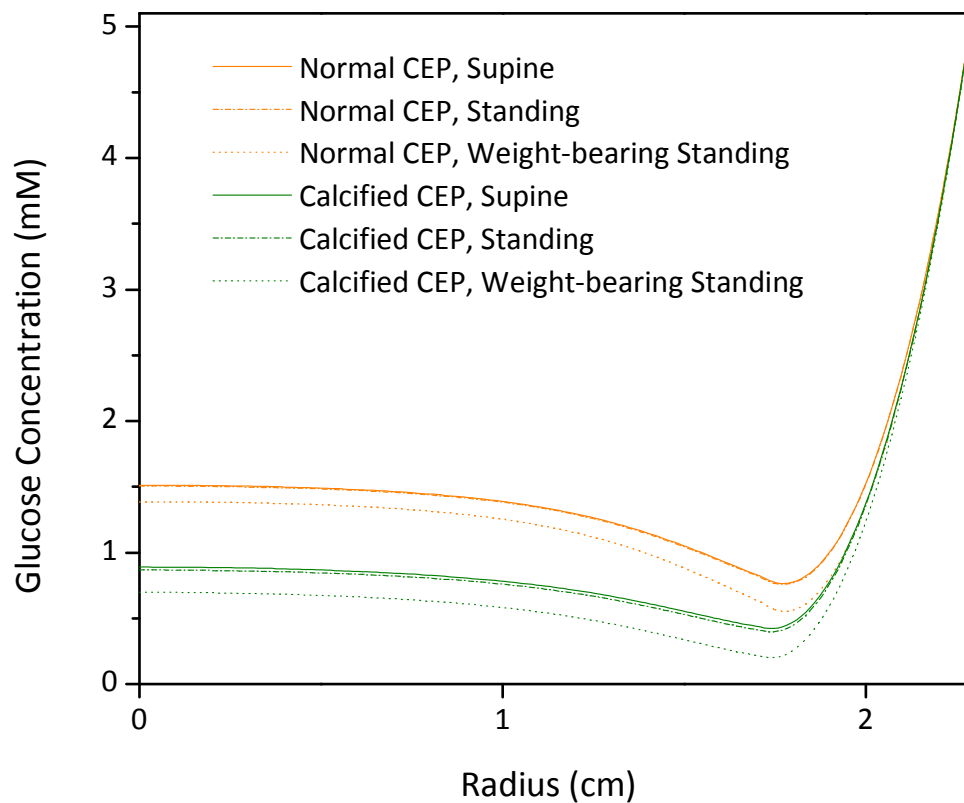


**Figure 7-6:** Distribution of glucose in the IVD under three loading conditions (supine, standing, and weight-bearing standing) and for normal (orange) and 'calcified' (green) endplate cases along the x axis at  $y = z = 0$  (from center to lateral edge, see figure).

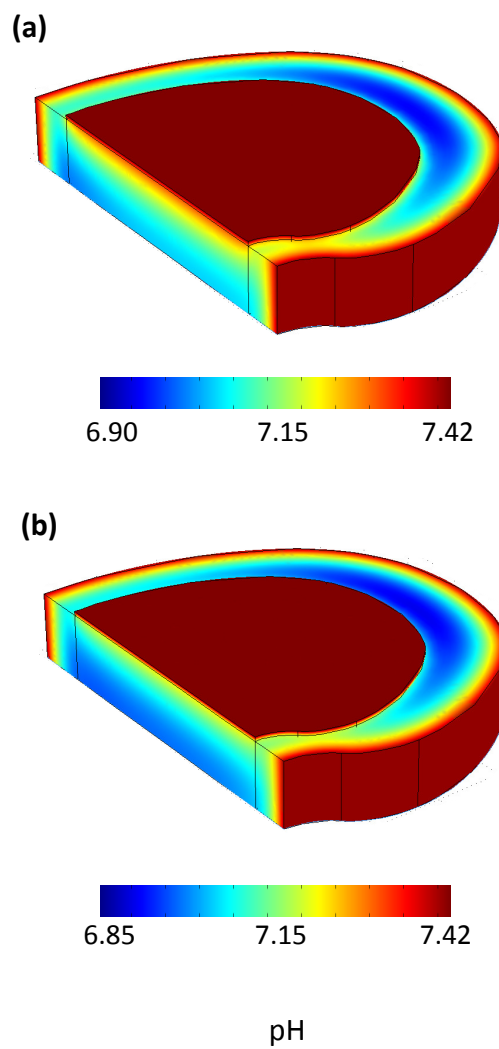


**Figure 7-7:** pH distribution in IVD for (a) normal and (b) 'calcified' endplate cases.

### 7.4.3 DISCUSSION

Our results indicate that reduced permeability associated with calcification of the cartilaginous endplates leads to a significant decrease in the minimum glucose concentrations in the disc, which is similar to the results presented in previous studies (Shirazi-Adl et al. 2010; Soukane et al. 2009). The minimum concentration of glucose fell from 0.748 mM in the normal endplate case to 0.408 mM for the ‘calcified’ case. The effects of reduced endplate permeability are most prominent in the NP region of the disc, as the NP receives its nutrient supply mainly from the capillary bed in the vertebral bone adjacent to the endplate (Brodin 1955; Brown and Tsaltas 1976; Holm et al. 1981; Maroudas et al. 1975; Nachemson et al. 1970; Ogata and Whiteside 1981; Urban et al. 1982). This decrease in the minimum concentration of glucose is significant as a previous study has shown that if glucose levels fall below 0.5 mM for more than 3 days, cells begin to die (Horner and Urban 2001). Endplate calcification occurs during the aging process of the disc. Although the exact mechanism of calcification is unknown, it is clear that this leads to a decrease in the transport of nutrients through the tissue (Nachemson et al. 1970). This, in turn, results in a decrease in the nutrient concentrations in the IVD, particularly in the NP region, as was seen here. Alterations in the concentrations and/or distribution of nutrients in the disc may lead to changes in the disc cellular metabolism and cell viability, which in turn would affect the function of the IVD.

Our results show that the *in vivo* loading configuration associated with the transition from supine to standing positions (Figure 7-2) results in a decrease in the minimum glucose concentration in the disc (Figures 7-3 to 7-6). This effect was augmented by endplate calcification; the decrease in minimum glucose concentration was



more than twice as large in the ‘calcified’ case as compared with the normal case. Additionally, the *in vivo* standing configuration led to an alteration in the distribution of glucose in the IVD, with that in the anterior region of the disc increased during standing, while that in the posterior region decreased (see dashed line in Figure 7-5), compared with results for the supine configuration. Results were similar for both the normal and ‘calcified’ endplate cases. This alteration is a result of a change in the tissue water content caused by the unique strain configuration. The anterior region of the disc is in tension, resulting in an increase in the water content, while the posterior region of the disc is in compression, causing a reduction in water content. In fact, for AF tissue with an initial tissue water content of 0.75, a 19% tensile strain results in an increase in the water content to 0.79, while a 16% compressive strain leads to a reduced water content of 0.70. These changes give rise to an alteration in the solute diffusivity through the tissue, see Equation (7-15), thereby varying the glucose concentration in the disc. These findings may have clinical implications, as the majority of disc herniations have been found to occur in the posterolateral region of the disc (Martin et al. 2002). A decrease in the nutrient levels in the posterior disc during standing may lead to regional degeneration of the tissue; this degeneration may disrupt the integrity of the tissue, thereby giving rise to herniation in this region.

This study also investigated the effects of 10% static compressive strain while in the standing configuration (i.e, weight-bearing standing configuration) on the glucose concentration in the disc. Results show that this strain configuration results in decreased glucose levels in the disc, whether the endplate is normal or calcified (see Figure 7-3 and dotted lines in Figures 7-5 and 7-6). This result was expected, as compressive loading

results in decreased water content and solute diffusivities, as discussed previously. Like the standing configuration, this weight-bearing configuration had a more pronounced effect on the minimum glucose level in the disc having endplates with reduced permeability ('calcified') (Figure 7-4), which had a decrease in minimum glucose concentration that was ~2.5 times greater as compared with the normal endplate case. This indicates that endplate calcification may cause more extreme glucose levels in the disc during loading, as compared to the normal, permeable endplate, leading to further degeneration of the tissue due to poor nutritional supply to disc cells.

Previous studies have also shown that the pH level in the disc tissue is an important factor in regulating cell viability and function (Horner and Urban 2001; Razaq et al. 2003). Furthermore, the cell metabolic rates incorporated into this model are pH-dependent, see Equations (7-9) and (7-10). Therefore, we also investigated how the pH profile in the disc was affected by loading configurations and endplate calcification. Results for pH values found here are similar to results previously reported for normal and symptomatic discs (Kitano et al. 1993). It is evident that CEP calcification leads to a decrease in the pH in the disc (see Figure 7-7). This is a result of the build-up of lactic acid, a by-product of anaerobic metabolism, caused by reduced endplate permeability during CEP calcification. These results indicate that CEP calcification may lead to acidic conditions in the IVD, resulting in subsequent changes in cellular activity as well as a loss of cell viability. These alterations would likely be detrimental to the health of the disc, resulting in degeneration and loss of function. It should also be noted that the loading configurations investigated here also led to more acidic conditions in the tissue, again likely the result of lactic acid accumulation in the tissue. Similar to the case for

glucose, the effect of compressive loading on pH was more pronounced for the ‘calcified’ endplate case (data not shown).

## **7.5 CASE 2: EFFECT OF DEGENERATION ON CELL VIABILITY IN IVD**

As has been mentioned, disc degeneration is a common phenomenon that happens early in life, especially compared to the degeneration of other connective tissues. Degeneration results in a change in tissue properties, which may in turn result in an alteration, or loss of, functioning of the tissue. Additionally, these changes may also cause cell death due to poor nutritional supply to the tissue. In this investigation, we analyze how changes in tissue properties resulting from degeneration affect the viability of cells in the tissue. We do this by incorporating criteria for maintaining cell viability in the tissue, based on threshold levels of glucose necessary for cells to survive.

### *7.5.1 TISSUE PROPERTIES AND MODEL PARAMETERS*

In this study, we compare the cell viability in normal, healthy disc to that in degenerated IVD using theoretical prediction. The normal disc investigated here has the same properties as those listed in Table 7-3. Degenerated tissue is known to have lower water content and fixed charge density, as well as reduced disc height as compared with non-degenerated tissue. Furthermore, the disc becomes stiffer with degeneration, altering the values of Lamé constants for the tissue. The properties used for modeling degenerated disc are shown in Table 7-4. Additionally, the heights of the AF and NP regions of the disc were reduced by 10% to  $h = 0.9$  cm. Other properties not listed in Table 7-4 (e.g., cell density, parameters for diffusivity and hydraulic permeability)

remained the same as those listed in Table 7-3. Solute concentrations at the tissue boundary are the same as those listed in Table 7-2.

**Table 7-4:** Tissue Properties Incorporated Into Finite Element Model for Degenerated Intervertebral Disc Tissue

	AF	NP	CEP
$\phi_o^w$	0.68	0.78	0.30
$c^f$ (mol/m <sup>3</sup> ) <sup>a</sup>	125	175	90
Lamé constants	$\lambda = 0.70$ MPa <sup>b</sup> $\mu = 0.15$ MPa <sup>b</sup>	$\lambda = 25.8$ kPa <sup>c</sup> $\mu = 0.61$ kPa <sup>c</sup>	$\lambda = 0.10$ MPa $\mu = 0.20$ MPa

<sup>a</sup>(Magnier et al. 2009)

<sup>b</sup>(Iatridis et al. 1999)

<sup>c</sup>Calculated from results in (Iatridis et al. 1997) and (Johannessen and Elliot 2005)

For the degenerated case, the water content of the degenerated CEP tissue was reduced by 50%, to 0.30. This reduction resulted in a 93% decrease in the hydraulic permeability of the tissue, based on the relationship in Equation (7-14). Like in our previous study, this reduction in permeability was used to simulate endplate calcification, which hinders the transport of solutes between the disc and the vasculature in the subchondral bone adjacent to the endplate.

In order to analyze the effect of degeneration on cell viability in the disc, the model includes cell viability criteria based on nutrient levels in the tissue. Previous studies have shown that disc cells begin to die when glucose levels fall below 0.5 mM, with all cells dying when glucose levels decrease to 0.2 mM (Bibby et al. 2002; Bibby and Urban 2004; Guehring et al. 2009; Horner and Urban 2001). This criteria for viability was incorporated into our theoretical formulation, with cells beginning to die when the glucose concentration decreases below 0.5 mM and continuing in a linear

fashion until levels fall to 0.2 mM, at which point all cells die. This is illustrated in Figure 7-8. Studies have also shown that pH levels also affect the viability of IVD cells; however, a previous analysis indicated that the effect of glucose is predominant in determining viability (Shirazi-Adl et al. 2010). Therefore, we have only incorporated the criteria based on glucose concentrations into this model.

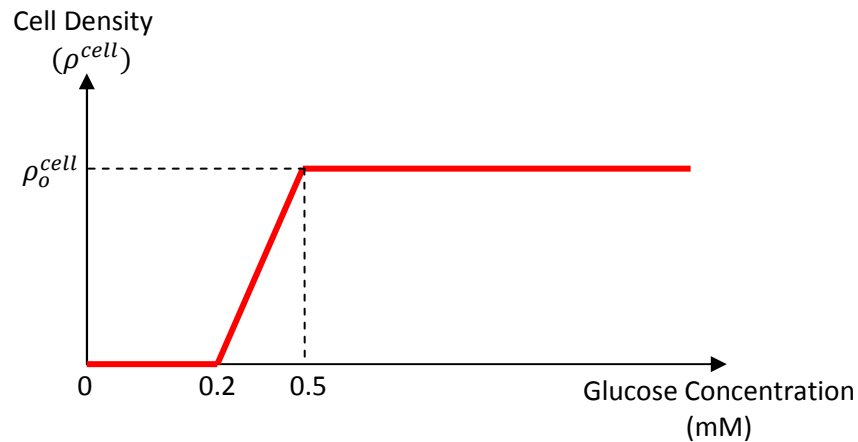


**Figure 7-8:** Schematic showing the criteria used for cell viability based on glucose concentrations in the tissue.

We have also investigated how mechanical compression affects cell viability in normal and degenerated IVD using our model. In this study, a 10% static compressive strain was applied to the tissue using a displacement boundary condition (see configuration in Figure 7-1d). The final results are for the disc in equilibrium after the application of strain to the IVD.

### 7.5.2 RESULTS

The results of this study indicate that degeneration and static compression both affect the glucose levels and related cell viability in the IVD. Typical results for glucose

distribution in normal and degenerated IVD are shown in Figure 7-9. Similar to our previous study, discussed above, the minimum glucose concentrations in the disc were located at the lateral interface between the AF and NP regions, at the center (or mid-plane) of the disc.

Our results show that degeneration results in a 70% decrease in the minimum glucose concentration in the IVD. This effect was predominant in the NP region of the IVD, which had a 68% decrease in the averaged glucose concentration, as compared with a 33.2% decrease in the AF region. This effect is visible in Figure 7-9, in which dark blue signifies low glucose concentration.

Disc degeneration was also found to significantly affect cell viability in the tissue. The averaged cell density fell 17% in the disc as a result of degenerative changes to the tissue. Similar to glucose concentrations, this was more prominent in the NP region, which had a 25% decrease in averaged cell density, compared with a 12% decrease in the AF region. This can be seen in Figure 7-12a. As expected, no cell death was found to occur in the normal tissue (not shown).

Static mechanical compression affected both the nutrient and cell density distributions in the IVD. For normal IVD, the minimum glucose concentration decreased by 19% following the application 10% static compressive strain. Comparatively, there was a 5% decrease in the minimum glucose concentration in the degenerated IVD. This can be seen in Figure 7-9(b and d). Cell viability in normal IVD was not affected by compression. In contrast, for degenerated IVD, the averaged cell density decreased by 8% following compression. The NP region, which had a 14% decrease, was more affected than AF, with a 5% decrease, see Figure 7-12.

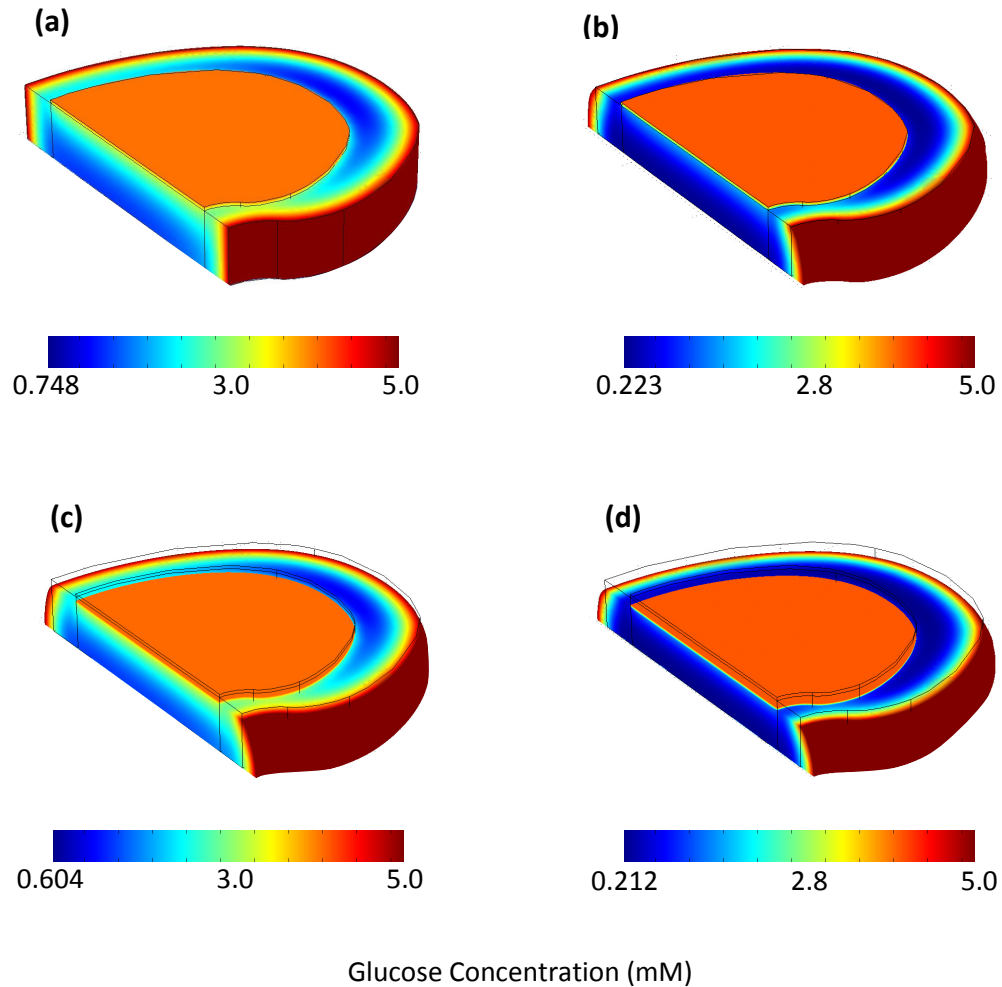


**Figure 7-9:** Typical glucose concentrations in the IVD for the four cases investigated: **(a)** normal disc, reference configuration; **(b)** normal disc, 10% static compressive strain; **(c)** degenerated disc, reference configuration; **(d)** degenerated disc, 10% static compressive strain. Note in (b) and (d), the deformed shape is shown, while the black outline signifies the original geometry.

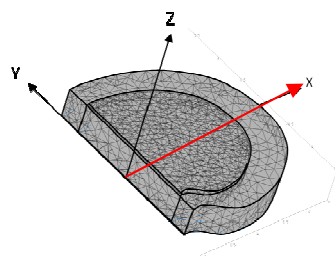
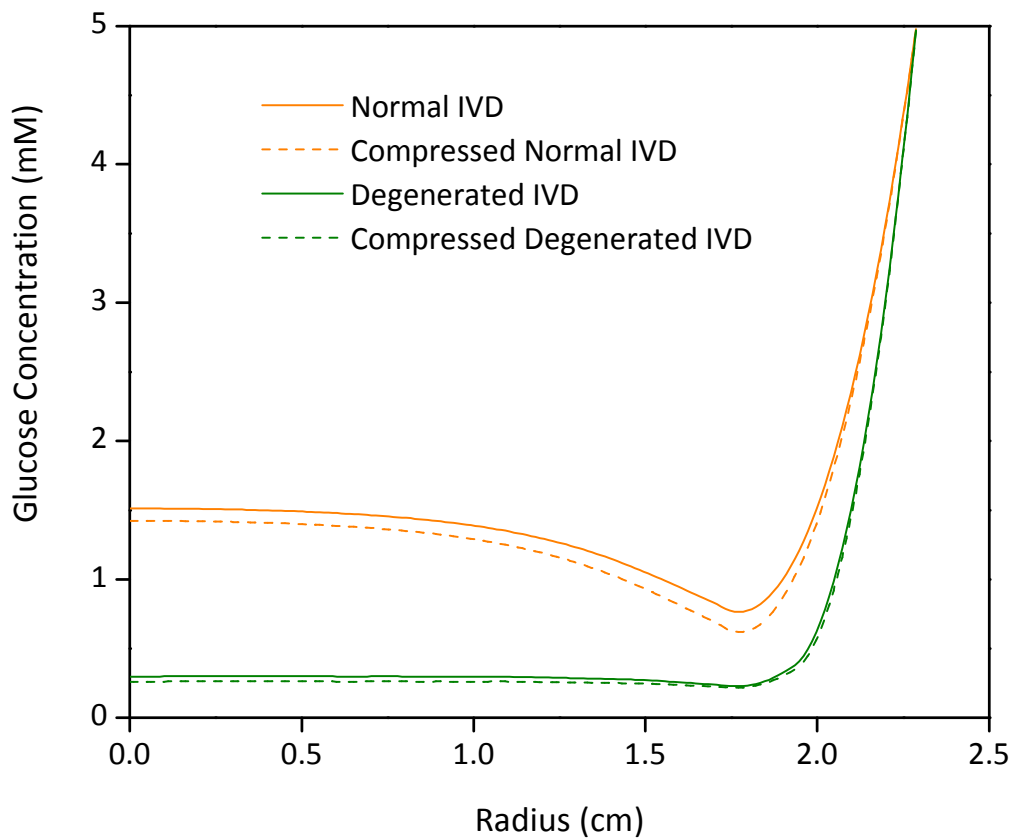


**Figure 7-10:** Distribution of glucose in the normal (orange) and degenerated (green) IVD under two loading conditions [supine or reference (solid) and 10% static compression (dashed)] along the x axis at  $y = z = 0$  (from center to lateral edge, see figure).



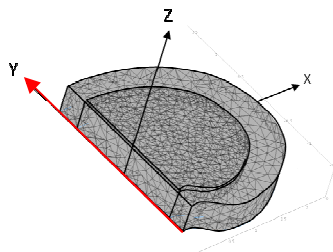
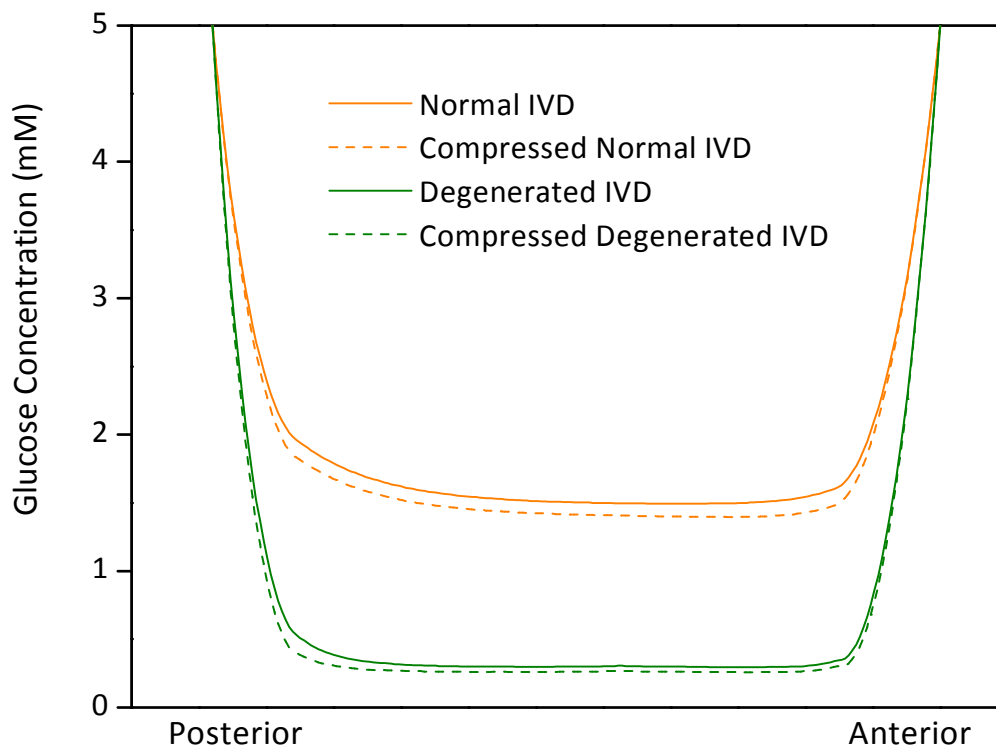


**Figure 7-11:** Distribution of glucose in the normal (orange) and degenerated (green) IVD under two loading conditions [supine or reference (solid) and 10% static compression (dashed)] along the y axis at  $x = z = 0$  (from posterior to anterior, see figure).

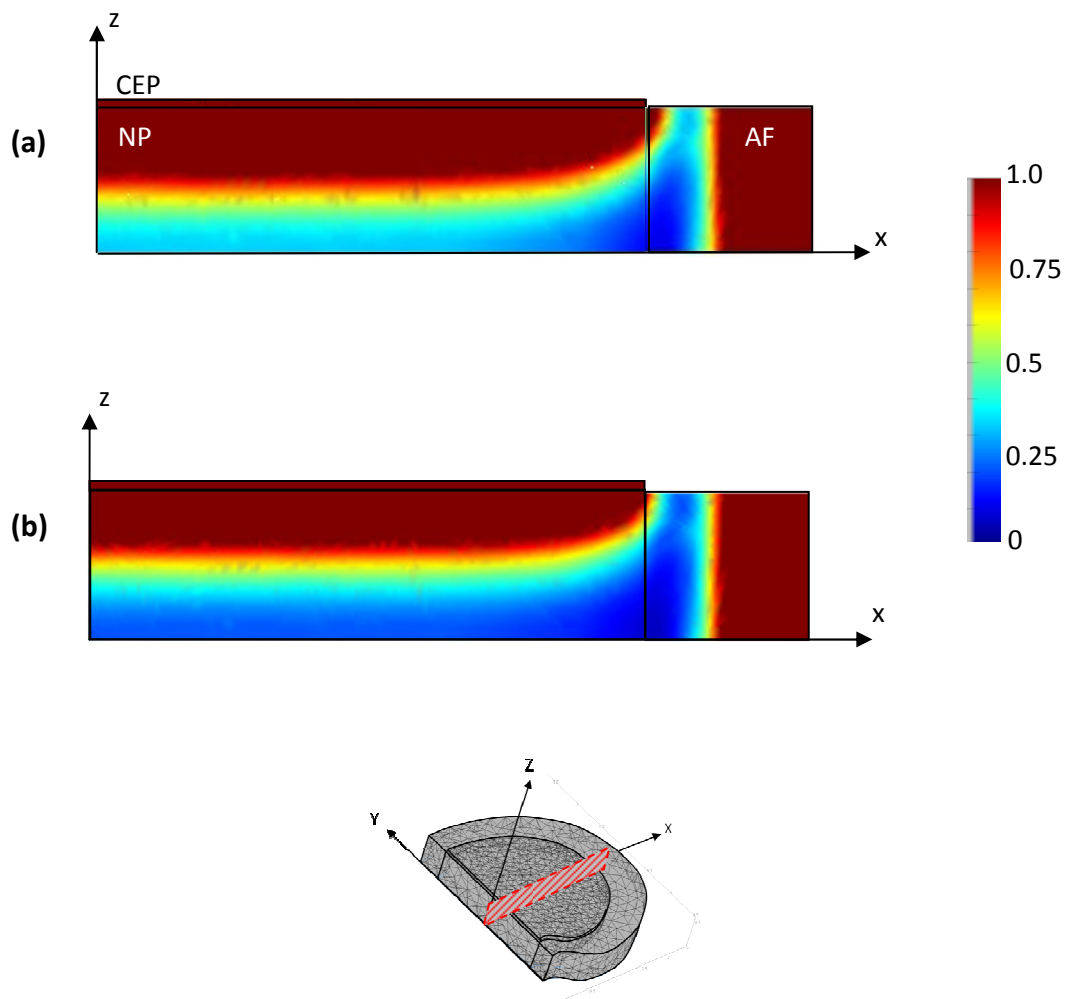


**Figure 7-12:** Cell density in degenerated IVD for **(a)** reference and **(b)** compressed tissue at cross section shown. Values are normalized by initial cell density (see Table 7-2). Note that cell death occurs moving away from nutritional supply.

### 7.5.3 DISCUSSION

To our knowledge, this is the first study to predict cell viability in IVD under mechanical compression using theoretical analysis. The results found here for minimum glucose concentrations in the IVD, ranging from 0.212 to 0.748 mM, are comparable with measurements in scoliotic discs in the literature (Bibby et al. 2002). Additionally, our results for concentrations distribution of glucose in the disc are also in agreement with previous studies [e.g., (Shirazi-Adl et al. 2010; Soukane et al. 2009)].

For normal IVD, no cell death was found to occur, either with or without compression. This is because glucose levels in the tissue did not fall below the minimum levels necessary for cell survival (i.e., 0.5 mM). This finding is in agreement with a previous study (Shirazi-Adl et al. 2010), which found that no cell death occurred in the uncompressed disc with permeable cartilage endplate. Glucose levels in the IVD were reduced following the application of static compression. This is likely due to the decreased diffusivity caused by decreased tissue water content during compression, see Equation (3-16).

For degenerated IVD, significant cell death was found to occur even without the application of compressive strain. This is in agreement with results in the literature, which found reduced cell viability in degenerated IVD and for calcified CEP (Shirazi-Adl et al. 2010). In general, cell death occurred moving away from the nutrition supply, see Figure 7-12. This was due to the fall in nutrient supply moving further from the nutritional source. Because our criterion for cell viability was based on glucose concentrations thresholds alone, the correlation between these two factors was expected.

Our results show that cell viability in the NP region is more affected by the reduced permeability of the endplates, as compared to the AF. As has been noted, the NP receives its nutritional supply primarily from the vasculature located in the subchondral bone adjacent to the CEP; endplate calcification, resulting in reduced permeability, reduces this supply, thereby leading to lower nutrition levels and subsequent cell death.

Mechanical compression led to increased cell death in degenerated tissue. This result is likely due to the lower glucose levels in the disc, resulting from slower diffusion rates caused by the decreased tissue porosity following compression. Compression did not have as large an effect on the glucose levels in degenerated tissue as compared with normal tissue. This can be explained by the lower cell density in degenerated tissue. For the degenerated case, there are fewer viable cells present to consume glucose, thereby easing the nutritional stress on the remaining cell population in the tissue; hence, there is less overall consumption as compared with the non-degenerated tissue.

The cell viability criteria incorporated into the model depends only on threshold levels of glucose. Previous studies have found that pH levels also affect cell viability, with cells beginning to die when pH falls below 6.8. However, it was previously shown that the inclusion of pH viability criteria did not significantly affect results, when compared to the glucose criteria alone (Shirazi-Adl et al. 2010). Therefore, only the glucose condition was incorporated into our model. It should be noted, however, that results are strongly-dependent upon the threshold levels chosen. The levels of glucose used here were chosen based on experimental results; however, variation of these values would alter the results for cell viability and glucose concentration distributions in the tissue.

## 7.6 LIMITATIONS

We believe the theoretical model developed here can provide accurate predictions of the *in vivo* environment in the IVD; however, the model does possess some limitations discussed here. For instance, in order to most accurately predict nutrient distributions in the disc, more information regarding nutrient consumption rates is needed. As an example, the rate of production of lactate, as well as the consumption rate of glucose, used in this study was based on results for bovine NP cells (Bibby et al. 2005). That is, metabolic rates for glucose and lactate were assumed to be the same for both AF and NP cells. Studies on the oxygen consumption rate for IVD cells have indicated a difference in metabolic rates for the two cell phenotypes (Huang et al. 2007); it is therefore likely that a difference would exist for glucose and lactate metabolism as well. However, although a recent study investigated the rate of lactate production by AF cells (Guehring et al. 2009), and our study (described in Chapter 6) provides a preliminary report of glucose consumption by AF cells, there is currently no quantitative relationship in the literature to describe the metabolic rates of glucose and lactate by AF cells. Such information is necessary in order to accurately predict nutrient distributions in the disc.

Additionally, further detailed studies on the consumption rate of glucose by IVD cells are needed, given that glucose is considered the limiting nutrient for cell viability. For example, in Equations (7-10) and (7-11), the glucose consumption rate is assumed to be dependent on the oxygen-tension level but independent of the glucose concentration. It is probable that glucose concentration levels affect the metabolic rate by disc cells, particularly at low (i.e., <0.5 mM) levels, thereby influencing the distribution of glucose in the IVD. Indeed, we found a Michaelis-Menton relationship for glucose consumption

by porcine NP cells (see Chapter 6), whereby the rate of consumption decreases with the glucose concentration. This phenomenon should be further investigated and incorporated into the model to provide more accurate results for glucose distributions in the disc.

Furthermore, many of the parameters used in this study (i.e., rates of cellular metabolism, solute diffusivities) are based on results from studies using animal tissues or cells. For instance, there are few studies in the literature regarding properties of animal CEP tissue [e.g., (Accadbled et al. 2008; Ayotte et al. 2000; Setton et al. 1993a)], but data regarding material properties of human endplate tissue are not available. Therefore, for convenience, material properties incorporated into the model were based on those of human articular cartilage. Additionally, the Lamé constants,  $\lambda$  and  $\mu$ , for the cartilaginous endplates incorporated into the model were assumed to be the same for both the normal and ‘calcified’ or degenerated cases. Changes in these properties caused by the degeneration or calcification processes should be incorporated into future models, in order to accurately reflect the disc *in vivo* environment.

## 7.7 SUMMARY AND CONCLUSIONS

We have developed a new, three-dimensional finite element model of the intervertebral disc in order to investigate nutritional supply to the tissue. This new formulation incorporates anatomical disc geometry, nutrient concentrations coupled to cellular metabolism, and mechanical loading conditions along with strain-dependent tissue properties. The integration of all of these aspects provides for accurate prediction of the *in vivo* environment in the disc. Using this model, we have shown that both *in vivo* loading conditions and reduced endplate permeability caused by calcification result in

decreased glucose levels in the disc. Furthermore, our model can predict cell death due to poor nutritional supply in degenerated IVD.

Our model is capable of predicting nutrient distributions, as well as stress and strain distributions, in the IVD. Moreover, it can be used to predict the cell density (or viability) in the IVD under a variety of conditions, and therefore may serve as a powerful tool in developing new strategies for treatment and/or retardation of disc degeneration. For instance, it has been suggested that there exists an ideal window of mechanical loading in which cells can survive and function (Stokes and Iatridis 2004). This phenomenon may be further investigated using our model, and ideal loading configurations (or exercise regimen) may be determined. These findings are a valuable supplement to experimental findings of nutrient distributions in IVD, and also provide important insight into the nutrition-related mechanisms of disc degeneration, which remain to be fully delineated.

## **CHAPTER 8. CONCLUSIONS AND RECOMMENDATIONS FOR FUTURE WORK**

### **8.1 SUMMARY AND CONCLUDING REMARKS**

Low back pain is a condition affecting millions of individuals each year, resulting in high costs. Degeneration of the intervertebral discs has been implicated as a possible source leading to back pain. Poor nutritional supply to the IVD is thought to be a primarily etiological factor leading to degenerative changes to the disc. Despite this, the transport and metabolic properties of the disc and its cells remain to be fully elucidated. In particular, glucose, which is considered a critical nutrient necessary for cell survival, has not been fully characterized in terms of transport and metabolism in the IVD.

Therefore, the major objectives of this dissertation were threefold: (1) to determine the strain-dependent transport properties of glucose in human IVD; (2) to determine the oxygen-tension-dependent rate of glucose consumption by IVD cells; and (3) to develop a new finite element model to investigate nutrient distributions in the IVD. In order to achieve these aims, four studies were carried out: (1) measurement of strain-dependent and anisotropic diffusivity of glucose in human AF (Chapter 3); (2) measurement of strain-dependent partitioning of glucose in human AF (Chapter 4); (3) development of a new technique for measuring glucose consumption rate by IVD cells and measurement of the consumption rate at various oxygen levels (Chapter 6); and (4) development of a new, 3-D finite element model of the IVD to analyze glucose distributions in the disc under mechanical loading and following disc degenerative changes (Chapter 7). The most important findings from these investigations are discussed below.



### *8.1.1 STRAIN-DEPENDENT TRANSPORT PROPERTIES IN IVD*

A one-dimensional steady-state diffusion experiment was carried out to measure the apparent diffusivity of glucose in human AF. Our results indicate that diffusivity decreases as the level of static compressive strain increases. Furthermore, we have found that glucose diffusivity in human AF is anisotropic, being higher in the axial and circumferential directions as compared with the radial direction. This trend was true from non-degenerated (Grade I) and mildly degenerated (Grade II) tissues, but not for degenerated tissues (Grade III).

The strain-dependent partition coefficient of glucose in human AF was also determined using a custom-designed chamber. We have found that the partition coefficient decreases with increasing static compression, similar to our findings for glucose diffusivity. Furthermore, we found that the partition coefficient in normal IVD (Grade I) is higher than that in degenerated tissue (Grades II and III).

Our results for apparent diffusivity and partition coefficient of glucose in human AF were combined to determine the effective diffusivity (Chapter 4). These findings are important for understanding transport pathways and mechanisms in the IVD, and their relation to disc degeneration.

### *8.1.2 GLUCOSE CONSUMPTION RATE BY IVD CELLS AT VARYING OXYGEN TENSION LEVELS*

We developed a new method for measuring the rate of glucose consumption by IVD cells using a diffusional uptake problem. The consumption rate for porcine IVD cells was determined based on the change in glucose concentration over time. Our results show porcine AF and NP cells exhibit a positive Pasteur effect, with the rate of glucose

consumption increasing at low oxygen levels. Furthermore, we found that the glucose consumption rate by NP cells was significantly higher than that by AF cells. These findings provide important insight into the metabolism of disc cells, and how cellular activity may be affected by *in vivo* environmental conditions. Furthermore, this study helps us to better understand nutritional demands by IVD cells and related disc degeneration.

### 8.1.3 FINITE ELEMENT MODEL OF THE IVD

We developed a new, 3-D finite element model of the intervertebral disc in order to predict nutrient distributions in the tissue. Our model incorporated anatomical disc geometry, nutrient transport coupled to cellular metabolism, and mechanical loading conditions, which are all essential for accurate theoretical prediction. Using this new finite element model, we investigated the effects of *in vivo* mechanical loading and endplate calcification on the distribution of glucose in IVD. Our findings show that mechanical loading results in decreased glucose levels in the tissue. Furthermore, we also found that endplate calcification causes lowered glucose concentrations in the disc.

We also investigated how disc degeneration affects cell viability in the IVD by incorporating cell viability criteria into the model formulation. We found changing tissue properties to reflect the degenerated case allows us to predict changes in cell viability with disc degeneration. Moreover, we determined that static mechanical loading of the degenerated disc leads to increased cell death. By comparison, there was no cell death in normal IVD (with or without static compression).

The model developed provides for accurate prediction of nutrient distributions in the IVD under a variety of conditions. It therefore serves as a useful tool in supplementing our experimental results, and helps us to better understand nutritional supply and related disc degeneration. Furthermore, the model may offer a useful means for developing new treatment strategies for disc degeneration (discussed below).

## **8.2 RECOMMENDATIONS FOR FUTURE WORK**

The overall objective of this research was to develop to strategies for the treatment of disc degeneration. Although the studies described in this dissertation provide valuable insight into transport and metabolic properties in IVD tissues, there still remains a great deal of information necessary for fully understanding nutrition in the disc and its relation to disc degeneration. Here, recommendations for future work are described.

Transport properties in AF tissue were investigated in these studies; however, those for NP tissues were not considered. This is due to the difficulty in measuring the diffusion coefficient in NP, given its gelatinous consistency, using the methods developed here. However, given that the composition and structure of the NP are unique to that of AF, transport properties in human NP tissue should be further investigated in a future study. This would allow for a more thorough understanding of transport in the IVD and nutritional supply to the center of the disc.

We investigated the rate of glucose consumption by IVD cells under various oxygen tension levels. However, a variety of factors may affect the activity and viability of disc cells. Cellular activity and viability depend on the extracellular environment,

including hydrostatic pressure, osmolarity, pH, nutrition levels, etc. The extracellular environment is regulated by the nutrition supply at the disc periphery, transport properties of the ECM, rates of nutrient metabolism by cells, and mechanical loading. Changes in these factors (either due to genetics, smoking, or mechanical loading) could affect disc cell metabolic activity (including viability), leading to disc degeneration. Currently, little is known about how different factors, including extracellular osmolarity, mechanical compression, hydrostatic pressure, growth factor concentration, and pH, quantitatively affect disc cell metabolic rates. Determining a functional relationship between these factors is important for better understanding of disc cell activity and viability *in vivo*; furthermore, such relationships are necessary in order to accurately predict the extracellular environment and cell viability in IVD using theoretical modeling. Additionally, the metabolic activity of human cells should be investigated in order to obtain an accurate understanding of what is happening *in vivo*, and to develop strategies for preventing disc degeneration.

The finite element model developed here is capable of predicting nutrient distributions and cell viability in the IVD under many conditions. In these studies, we have only investigated static compressive loading conditions. However, during normal daily activities, the IVD is subjected to a wide range of motion, which is often dynamic. Our model should be employed to further investigate the effects of a variety of loading conditions, including dynamic loading, on the nutrient and cell distributions in the disc. This may serve as a useful tool for determining which loading configuration may allow for optimal nutritional transport to disc cells, thereby allow for decreased cell loss.

Hence, we may be able to develop new treatment strategies, perhaps in the form of an exercise regimen, for retarding or reversing disc degenerative changes.

In all, the recommended studies would greatly enhance the results found in this investigation, and would allow us to achieve the long-term goals of our research: to better understand the pathophysiology involved in the development of low back pain, to further elucidate transport and metabolic properties in normal and degenerated intervertebral discs; and to develop new strategies for assessing and treating the changes occurring in tissue during disc degeneration.

## REFERENCES

- Accadbled, F., Laffosse, J.-M., Ambard, D., Gomez-Brouchet, A., de Guazy, J. S. & Swider, P. 2008. Influence of location, fluid flow direction, and tissue maturity on the macroscopic permeability of vertebral end plates. *Spine*, 33, (6) 612-619.
- Adams, M. A. & Hutton, W. C. 1986. The effect of posture on diffusion into lumbar intervertebral discs. *J Anat*, 147, 121-134.
- Adams, M. A. & Hutton, W. C. 1983. The effect of posture on the fluid content of lumbar intervertebral discs. *Spine*, 8, (6) 665-671.
- Adams, M. A., McNally, D. S. & Dolan, P. 1996. 'Stress' distributions inside intervertebral discs. The effects of age and degeneration. *J Bone Joint Surg Br*, 78, (6) 965-972.
- Allhands, R. V., Torzilli, P. A. & Kallfelz, F. A. 1984. Measurement of diffusion of uncharged molecules in articular cartilage. *Cornell Vet*, 74, (2) 111-123.
- Arun, R., Freeman, B. J. C., Scammell, B. E., McNally, D. S., Cox, E. & Gowland, P. 2009. 2009 ISSLS Prize Winner: What influence does sustained mechanical load have on diffusion in the human intervertebral disc?: an in vivo study using serial postcontrast magnetic resonance imaging. *Spine*, 34, (21) 2324-2337.
- Ayotte, D. C., Ito, K., Perren, S. M. & Tepic, S. 2000. Direction-dependent constriction flow in a poroelastic solid: the intervertebral disc valve. *J Biomech Engng*, 122, (6) 587-593.
- Beattie, P. F., Morgan, P. S. & Peters, D. 2008. Diffusion-weighted magnetic resonance imaging of normal and degenerative lumbar intervertebral discs: A new method to potentially quantify the physiological effect of physical therapy intervention. *J Orthop & Sports Phys Therapy*, 38, (2) 42-49.
- Bernick, S. & Cailliet, R. 1982. Vertebral end-plate changes with aging of human vertebrae. *Spine*, 7, (2) 97-102.
- Bibby, S. R., Fairbank, J. C., Urban, M. R. & Urban, J. P. 2002. Cell viability in scoliotic discs in relation to disc deformity and nutrient levels. *Spine*, 27, (20) 2220-2228.
- Bibby, S. R. & Urban, J. P. 2004. Effect of nutrient deprivation on the viability of intervertebral disc cells. *Eur Spine J*, 13, (8) 695-701.
- Bibby, S. R. S. (2002) *Cell Metabolism and Viability in the Intervertebral Disc*. PhD Dissertation, University of Oxford.

- Bibby, S. R. S., Jones, D. A., Ripley, R. M. & Urban, J. P. 2005. Metabolism of the intervertebral disc: effects of low levels of oxygen, glucose, and pH on rates of energy metabolism of bovine nucleus pulposus cells. *Spine*, 30, (5) 487-496.
- Bonassar, L. J., Grodzinsky, A. J., Frank, E. H., Davila, S. G., Bhaktav, N. R. & Trippel, S. B. 2001. The effect of dynamic compression on the response of articular cartilage to insulin-like growth factor-I. *J Orthop Res*, 19, (1) 11-17.
- Boos, N., Wallin, A., Gbedegbegnon, T., Aebi, M. & Boesch, C. 1993. Quantitative MR imaging of lumbar intervertebral disks and vertebral bodies: influence of diurnal water content variations. *Radiology*, 188, (2) 351-354.
- Boubriak, O. and Urban, J. P. G. 2002. Measurement of Diffusion Coefficients in the Nucleus and Annulus of the Intervertebral Disc. 84-B ed.
- Bressler, H. B., Keyes, W. J., Rochon, P. A. & Bradley, E. 1999. The prevalence of low back pain in the elderly. A systematic review of the literature. *Spine*, 24, (17) 1813-1819.
- Brodin, H. 1955. Path of nutrition in articular cartilage and intervertebral disk. *Acta Ortho Scand*, 24, 177.
- Brown, M. D. & Tsaltas, T. T. 1976. Studies on the permeability of the intervertebral disc during skeletal maturation. *Spine*, 1, 240-244.
- Buckwalter, J. A. 1995. Aging and degeneration of the human intervertebral disc. *Spine*, 20, (11) 1307-1314.
- Burstein, D., Gray, M. L., Hartman, A. L., Gipe, R. & Foy, B. D. 1993. Diffusion of small solutes in cartilage as measured by nuclear magnetic resonance (NMR) spectroscopy and imaging. *J Orthop Res*, 11, (4) 465-478.
- Chelberg, M. K., Banks, G. M., Geiger, D. F. & Oegema, T. R., Jr. 1995. Identification of heterogeneous cell populations in normal human intervertebral disc. *J Anat.*, 186 ( Pt 1), 43-53.
- Chen, J., Yan, W. & Setton, L. A. 2006. Molecular phenotypes of notochordal cells purified from immature nucleus pulposus. *Eur Spine J*, 15 Suppl 3, S303-S311.
- Chiba, K., Andersson, G. B., Masuda, K. & Thonar, E. J. 1997. Metabolism of the extracellular matrix formed by intervertebral disc cells cultured in alginate. *Spine*, 22, (24) 2885-2893.
- Chiu, E. J., Newitt, D. C., Segal, M. R., Hu, S. S., Lotz, J. C. & Majumdar, S. 2001. Magnetic resonance imaging measurement of relaxation and water diffusion in the human lumbar intervertebral disc under compression in vitro. *Spine*, 26, (19) E437-E444.

- Das, D. B., Welling, A., Urban, J. P. G. & Boubriak, O. A. 2009. Solute transport in intervertebral disc: Experiments and finite element modeling. *Ann New York Acad Sci*, 1161, 44-61.
- Deen, W. M. (1998) *Analysis of Transport Phenomena*, 1st ed. New York, Oxford University Press.
- Drew, S. C., Silva, P., Crozier, S. & Percy, M. J. 2004. A diffusion and T2 relaxation MRI study of the ovine lumbar intervertebral disc under compression in vitro. *Phy Med Biol*, 49, 3585-3592.
- Ebara, S., Iatridis, J. C., Setton, L. A., Foster, R. J., Mow, V. C. & Weidenbaum, M. 1996. Tensile properties of nondegenerate human lumbar annulus fibrosus. *Spine*, 21, (4) 452-461.
- Errington, R. J., Puustjarvi, K., White, I. R., Roberts, S. & Urban, J. P. 1998. Characterisation of cytoplasm-filled processes in cells of the intervertebral disc. *J Anat*, 192 ( Pt 3), 369-378.
- Eyre, D. R., Benya, P., Buckwalter, J., Caterson, B., Heinegard, D., Oegema, T., Pearce, R., Pope, M. and Urban, J. (1989) Intervertebral disk: Basic science perspectives. IN J. W. Frymoyer & S. L. Gordon (Eds.) *New Perspectives on Low Back Pain*, Park Ridge, IL, American Academy of Orthopaedic Surgeons.
- Fetter N.L., Leddy, H. A., Guilak, F. & Nunley, J. A. 2006. Composition and transport properties of human ankle and knee cartilage. *J Orthop Res*, 24, (2) 211-219.
- Fischer, A. E., Carpenter, T. A., Tyler, J. A. & Hall, L. D. 1995. Visualisation of mass transport of small organic molecules and metal ions through articular cartilage by magnetic resonance imaging. *Magn Reson Imaging*, 13, (6) 819-826.
- Flagler, D. J., Huang, C.-Y., Yuan, T.-Y., Lu, Z., Cheung, H. S. & Gu, W. Y. 2009. Intracellular flow cytometric measurement of extracellular matrix components in porcine intervertebral disc cells. *Cell Molec Bioeng*, 2, 264-273.
- Foy, B. D. & Blake, J. 2001. Diffusion of paramagnetically labeled proteins in cartilage: enhancement of the 1-D NMR imaging technique. *J Magn Reson*, 148, (1) 126-134.
- Frymoyer, J. W. & Cats-Baril, W. L. 1991. An overview of the incidences and costs of low back pain. *Orthop Clin North Am*, 22, (2) 263-271.
- Fujita, Y., Lotz J.C & Soejima O. 1995. Site specific radial tensile properties of the lumbar annulus fibrosus. *Trans Orthop Res Soc*, 20, 673.
- Galante, J. O. 1967. Tensile properties of the human lumbar annulus fibrosus. *Acta Orthop Scand Suppl*-91.



Garcia, A. M., Frank, E. H., Grimshaw, P. E. & Grodzinsky, A. J. 1996. Contributions of fluid convection and electrical migration to transport in cartilage: relevance to loading. *Arch Biochem Biophys.*, 333, (2) 317-325.

Gruber, H. E., Fisher, E. C., Jr., Desai, B., Stasky, A. A., Hoelscher, G. & Hanley, E. N., Jr. 1997. Human intervertebral disc cells from the annulus: three-dimensional culture in agarose or alginate and responsiveness to TGF-beta1. *Exp Cell Res*, 235, (1) 13-21.

Gruber, H. E. & Hanley, E. N., Jr. 2002. Ultrastructure of the human intervertebral disc during aging and degeneration: comparison of surgical and control specimens. *Spine*, 27, (8) 798-805.

Gruber, H. E., Leslie, K., Ingram, J., Hoelscher, G., Norton, H. J. & Hanley, E. N., Jr. 2004. Colony formation and matrix production by human annulus cells: modulation in three-dimensional culture. *Spine*, 29, (13) E267-E274.

Gu, W. Y. & Justiz, M. A. 2002. Apparatus for measuring the swelling dependent electrical conductivity of charged hydrated soft tissues. *J Biomech Engng*, 124, 790-793.

Gu, W. Y., Justiz, M. A. & Yao, H. 2002. Electrical conductivity of lumbar annulus fibrosis: Effects of porosity and fixed charge density. *Spine*, 27, 2390-2395.

Gu, W. Y., Lai, W. M. & Mow, V. C. 1998. A mixture theory for charged-hydrated soft tissues containing multi- electrolytes: passive transport and swelling behaviors. *J Biomech Engng*, 120, (2) 169-180.

Gu, W. Y., Mao, X. G., Foster, R. J., Weidenbaum, M., Mow, V. C. & Rawlins, B. A. 1999. The anisotropic hydraulic permeability of human lumbar annulus fibrosus. Influence of age, degeneration, direction, and water content. *Spine*, 24, (23) 2449-2455.

Gu, W. Y. & Yao, H. 2003. Effects of hydration and fixed charge density on fluid transport in charged hydrated soft tissue. *Ann Biomed Engng*, 31, (10) 1162-1170.

Gu, W. Y., Yao, H., Huang, C.-Y. & Cheung, H. S. 2003. New insight into deformation-dependent hydraulic permeability of gels and cartilage, and dynamic behavior of agarose gels in confined compression. *J Biomech*, 36, 593-598.

Gu, W. Y., Yao, H., Vega, A. L. & Flagler, D. 2004. Diffusivity of ions in agarose gels and intervertebral disc: Effect of porosity. *Ann Biomed Engng*, 32, 1710-1717.

Guehring, T., Wilde, G., Sumner, M., Grünhagen, T., Karney, G. B., Tirlapur, U. K. & Urban, J. P. 2009. Notochordal intervertebral disc cells: sensitivity to nutrient deprivation. *Arthritis Rheum*, 60, (4) 1026-1034.

Guiot, B. H. & Fessler, R. G. 2000. Molecular biology of degenerative disc disease. *Neurosurgery*, 47, (5) 1034-1040.

Helferich, F. (1962) *Ion Exchange* New York, McGraw Hill Book Company, Inc.

Heller, A. & Feldman, B. 2008. Electrochemical glucose sensors and their applications in diabetes management. *Chem Rev*, 108, 2482-2505.

Hendry, N. G. C. 1958. The hydration of the nucleus pulposus and its relation to intervertebral disc derangement. *J Bone Joint Surg*, 40 B, 132-144.

Hickey, D. S. & Hukins, D. W. L. 1980. Relation between the structure of the annulus fibrosus and the function and failure of the intervertebral disc. *Spine*, 5, 106-116.

Holm, S., Maroudas, A., Urban, J. P., Selstam, G. & Nachemson, A. 1981. Nutrition of the intervertebral disc: solute transport and metabolism. *Connect Tissue Res*, 8, (2) 101-119.

Holm, S. & Nachemson, A. 1982. Nutritional changes in the canine intervertebral disc after spinal fusion. *Clin Orthop*, 169, 243-258.

Holm, S., Selstam, G. & Nachemson, A. 1982. Carbohydrate metabolism and concentration profiles of solutes in the canine lumbar intervertebral disc. *Acta Physiol Scand*, 115, (1) 147-156.

Horner, H. A., Roberts, S., Bielby, R. C., Menage, J., Evans, H. & Urban, J. P. 2002. Cells from different regions of the intervertebral disc: effect of culture system on matrix expression and cell phenotype. *Spine*, 27, (10) 1018-1028.

Horner, H. A. & Urban, J. P. 2001. 2001 Volvo Award Winner in Basic Science Studies: Effect of nutrient supply on the viability of cells from the nucleus pulposus of the intervertebral disc. *Spine*, 26, (23) 2543-2549.

Hsu, E. W. & Setton, L. A. 1999. Diffusion tensor microscopy of the intervertebral disc annulus fibrosus. *Magn Reson Med*, 41, (5) 992-999.

Huang, C.-Y. & Gu, W. Y. 2008. Effects of mechanical compression on metabolism and distribution of oxygen and lactate in intervertebral disc. *J. Biomech*, 41, (6) 1184-1196.

Huang, C.-Y., Yuan, T.-Y., Jackson, A. R., Hazbun, L. & Gu, W. Y. 2007. Effects of low glucose concentrations on oxygen consumption rates of intervertebral disc cells. *Spine*, 32, (19) 2063-2069.

Iatridis, J. C. & ap Gwynn, I. 2004. Mechanisms for mechanical damage in the intervertebral disc annulus fibrosus. *J Biomech*, 37, 1165-1175.

Iatridis, J. C., Kumar, S., Foster, R. J., Weidenbaum, M. & Mow, V. C. 1999. Shear mechanical properties of human lumbar annulus fibrosus. *J Orthop Res*, 17, (5) 732-737.

Iatridis, J. C., Setton, L. A., Weidenbaum, M. & Mow, V. C. 1997. Alterations in the mechanical behavior of the human lumbar nucleus pulposus with degeneration and aging. *J Orthop Res*, 15, (2) 318-322.

- Ishihara, H. & Urban, J. P. 1999. Effects of low oxygen concentrations and metabolic inhibitors on proteoglycan and protein synthesis rates in the intervertebral disc. *J Orthop Res*, 17, (6) 829-835.
- Jackson, A. R. & Gu, W. Y. 2009. Transport properties of cartilaginous tissues. *Curr Rheum Rev*, 5, 40-50.
- Jackson, A. R., Yao, H., Brown, M. D. & Gu, W. Y. 2006. Anisotropic ion diffusivity in intervertebral disc: an electrical conductivity approach. *Spine*, 31, 2783-2789.
- Jackson, A. R., Yuan, T. Y., Huang, C. Y., Travascio, F. & Gu, W. Y. 2008. Effect of compression and anisotropy on the diffusion of glucose in annulus fibrosus. *Spine*, 33, (1) 1-7.
- Johannessen, W. & Elliot, D. M. 2005. Effects of degeneration on the biphasic material properties of human nucleus pulposus in confined compression. *Spine*, 30, (24) E724-E729.
- Johnstone, B., Urban, J. P., Roberts, S. & Menage, J. 1992. The fluid content of the human intervertebral disc. Comparison between fluid content and swelling pressure profiles of discs removed at surgery and those taken postmortem. *Spine*, 17, (4) 412-416.
- Kealey, S. M., Aho, T., Delong, D., Barboriak, D. P., Provenzale, J. M. & Eastwood, J. D. 2005. Assessment of apparent diffusion coefficient in normal and degenerated intervertebral lumbar disks: Initial experience. *Radiology*, 235, (2) 569-574.
- Kelsey, J. L., Mundt, D. F. and Golden, A. L. (1992) Epidemiology of low back pain. IN J. I. V. Malcolm (Ed.) *The Lumbar Spine and Back Pain*, 4th ed. New York, Churchill Livingstone.
- Kelsey, J. L., Pastides, H. and Bisbee, G. E. (1978) *Musculoskeletal Disorders: Their Frequency of Occurrence and Their Impact on the Population of the United States* New York, Prodist.
- Kelsey, J. L. & White, A. A. 1980. Epidemiology and impact of low-back pain. *Spine*, 5, 133-142.
- Kelsey, J. L., White, A. A., III, Pastides, H. & Bisbee, G. E., Jr. 1979. The impact of musculoskeletal disorders on the population of the United States. *J Bone Joint Surg Am*, 61, (7) 959-964.
- Kerttula, L., Kurunlahti, M., Jauhiainen, J., Koivula, A., Oikarinen, J. & Tervonen, O. 2001. Apparent diffusion coefficients and T2 relaxation time measurements to evaluate disc degeneration. A quantitative MR study of young patients with previous vertebral fracture. *Acta Radiol*, 42, (6) 585-591.

- Kitano, T., Zerwekh, J. E., Usui, Y., Edwards, M. L., Flicker, P. L. & Mooney, V. 1993. Biochemical changes associated with the symptomatic human intervertebral disc. *Clin Orthop*, 293, 372-377.
- Kraemer, J., Kolditz, D. & Gowin, R. 1985. Water and electrolyte content of human intervertebral discs under variable load. *Spine*, 10, (1) 69-71.
- Kurunlahti, M., Kerttula, L., Jauhiainen, J., Karppinen, J. & Tervonen, O. 2001. Correlation of diffusion in lumbar intervertebral disks with occlusion of lumbar arteries: a study in adult volunteers. *Radiology*, 221, (3) 779-786.
- Lai, W. M., Hou, J. S. & Mow, V. C. 1991. A triphasic theory for the swelling and deformation behaviors of articular cartilage. *J Biomech Engng*, 113, (3) 245-258.
- Leddy, H. A. & Guilak, F. 2003. Site-specific molecular diffusion in articular cartilage measured using fluorescence recovery after photobleaching. *Ann Biomed Engng*, 31, (7) 753-760.
- Lee, R. B. & Urban, J. P. 1997. Evidence for a negative Pasteur effect in articular cartilage. *Biochem J*, 321 ( Pt 1), 95-102.
- Longworth, L. G. 1953. Diffusion measurements, at 25°C, of aqueous solutions of amino acids, peptides, and sugars. *J Am Chem Soc*, 75, 5705-5709.
- Lundon, K. & Bolton, K. 2001. Structure and function of the lumbar intervertebral disk in health, aging, and pathologic conditions. *J Orthop Sports Phys Ther*, 31, (6) 291-303.
- Lyons, G., Eisenstein, S. M. & Sweet, M. B. 1981. Biochemical changes in intervertebral disc degeneration. *Biochim Biophys Acta*, 673, (4) 443-453.
- Magnier, C., Boiron, O., Wendling-Mansuy, S., Chabrand, P. & Deplano, V. 2009. Nutrient distribution and metabolism in the intervertebral disc in the unloaded state: a parametric study. *J Biomech*, 42, (2) 100-108.
- Maldonado, B. A. & Oegema, T. R., Jr. 1992. Initial characterization of the metabolism of intervertebral disc cells encapsulated in microspheres. *J Orthop Res*, 10, (5) 677-690.
- Marchand F. & Ahmed A.M 1989. Mechanical properties and failure mechanisms of the lumbar disc annulus. *Trans Orthop Res Soc*, 14, 355.
- Marchand, F. & Ahmed, A. M. 1990. Investigation of the laminate structure of lumbar disc annulus fibrosus. *Spine*, 15, (5) 402-410.
- Maroudas, A. 1976. Transport of solutes through cartilage: permeability to large molecules. *J Anat*, 122, (2) 335-347.
- Maroudas, A. 1968. Physicochemical properties of cartilage in the light of ion exchange theory. *Biophys J*, 8, (5) 575-595.

- Maroudas, A. 1975. Biophysical chemistry of cartilaginous tissues with special reference to solute and fluid transport. *Biorheology*, 12, 233-248.
- Maroudas, A., Bullough, P., Swanson, S. A. & Freeman, M. A. 1968. The permeability of articular cartilage. *J Bone Joint Surg Br*, 50, (1) 166-177.
- Maroudas, A., Stockwell, R. A., Nachemson, A. & Urban, J. 1975. Factors involved in the nutrition of the human lumbar intervertebral disc: cellularity and diffusion of glucose in vitro. *J Anat*, 120, (1) 113-130.
- Martin, M. D., Boxell, C. M. & Malone, D. G. 2002. Pathophysiology of lumbar disc degeneration: a review of the literature. *Neurosurg Focus*, 13, (2) E1.
- Masaro, L. & Zhu, X. X. 1999. Physical models of diffusion for polymer solutions, gels and solids. *Progress in Polymer Science*, 24, 731-775.
- Mauck, R. L., Hung, C. T. & Ateshian, G. A. 2003. Modeling of neutral solute transport in a dynamically loaded porous permeable gel: Implications for articular cartilage biosynthesis and tissue engineering. *J Biomech Engng*, 125, (5) 602-614.
- Melrose, J., Smith, S., Ghosh, P. & Taylor, T. K. 2001. Differential expression of proteoglycan epitopes and growth characteristics of intervertebral disc cells grown in alginate bead culture. *Cells Tissues Organs*, 168, (3) 137-146.
- Miller, J. A. A., Schmatz, C. & Schultz, A. B. 1988. Lumbar disc degeneration: Correlation with age, sex, and spine level in 600 autopsy specimens. *Spine*, 13, 173-178.
- Mirza, S. K. & White, A. A., III 1995. Anatomy of intervertebral disc and pathophysiology of herniated disc disease. *J Clin Laser Med Surg*, 13, (3) 131-142.
- Nachemson, A. 1966. The load on lumbar disks in different positions of the body. *Clin Orthop Rel Res*, 45, 107-122.
- Nachemson, A., Lewin, T., Maroudas, A. & Freeman, M. A. 1970. In vitro diffusion of dye through the end-plates and the annulus fibrosus of human lumbar inter-vertebral discs. *Acta Orthop Scand*, 41, (6) 589-607.
- Nerlich, A. G., Boos, N., Wiest, I. & Aebi, M. 1998. Immunolocalization of major interstitial collagen types in human lumbar intervertebral discs of various ages. *Virchows Arch*, 432, (1) 67-76.
- Nguyen-minh, C., Houghton, V. M., Papke, R. A., An, H. & Censky, S. C. 1998. Measuring diffusion of solutes into intervertebral disks with MR imaging and paramagnetic contrast medium. *Am J Neuroradiol*, 19, (9) 1781-1784.
- Ngwa, W., Geier, O., Stallmach, F., Naji, L., Schiller, J. & Arnold, K. 2002. Cation diffusion in cartilage measured by pulsed field gradient NMR. *Eur Biophys J*, 31, (1) 73-80.

NIH 1997. Research on low back pain and common spinal disorders. NIH Guide, 26, (Number 16).

Niinimäki, J., Korkiakoski, A., Ojala, O., Karppinen, J., Ruohonen, J., Haapea, M., Korpelainen, R., Natri, A. & Tervonen, O. 2009. Association between visual degeneration of intervertebral discs and the apparent diffusion coefficient. *Magn Reson Imaging*, 27, 641-647.

Nimer, E., Schneiderman, R. & Maroudas, A. 2003. Diffusion and partition of solutes in cartilage under static load. *Biophys Chem*, 106, 125-146.

O'Hara, B. P., Urban, J. P. & Maroudas, A. 1990. Influence of cyclic loading on the nutrition of articular cartilage. *Ann Rheum Dis*, 49, (7) 536-539.

O'Hare, D., Winlove, C. P. & Parker, K. H. 1991. Electrochemical method for direct measurement of oxygen concentration and diffusivity in the intervertebral disc: electrochemical characterization and tissue-sensor interactions. *J Biomed Engng*, 13, (4) 304-312.

Ogata, K. & Whiteside, L. A. 1981. 1980 Volvo award winner in basic science. Nutritional pathways of the intervertebral disc. An experimental study using hydrogen washout technique. *Spine*, 6, (3) 211-216.

Ohshima, H., Tsuji, H., Hiarano, N., Ishihara, H., Katoh, Y. & Yamada, H. 1989. Water diffusion pathway, swelling pressure, and biomechanical properties of the intervertebral disc during compression load. *Spine*, 14, 1234-1244.

Ohshima, H. & Urban, J. P. 1992. The effect of lactate and pH on proteoglycan and protein synthesis rates in the intervertebral disc. *Spine*, 17, (9) 1079-1082.

Panagiotacopoulos, N. D., Pope, M. H., Krag, M. H. & Block, R. 1987. Water content in human intervertebral discs. Part I. Measurement by magnetic resonance imaging. *Spine*, 12, (9) 912-917.

Pearce, R. H. (1993) Morphologic and Chemical Aspects of Aging. IN D. O. Wood, V. M. Goldberg, & S. L. Woo (Eds.) *Musculoskeletal Soft-Tissue Aging: Impact on Mobility*, Rosemont, IL, American Academy of Orthopaedic Surgeons.

Quinn, T. M., Kocian, P. & Meister, J. J. 2000. Static compression is associated with decreased diffusivity of dextrans in cartilage explants. *Arch Biochem Biophys*, 384, 327-334.

Quinn, T. M., Morel, V. & Meister, J. J. 2001. Static compression of articular cartilage can reduce solute diffusivity and partitioning: implications for the chondrocyte biological response. *J Biomech*, 34, (11) 1463-1469.

Quinn, T. M., Studer, C., Grodzinsky, A. J. & Meister, J. J. 2002. Preservation and analysis of nonequilibrium solute concentration distributions within mechanically compressed cartilage explants. *J Biochem Biophys Methods*, 31, (2) 83-95.

Razaq, S., Wilkins, R. J. & Urban, J. P. 2003. The effect of extracellular pH on matrix turnover by cells of the bovine nucleus pulposus. *Eur Spine J*, 12, 341-349.

Roberts, S., Menage, J. & Eisenstein, S. M. 1993. The cartilage end-plate and intervertebral disc in scoliosis: calcification and other sequelae. *J Orthop Res*, 11, (5) 747-757.

Roberts, S., Menage, J. & Urban, J. P. 1989. Biochemical and structural properties of the cartilage end-plate and its relation to the intervertebral disc. *Spine*, 14, (2) 166-174.

Roberts, S., Urban, J. P., Evans, H. & Eisenstein, S. M. 1996. Transport properties of the human cartilage endplate in relation to its composition and calcification. *Spine*, 21, (4) 415-420.

Selard, E., Shirazi-Adl, A. & Urban, J. 2003. Finite element study of nutrient diffusion in the human intervertebral disc. *Spine*, 28, (17) 1945-1953.

Setton, L. A. & Chen, J. 2006. Mechanobiology of the intervertebral disc and relevance to disc degeneration. *J Bone Joint Surg Am*, 88, (Suppl. 2) 52-57.

Setton, L. A., Zhu, W., Weidenbaum, M., Ratcliffe, A. & Mow, V. C. 1993a. Compressive properties of the cartilaginous end-plate of the baboon lumbar spine. *J Orthop Res*, 11, (2) 228-239.

Setton, L. A., Zhu, W. B. & Mow, V. C. 1993b. The biphasic poroviscoelastic behavior of articular cartilage: Role of the surface zone in governing the compressive behavior. *J Biomech*, 26, 581-592.

Shirazi-Adl, A., Taheri, M. & Urban, J. P. 2010. Analysis of cell viability in intervertebral disc: Effect of endplate permeability on cell population. *J Biomech*, 43, (7) 1330-1336.

Soukane, D. M., Shirazi-Adl, A. & Urban, J. 2005. Analysis of nonlinear coupled diffusion of oxygen and lactic acid in intervertebral discs. *J Biomech Engng*, 127, (7) 1121-1126.

Soukane, D. M., Shirazi-Adl, A. & Urban, J. P. 2007. Computation of coupled diffusion of oxygen, glucose and lactic acid in an intervertebral disc. *J Biomech*, 40, (12) 2645-2654.

Soukane, D. M., Shirazi-Adl, A. & Urban, J. P. G. 2009. Investigation of solute concentrations in a 3D model of intervertebral disc. *Eur Spine J*, 18, 254-262.



Stairmand, J. W., Holm, S. & Urban, J. P. 1991. Factors influencing oxygen concentration gradients in the intervertebral disc. A theoretical analysis. *Spine*, 16, (4) 444-449.

Stokes, I. A. & Iatridis, J. C. 2004. Mechanical conditions that accelerate intervertebral disc degeneration: overload versus immobilization. *Spine*, 29, (23) 2724-2732.

Sun, D. N., Gu, W. Y., Guo, X. E., Lai, W. M. & Mow, V. C. 1999. A mixed finite element formulation of triphasic mechano-electrochemical theory for charged, hydrated biological soft tissues. *Intl J Num Meth Engng*, 45, 1375-1402.

Terahata, N., Ishihara, H., Ohshima, H., Hirano, N. & Tsuji, H. 1994. Effects of axial traction stress on solute transport and proteoglycan synthesis in the porcine intervertebral disc in vitro. *Eur Spine J*, 3, (6) 325-330.

Thompson, J. P., Pearce, R. H., Schechter, M. T., Adams, M. E., Tsang, I. K. Y. & Bishop, P. B. 1990. Preliminary evaluation of a scheme for grading the gross morphology of the human intervertebral disc. *Spine*, 15, 411-415.

Torzilli, P. A., Adams, T. C. & Mis, R. J. 1987. Transient solute diffusion in articular cartilage. *J Biomech*, 20, (2) 203-214.

Torzilli, P. A., Dethmers, D. A., Rose, D. E. & Schryuer, H. F. 1983. Movement of interstitial water through loaded articular cartilage. *J Biomech*, 16, (3) 169-179.

Torzilli, P. A., Grande, D. A. & Arduino, J. M. 1998. Diffusive properties of immature articular cartilage. *J Biomed Mater Res*, 40, (1) 132-138.

Travascio, F. & Gu, W. Y. 2007. Anisotropic diffusive transport in annulus fibrosus: experimental determination of the diffusion tensor by FRAP technique. *Ann Biomed Engng*, 35, (10) 1739-1748.

Travascio, F., Jackson, A. R., Brown, M. D. & Gu, W. Y. 2009. Relationship between solute transport properties and tissue morphology in human annulus fibrosus. *J Orthop Res*, 27, 1625-1630.

Urban, J. P. 2001. The role of the physicochemical environment in determining disc cell behaviour. *Biochem Soc Trans*, 30, (6) 858-864.

Urban, J. P., Holm, S. & Maroudas, A. 1978. Diffusion of small solutes into the intervertebral disc: as in vivo study. *Biorheology*, 15, (3-4) 203-221.

Urban, J. P., Holm, S., Maroudas, A. & Nachemson, A. 1982. Nutrition of the intervertebral disc: Effect of fluid flow on solute transport. *Clin Orthop*, 170, 296-302.

Urban, J. P. & McMullin, J. F. 1988. Swelling pressure of the lumbar intervertebral discs: influence of age, spinal level, composition, and degeneration. *Spine*, 13, (2) 179-187.



- Urban, J. P. & Roberts, S. 1995. Development and degeneration of the intervertebral discs. *Mol.Med Today*, 1, (7) 329-335.
- Urban, J. P., Smith, S. & Fairbank, J. C. 2004. Nutrition of the intervertebral disc. *Spine*, 29, 2700-2709.
- Urban, J. P. G. (1977) *Fluid and Solute Transport in the Intervertebral Disc*. Ph.D. Dissertation, London University.
- Urban, J. P. G. & Roberts, S. 2003. Degeneration of the intervertebral disc. *Arth Res Ther*, 5, (3) 120-130.
- Urban, J. P. G., Roberts, S. & Ralphs, J. R. 2000. The nucleus of the intervertebral disc from development to degeneration. *American Zoologist*, 40, 53-61.
- Urban, M. R., Fairbank, J. C., Etherington, P. J., Loh, F. L., Winlove, C. P. & Urban, J. P. 2001. Electrochemical measurement of transport into scoliotic intervertebral discs in vivo using nitrous oxide as a tracer. *Spine*, 26, (8) 984-990.
- Wang, J. Y., Baer, A. E., Kraus, V. B. & Setton, L. A. 2001. Intervertebral disc cells exhibit differences in gene expression in alginate and monolayer culture. *Spine*, 26, (16) 1747-1751.
- Wang, S., Xia, Q., Passias, P., Wood, K. & Li, G. 2009. Measurement of geometric deformation of lumbar intervertebral discs under in-vivo weightbearing condition. *J Biomech*, 42, (6) 705-711.
- White, A. A. (1981) Biomechanics of lumbar spine and sacroiliac articulation: relevance to idiopathic low back pain. IN A. A. White & S. L. Gordon (Eds.) *Symposium on Idiopathic Low Back Pain*, St. Louis, CV Mosby Co.
- White, A. A. and Panjabi, M. M. (1990) *Clinical Biomechanics of the Spine*, 2nd ed. Philadelphia, J.B. Lippincott Company.
- White, A. A. and Panjabi, M. M. (1978) Physical properties and functional biomechanics of the spine. IN A. A. White & M. M. Panjabi (Eds.) *Clinical Biomechanics of the Spine*, Philadelphia, JB Lippincott.
- Wilke, H. J., Neef, P., Caimi, M., Hoogland, T. & Claes, L. E. 1999. New in vivo measurements of pressures in the intervertebral disc in daily life. *Spine*, 24, (8) 755-762.
- Windhaber, R. A. J., Wilkins, R. J. & Meredith, D. 2003. Functional characterisation of glucose transport in bovine articular chondrocytes. *Eur J Physiol*, 446, 572-577.
- Woolfe, A. D. & Pflieger, B. 2003. Burden of major musculoskeletal conditions. *Bull World Health Organ*, 81, 646-656.

Yao, H. & Gu, W. Y. 2006. Physical signals and solute transport in human intervertebral disc during compressive stress relaxation: 3D finite element analysis. *Biorheology*, 43, 323-335.

Yao, H. & Gu, W. Y. 2004. Physical signals and solute transport in cartilage under dynamic unconfined compression: finite element analysis. *Ann Biomed Engng*, 32, 380-390.

Yao, H. & Gu, W. Y. 2007. Three-dimensional inhomogeneous triphasic finite-element analysis of physical signals and solute transport in human intervertebral disc under axial compression. *J Biomech*, 40, (9) 2071-2077.

Yao, H., Justiz, M. A., Flagler, D. & Gu, W. Y. 2002. Effects of swelling pressure and hydraulic permeability on dynamic compressive behavior of lumbar annulus fibrosus. *Ann Biomed Engng*, 30, 1234-1241.

Yuan, T. Y., Jackson, A. R., Huang, C. Y. & Gu, W. Y. 2009. Strain-dependent oxygen diffusivity in bovine annulus fibrosus. *J Biomech Engng*, 131, 074503-1-074503-4.

